Magnesium Polyolefin Interactions during Thermal Debinding in the MIM Process of Magnesium

Dissertation

zur Erlangung des akademischen Grades

Doktor der Ingenieurwissenschaften (Dr.-Ing.)

der Technischen Fakultät

der Christian-Albrechts-Universität zu Kiel

vorgelegt von

Johannes Geronimo Schaper

Kiel 2019

Erstgutachterin: Prof. Dr. Regine Willumeit-Römer

Zweitgutachter: Prof. Dr. Franz Faupel

Datum der mündlichen Prüfung: 08.07.2019

Abstract

Metal injection moulding (MIM) of magnesium has been developed in the recent years with the aim to produce metallic implants for the biomedical sector with unique properties such as a special microstructure which is independent of the part geometry. Powder metallurgy (PM) possesses the benefit of easy and fast alloy development by the mixing of elemental or pre-alloyed powders. MIM of magnesium has the potential to combine the benefits of the metallic material, for example the strength and the ones of the plastic injection moulding such as cheap mass production of small and complex shaped parts. However, due to the reactive nature of magnesium a few challenges have to be overcome. Once the sinterability of magnesium was proven the MIM process could be introduced. First trials showed that polyethylene (PE) based polymers, typically used for MIM of reactive materials such as titanium, cause a strong sintering inhibiting effect, while polypropylene (PP) based polymers do not show this effect. Within this work a fundamental understanding of the mechanisms taking place during the thermal debinding of PE and PP based polymers in combination with magnesium powder is developed by using literature and different experimental setups.

Based on a literature review it was found that PE based polymers decompose into straight alkanes and alkenes while PP based polymers decompose into branched ones. Experiments using different straight and branched alkanes and alkenes revealed that this treatment results in differences in sintering activity and carbon content. An opposing correlation between carbon content and sintering activity could be proved. This correlation is caused by the fact that magnesium has no solubility for carbon and that there are no stable compounds at the conditions used during MIM processing. This leads to the fact that carbon on the powder surfaces can act as a barrier between neighbouring powder particles preventing the contact needed for solid state diffusion which is the fundamental process of sintering. Furthermore, it could be proven that hydrogen atmosphere during thermal treatment can be used to remove carbon residuals resulting in increased sintering activity. By using hydrogen, the negative effect of PE based polymers can be reversed. However, it could also be shown that the use of hydrogen is limited to alloys that are not prone to react with hydrogen.

Based on a literature review and conducted experiments it could be found that the decomposition products of PE prone to react with magnesium forming metastable carbides on the powder surfaces while the decomposition products of PP do not show this reaction. The carbides decompose leaving carbon on the powder surfaces. The decomposition is intensified by the heat and vacuum conditions applied during thermal debinding.

Based on the knowledge of this work a suitable binder polymer for MIM of magnesium could be identified and processing parameters could be optimised. Thus, it is concluded that MIM of magnesium is ready for commercial application and further magnesium alloys can be introduced into the process.

Zusammenfassung

Metallpulverspritzguss (MIM) von Magnesium wurde in den letzten Jahren mit dem Ziel entwickelt metallische Implantate für biomedizinische Anwendungen mit einzigartigen Eigenschaften wie insbesondere einer speziellen, geometrieunabhängigen Mikrostruktur herzustellen. Die Pulvermetallurgie (PM) bietet den Vorteil einfacher und schneller Legierungsentwicklung durch das Mischen von elementar oder vorlegierten Pulvern. MIM von Magnesium bietet das Potential die Vorzüge von metallischen Materialien, unter anderem deren Festigkeit, mit denen des Spritzgussprozesses, insbesondere die günstige Herstellung von kleinen komplex geformten Teilen in hohen Stückzahlen, zu verbinden. Durch die reaktive Natur von Magnesium müssen jedoch einige Herausforderungen überwunden werden. Nach dem erfolgreichen Nachweis der Sinterbarkeit von Magnesium konnte dieses in den MIM Prozess eingeführt werden. Erste Versuche haben gezeigt, dass Polyethylen (PE) basierte Polymere, welche typischerweise für den MIM Prozess von reaktiven Metallen wie zum Beispiel Titan genutzt werden, einen stark sinterhemmenden Effekt haben. Polypropylen (PP) basierte Polymere zeigen diesen Effekt nicht. Im Rahmen dieser Arbeit wird, durch den Gebrauch von Literatur und diversen experimentellen Aufbauten, ein grundlegendes Verständnis über die Mechanismen, welche während des thermischen Entbinderns von PP und PE basierten Polymeren in Kombination mit Magnesium auftreten, erarbeitet.

Basierend auf einer Literaturrecherche konnte herausgefunden werden, dass PE basierte Polymere in unverzweigte und PP basierte Polymere in verzweigte Alkane und Alkene zerfallen. Experimente mit verschiedenen unverzweigten und verzweigten Alkanen und Alkenen haben gezeigt, dass es zu Unterschieden in der Sinteraktivität und im Kohlenstoffgehalt der Proben kommt. Es konnte bewiesen werden, dass es ein gegenläufiges Verhältnis zwischen Sinteraktivität und Kohlenstoffgehalt gibt. Dieses Verhältnis wird dadurch hervorgerufen, dass Magnesium unter den beim MIM Prozess herrschenden Bedingungen keine Löslichkeit für Kohlenstoff hat, und es außerdem keine stabilen Magnesium-Kohlenstoffverbindungen gibt. Dies führt dazu, dass Kohlenstoff auf den Pulveroberflächen als Kontaktbarriere zwischen benachbarten Pulverpartikeln wirken kann. Ohne den direkten Kontakt kann es zu keiner Festphasendiffusion zwischen den Partikeln, einer der grundlegenden Prozesse beim Sintern, kommen. Des Weiteren konnte gezeigt werden, dass eine Wasserstoffatmosphäre während des thermischen Behandlung Kohlenstoffrückstände entfernen und dadurch die Sinteraktivität erhöhen kann. Durch den Einsatz von Wasserstoff kann der negative Effekt von PE basierten Polymeren rückgängig gemacht werden. Jedoch konnte auch gezeigt werden, dass der Einsatz von Wasserstoff auf Legierungen beschränkt ist, welche nicht dazu neigen mit dem Wasserstoff zu reagieren.

Basierend auf einer Literaturrecherche und den Experimenten wurde herausgefunden, dass die Zersetzungsprodukte von PE dazu neigen mit Magnesium zu reagieren, um metastabile Magnesiumkarbide auf den Pulveroberflächen zu bilden, während die Zersetzungsprodukte von PP diese Reaktion nicht zeigen. Diese Karbide zerfallen und hinterlassen dadurch Kohlenstoffrückstände auf den Pulveroberflächen. Diese Zerfallsreaktion wird durch die Wärme und das Vakuum während des thermischen Entbinderns verstärkt.

Basierend auf den Erkenntnissen dieser Arbeit konnte ein geeignetes Binderpolymer für MIM von Magnesium gefunden werden und die Prozessparameter konnten optimiert werden. Dadurch kann nunmehr geschlussfolgert werden, dass MIM von Magnesium reif für eine kommerzielle Nutzung ist und weitere Legierungen in den Prozess eingeführt werden können.

Erklärung

Hiermit erkläre ich, dass die beigefügte Dissertation, abgesehen von der Beratung durch die Betreuerin, nach Inhalt und Form meine eigene Arbeit ist.

Die Arbeit, ganz oder zum Teil, wurde nie schon einer anderen Stelle im Rahmen eines Prüfungsverfahrens vorgelegt und ist abgesehen, von den in den angegebenen Veröffentlichungen, nicht anderweitig zur Veröffentlichung vorgelegt worden.

Außerdem ist die Arbeit unter Einhaltung der Regeln guter wissenschaftlicher Praxis der Deutschen Forschungsgemeinschaft entstanden.

Ich gebe außerdem an, dass mir kein akademischer Grad entzogen wurde.

Kiel, 04.06.2019
(Ort, Datum)

J. Schaper
(Unterschrift)
Johannes Geronimo Schaper

Supporting Academic Works

The following publications have either been produced in direct or indirect context of this work.

M. Wolff, J. G. Schaper, M. Dahms, T. Ebel, K.U. Kainer, T. Klassen: *Magnesium Powder Injection Moulding for biomedical application.* Conference oral presentation and Proceedings, EuroPM2014, Salzburg, Austria, 2014.

M. Wolff, J. G. Schaper, M. Dahms, T. Ebel, K.U. Kainer, T. Klassen: *Magnesium powder injection moulding for biomedical application.* Powder Metallurgy, 2014, 57, 331-340.

M. Wolff, J. G. Schaper, M. Dahms, T. Ebel, K. U. Kainer, T. Klassen, *Benefits and limitations of biodegradable Mg implants and parts, produced by MIM (Metal Injection Moulding)*. Conference oral presentation and proceedings, Biometal 6th symposium on biodegradable Metals, Maratea, Italy, Aug 24th-29th 2014.

M. Wolff, J. G. Schaper, M. Dahms, N. Rüder, C. Vogt, T. Ebel, F. Feyerabend, R. Willumeit-Römer, T. Klassen, *Investigation of impurity levels of biodegradable Mg-materials and their influence on biocorrosion*. Conference oral presentation and Proceedings, Biometal 7th symposium on biodegradable Metals, Carovigno, Italy, Aug 23rd-28th 2015.

M. Wolff, J. Schaper, N. Rüder, C. Vogt, F. Feyerabend, M. Dahms, R. Willumeit-Römer, T. Ebel, T. Klassen, *Untersuchung des Einflusses von Verunreinigungen auf das Bioabbauverhalten metallischer Mg-Ca basierter Implantate*, Conference oral presentation and proceedings, Jahrestagung der DGBM, Freiburg, Germany, 2015.

M. Wolff, M. R. Suckert, J. G. Schaper, M. Dahms, T. Ebel, K. U. Kainer, T. Klassen, *Metal Injection Molding (MIM) of Magnesium Alloys for Orthopedic Implant Applications*. Conference oral presentation and Proceedings, Int. Conference on Frontiers in Materals Processing, Applications Research & Technology - FIMPART´15, Hyderabad, India, 2015.

M. Wolff, J. Schaper, M. Dahms, T. Ebel, K. U. Kainer, T. Klassen, *Magnesium Powder Injection Moulding for biomedical applications.* Powder Injection Moulding-International, 2015, 9, 61-64.

M. Wolff, J. G. Schaper, M. R. Suckert, M. Dahms, T. Ebel, R. Willumeit-Römer, T. Klassen, *Magnesium Powder Injection Molding (MIM) of Orthopedic Implants for Biomedical Applications.* JOM, 2016, 68, 1191-1197

Martin Wolff, Johannes G. Schaper, Marc René Suckert, Michael Dahms, Frank Feyerabend, Thomas Ebel, Regine Willumeit-Römer, Thomas Klassen, *Metal Injection Molding (MIM) of Magnesium and Its Alloys.* Metals, 2016, 6, 118.

M. Wolff, J. Schaper, *Magnesium implant demonstrator parts successfully produced by MIM.* Powder Injection Moulding International, 2016, 10, 50-51.

M. Wolff, J. G. Schaper, M. R. Suckert, N. Rüder, M. Dahms, T. Ebel, F. Feyerabend, R. Willumeit-Römer, T. Klassen, *Magnesium Powder Injection Moulding (MIM) of Orthopaedic Implants for Biomedical Applications.* Conference oral presentation and Proceedings, TMS2016 145th annual meeting and exhibition, Nashville, USA, 2016.

M. Wolff, J. G. Schaper, M. R. Suckert, M. Dahms2 T. Ebel, R. Willumeit-Römer, T. Klassen, *Enhancement of Thermal Debinding and Sintering of Biodegradable MIM-Magnesium Parts for Biomedical Applications.* Conference oral presentation and Proceedings, WorldPM2016, Hamburg, Germany, 2016.

M. Wolff, M. Luczak, J. G. Schaper, B. Wiese, T. Ebel, R. Willumeit-Römer, T. Klassen, *Manufacturing and Assessment of high strength Mg-Nd-Gd-Zr-Zn alloy implant prototypes and test specimen, using PM (Powder Metallurgy) methods*. Conference oral presentation and Proceedings, Biometal 9th symposium on biodegradable Metals, Bertinoro, Italy, Aug 27rd-Sep 1st 2017.

Johannes G. Schaper, Martin Wolff, Thomas Ebel, Michael Dahms, Regine Willumeit-Römer, *MIM Processing of Complex Mg-Alloys,* Conference oral presentation and Proceedings, EuroPM2017, Milan, Italy, 2017.

M. Wolff, M. Luczak, J. G. Schaper, B. Wiese, M. Dahms, T. Ebel, R. Willumeit-Römer, T. Klassen, *In vitro biodegradation testing of Mg-alloy EZK400 and manufacturing of implant prototypes using PM (powder metallurgy) methods*. Bioactive Materials, 2018, 3, 213-217.

M. Wolff, J. G. Schaper, M. Dahms, T. Ebel, R. Willumeit-Römer, T. Klassen, *Metal Injection Moulding (MIM) of Mg alloys*. Conference oral presentation and Proceedings, TMS 2018 147th Annual Meeting & Exhibition Supplemental Proceedings, 239-251.

Johannes G. Schaper, Nico Scharnagl, Martin Wolff, Thomas Ebel, Silvio Neumann and Regine Willumeit-Römer, *Polyolefin-Magnesium Interactions Performing Powder Injection Molding Process,* Advanced Engineering Materials, 2018.

Johannes G. Schaper, Martin Wolff, Thomas Ebel, Regine Willumeit-Römer, *Sintering of Mg and its alloys under Hydrogen Atmospheres,* Conference oral presentation and Proceedings, EuroPM2018, Bilbao, Spain, 2018.

Johannes G. Schaper, Martin Wolff, Björn Wiese, Thomas Ebel, Regine Willumeit-Römer, *Powder metal injection moulding and heat treatment of AZ81 Mg alloy,* Journal of Materials Processing Technology, 2019, 267, 241-246.

Acknowledgements

This thesis was completed in the department WBM of the Institute of Materials Research at the Helmholtz-Zentrum Geesthacht.

I would like to thank all members of the Helmholtz-Zentrum that helped me in conducting the work for this thesis especially Dr. Thomas Ebel for his support and guidance during the whole time of the preparation of this work. I like to thank Martin Wolff for the intense and fruitful discussions of scientific and technical but also on many other topics. I would like to thank

Andreas Dobernowsky for his help in the laboratory work.
For helping me with measurements and evaluation of the results I would like to thank Silvio Neumann for his help in the FTIR measurements, Dr. Nico Scharnagl for his help in the XPS measurements and Dr. Alexander Welle for his help in the ToF-SIMS measurements. Also, I would like to thank the companies LECO Instrumente GmbH, ELTRA GmbH and HUK Umweltlabor for their help in conduction the carbon combustion analysis.
Prof. Dr. Michael Dahms suggested to me to perform my master thesis at the Helmholtz-Zentrum Geestacht which resulted in the opportunity to follow up on the topic of this work. I would like to thank him for his scientific guidance.

A special thanks goes to my wife Kristin Schaper who always supported me in all matters during the time of this work and always had an understanding when I had to spend weekends or days of our holidays with the writing of this work.

Table of Contents

Table of Figures

Table Directory

Table of Abbreviations

$A_{BET,Mg}$	BET surface area of magnesium
A_C	Surface area of carbon (graphene)
A_{Mg}	Surface area of magnesium
$A_{th,C}$	Theoretical surface area of graphene
BET	Brunauer-Emmett-Teller: method for determination of specific surface area of solids
E	Young's modulus
EBS	Ethylenbisstearamide
EDXS	Energy-dispersive X-ray spectroscopy
FCC	Face centred cubic (crystal structure)
FTIR	Fourier transformed infrared spectroscopy
GD-OES	Glow discharge optical emission spectrometry
HCP	Hexagonal close-packed (crystal structure)
HDPE	High density polyethylene
IR	Infrared
LDPE	Low density polyethylene
L_e	Starting length of test area during tensile testing
l_g	Green length
l_s	Sintered length
m_C	Mass of carbon
MIM	Metal Injection Moulding
m_{Mg}	Mass of magnesium
m_s	Weight sintered part
P_{closed}	Closed porosity
PE	Polyethylene
PEcoOc	Polyethylene octene copolymer
PE-EVA	Polyethylene-vinyl acetate
PIB	Polyisobutylene
PM	Powder Metallurgy

PP	Polypropylene
PPcoPB	Polypropylene-co-1-butene
PS	Polystyrene
PVS	Polyvinyl alcohol
R_m	Tensile strength
$R_{p0,2}$	Yield strength
SDS	Shaping debinding sintering
SEM	Scanning electron microscope
S_L	Longitudinal shrinkage
TGA	Thermos gravimetric analysis
T_m	Melting point
ToF-SIMS	Time-of-Flight Secondary Ion Mass Spectrometry
V	Volume
XPS	X-ray photoelectron spectroscopy
XRD	X-ray diffraction
ρ_a	Archimedes density
ρ_{geo}	Geometrical density
ρ_{th}	Theoretical density

1 Introduction

Metal injection moulding (MIM) enables the production of small complex shaped parts in high quantities at low costs. MIM is used to produce components in a broad field of applications out of a large choice of materials. Steel and hard metals are by far the most processed materials in the MIM sector [1]. Reactive metals such as titanium are also processed by MIM but their percentage of the entire MIM sector is very low; nevertheless, MIM of titanium and other "advanced" materials is growing [2]. MIM combines the cheap and fast shaping technology of plastics injection moulding with the properties of metals. This is possible due to mixing of metal powder with polymeric binder components. This mixture can be processed on injection moulding machines for shaping of the components without melting the metal. After shaping, the binder components are removed and the powder is consolidated due to sintering resulting in a metal part. [3]

Magnesium is the lightest of all structural metals and is therefore of great interest in lightweight applications. The demand for energy saving transport is a driving force for the growing applications in the transport sector. Another driving force is the growing market for electronics and "wearables" that need to be light for better ergonomics. [4, 5]

An additional interesting sector for the application of magnesium parts is the medical sector where magnesium can be used as biodegradable material for implants that dissolve after their temporary function such as the fixation of a bone or suture is fulfilled. Magnesium can be advantageous in this sector due to the fact that magnesium is an essential element in the human body and the non-toxic degradation products might directly be used for e.g. bone remodelling [4, p. 672].

To combine the benefits of the production technique MIM with the benefits of the metal magnesium the development of the magnesium MIM process was investigated [6, 7]. Once the most critical part, the sintering, was proven feasible using Mg-Ca alloys [8] the first parts could be produced. These first trials were performed using a binder system typically used for MIM of titanium. However, it turned out that the binder system used for MIM of titanium has a strong sintering inhibiting effect [9, 10]. Subsequent experiments showed that this could be traced back to the used polyolefin backbone polymer. It was found that the polyethylene (PE) based polymer (polyethylene-vinyl acetate (PE-EVA)) has a strong negative effect while polypropylene (PP) based ones do not show this effect [10, 11]. This result was surprising due to the comparable molecular structure and chemical composition of the two polyolefins. As yet. a sound explanation for this strong difference in sintering results using these two types of backbone polymers has not been found.

The overall aim of the development of the magnesium MIM processing is the commercial application of the process. To achieve this goal several challenges need to be overcome.

After the successful proof of the sinterabilty of magnesium and magnesium alloys the aim of this work is to face the problem that occurs in combination with the backbone polymer and the necessary thermal removal thereof. The main function of the backbone polymer is to ensure the shape stability between the shaping process and the sintering process. As mentioned above the thermal removal of the backbone polymer without negative effects on the subsequent sintering process was unexpectedly found to be completely opposite with PP and PE based polymers. Finding a fundamental explanation for this unexpected phenomenon is the main focus of this work. Based on this understanding of the interactions of the magnesium powder with the backbone polymer during thermal debinding will help to design a suitable binder system and also to optimise the processing conditions during MIM processing of magnesium. However, the thermal removal of the backbone polymer can be performed without negatively effecting the sintering results of magnesium is not the only issue to overcome. Other aspects such as the miscibility with other binder components and the resulting rheological behaviour also need to be suitable especially for the shaping process also need to be taken into account. The outcome of the work should therefore not only be to understand the mechanisms during thermal debinding but also to find a suitable binder system for MIM of magnesium. Based on this knowledge and improvements together with the already existing knowledge in this field a commercial application of magnesium MIM processing should be feasible.

Previous developments of MIM of magnesium have been mainly performed using Mg-0.9Ca alloy. Mg-Ca alloys have the benefit that calcium increases the sintering activity of magnesium [8] and that it is also a non-toxic essential element in the human body making Mg-Ca alloys attractive for biomedical applications [12]. Therefore, also in this work most experiments are performed using Mg-0.9Ca. However, pure magnesium, AZ91 as well as Mg-Gd are used for certain experiments. Titanium is used as reference material in certain experiments as it is also an oxygen sensitive and rather reactive material already established in MIM processing.

A polymer screening is performed to determine the influence of different polyolefins on the sintering behaviour of magnesium. The influence of carbon on the sintering is investigated using different approaches such as pure carbon additions as well as determination of carbon residuals after treatment with different polymers and hydrocarbon gases using different measurement techniques. Thermal treatment under hydrogen is performed to investigate the possibility of carbon removal by hydrogenation and the influence on the sintering results.

Different measurement equipment and procedures are used for analysing samples and gathering experimental data such as dimensional and weight changes, mechanical testing, light and electron microscopy and thermo-gravimetric analysis also coupled with infrared spectroscopy for analysis of thermal decomposition products. X-Ray diffraction and

X-Ray photoelectron spectroscopy as well as Time-of-Flight Secondary Ion Mass Spectrometry and combustion analysis are used to determine composition of samples especially in respect to carbon residuals.

2 Literature Review

This chapter reviews the state of the art of sintering and MIM of magnesium. Material properties, compounds and reactions that are of interest for this work are presented. Furthermore, the thermal decomposition of PE and PP and measurements techniques that are of interest for this work such as evolved gas evolution measurements during thermal debinding of powder metallurgy (PM) compounds are explained as well.

2.1 Powder Metallurgy

Powder metallurgy comprises the production of metallic powders and the production of parts using these powders. The near-net shape PM processes have been used since the early 1900s to produce a wide range of parts. Starting from structural components over self-lubricating bearings (sinter compound materials) and cutting tools (high melting temperature hard metals and compounds) [13]. PM are mostly near net shape or net shape processing technologies involving a high material yield from the primary shaping to the ready part (in aeronautics called “buy to fly ratio”). Depending on the material PM can bring several advantages.

- High temperature materials are typically processed by PM due to their high melting points. They can be sintered at temperatures considerably below the melting point. This can save energy and equipment costs. Tungsten and Molybdenum were first processed by PM because suitable melting furnaces did not exist at the turn of the 20th century [14].
- Material combinations which are difficult or impossible to produce by conventional techniques due to high differences in melting point, have limited mutual solubility in the liquid state, have very different densities or a refractory constituent in solid form is attacked by the liquid metal can be produced and processed. E.g. WC, WC-TiC or WC-TiC-TaC can be used for wear resistant tools when combined with Co as binding agent [14].
- Materials with tailored microstructures and porosities can be produced. Porosity can be used e.g. for implementing a lubricant for self-lubrication bearings in technical applications, for filter applications or for bone ingrowth and drug delivery in medical applications [14, 15, 16].
- Parts in large quantities with net-shape or near net-shape geometries can be produced at low costs compared to conventional production techniques [1, 14].
- Powder based additive manufacturing (3D-Printing) is an intensively growing field in the PM sector. Selective laser melting (SLM) and electron beam melting (EBM) locally melt a powder which is spread layer by layer over the building platform [17]. Fused filament fabrication (FFF), feedstock extrusion and binder

jetting are using a binding agent or binder system to hold the powders in place before sintering [18, 19, 20]. The printing is followed by conventional debinding and sintering. Therefore, these techniques can be classified as related to MIM in the aspect of shaping, debinding and sintering (SDS).

PM of reactive materials such as titanium and aluminium is relatively recent technique and still only applied in niche applications [13]. MIM of titanium has been of great interest in the past years [2]. Sintering based PM of magnesium is only reported by a few research groups and not established yet [8, 21, 22, 23, 24].

2.2 Magnesium

Magnesium is a silver-white metal. In presence of air magnesium is covered with a thin oxide layer. In contact with oxygen it reacts to form magnesium oxide. The density of pure magnesium is 1.74 g/cm³ (for comparison steel 7.2 g/cm³) [25, p. 3]. This makes magnesium a promising material where light weight is of great interest. The crystal structure of magnesium is hexagonal close-packed (HCP). The melting and boiling point of magnesium are at 650 °C and 1107 °C (under air exclusion), respectively [26].

An important factor needs to be considered when taking magnesium in account as material for certain applications, magnesium has a low corrosion resistance. Protective layers, alloying elements and construction guidelines can reduce the risks of unwanted corrosion. This property can be an advantage when magnesium is used as sacrificial anode to protect other materials [4].

Another possible application for magnesium and its alloys, where the low corrosion resistance is beneficial, is the biomedical sector where magnesium can be used as a degradable implant material. A degradable implant can reduce the costs and risks of a second surgery for removal of the implant after the temporary function of the implant is fulfilled [27].

Magnesium is known to form metastable carbides at evolved temperatures when in contact with hydrocarbons (more detailed in section 2.3).

2.2.1 Magnesium in Technical Applications

Pure magnesium is rarely used in technical applications because of its mechanical and chemical properties such as low yield strength, low ductility, its tendency to creep and the low corrosion resistance [4, p. 77 ff.].

Generally, magnesium is used in alloy form. Pure magnesium is used as a reductive in the production of other metals e.g. uranium, zirconium, copper, nickel, chromate, or titanium or in pyrotechnics because of its bright light when being burned [4, p. 77]. The

largest consumer of magnesium is aluminium production where magnesium is used as an alloying element [4, p. 651].

Its specific strength is considerably higher compared to aluminium and iron. This makes magnesium a promising material where light weight is of great interest in sectors such as aerospace, automotive, tools, electronics, "wearables" and sports. Aluminium, zinc, manganese, silicon, rare earth elements, lithium, calcium and silver are mainly used as alloying elements to improve mechanical properties, processability and corrosion resistance [4, 5, 25].

Alloying elements such as aluminium and zinc improve the strength, ductility and the notch sensitivity due to curing. Manganese and calcium in moderate amounts improve the corrosion properties [28].

Magnesium alloys are used in different technical applications e.g. automotive (engine and gear box housings e.g. Porsche G1 Panamera and E2 Cayenne [29]), aviation and electric industry. Mostly casting or die casting production methods are used. Those alloys contain up to 15 m.% alloying elements. [4, p. 662 ff.].

2.2.2 Magnesium in Biomedical Applications

The success of an implant depends on its biological and mechanical properties. Mechanical incompatibilities result from geometrical and material characteristic mismatches. Differences in the Young's modulus of the implant and the bone can cause an effect called stress-shielding[1]. Due to the mechanical properties of titanium are closer to those of cortical bone than of other considered materials (e.g. chrome-nickel steels) and because of its inert behaviour in the human body, titanium is well established for long term implants [4, pp. 670-675].

To avoid a second surgery to remove the implant and uncomfortable influences caused by a permanent implant such as physical irritation or chronic inflammatory discomfort, absorbable implants have been developed. Current biodegradable implants are made of polymers (e.g. poly-L-Lactic acid). These polymers suffer from unsatisfactory mechanical strength. Furthermore, these biodegradable polymers are prone to water absorption and swelling, which leads to a supplemental reduction of strength and Young's modulus [27].
These disadvantages of the conventional degradable implant materials lead to the development of new biodegradable materials. These materials should have better bone matching material properties compared to the currently used materials. These new materials

[1] Stress-shielding: Implant loosening due to unphysiologically force transmission in in combination with the loss of bearing bone structure [164].

should mainly contain elements which are uncritical related to the biocompatibility [4, p. 671].

In the search of eligible materials for biodegradable implants magnesium alloys seem to be a promising approach according to the essential need of magnesium in the human body. Toxic reactions, caused by too much magnesium, are unknown [27]. Compared to other implant materials, magnesium has the most closely related Young's modulus to cortical bone [4, p. 672]. Moreover, magnesium is osteoinductive[2] and promotes bone remodelling [30].

Magnesium is an essential element in the human body, to meet the demand the body needs approximately 4.5 mg of magnesium per kg of bodyweight per day. Magnesium is involved in many enzyme reactions, bone formation and it takes part, together with calcium, in the signal transmission of the neurones [26].

The idea to use magnesium as a biodegradable medical material is not new. In 1878, for example, a magnesium wire was used as a degradable thread for ligation of vasculature [31]. However, magnesium as a biodegradable material is not well established yet. This is due to the fact that the degradation speed as well as the mechanical properties of the alloys need to be well adjusted and problems such as hydrogen evolution need to be controlled to meet the demands of the desired implant applications. Nonetheless, first implants were successfully introduced into the market and passed the necessary clinical trials [32].

2.2.3 Processing of Magnesium

Magnesium and most of its alloys possess good castability and are easy to machine [4, p. 345].
Besides casting, die casting techniques, hot forging and extrusion are most commonly used to produce magnesium parts. [4, 5] However, magnesium shows poor formability at room temperature because of its HCP crystal structure. Above 225 °C additional gliding planes are activated resulting in better formability [4, p. 199]. The high reactivity of magnesium at high temperatures requires the use of protective atmospheres such as argon and the extremely potent greenhouse gas SF_6 during processing of magnesium [4, 5].

Powder based techniques such as powder forging and powder extrusion are becoming more and more established. Powder metallurgy is typically a technique for mass production [4, p. 410]. For instance, the first magnesium-based implant screw is produced by

[2] From [165]: "Osteoinduction is the process by which osteogenesis is induced. It is a phenomenon regularly seen in any type of bone healing process. Osteoinduction implies the recruitment of immature cells and the stimulation of these cells to develop into preosteoblasts. In a bone healing situation such as a fracture, the majority of bone healing is dependent on osteoinduction. Osteoconduction means that bone grows on a surface."

powder extrusion and subsequent machining [33], because extruded powder yields in high mechanical properties and homogeneous microstructure.

Conventional press and sintering and especially MIM are not yet established for magnesium part production, but interest and successes in this field are growing [7, 6, 34] (see also section 2.4.3). These techniques have the advantage of net shape or near net shape production to reduce the costs of subsequent machining.

2.2.4 Calcium as an Alloying Element in Magnesium

A common notation for magnesium alloys is given by the ASTM[3] specification B275-05 [35]. In this specification calcium is designated by an X followed by the content in wt.% rounded to the nearest integer. The alloy examined in this work would be designated as X1. This notification is improper according to the calcium content. Due to this, a notification according to the nomenclature of titanium alloys such as in [36] is used. The examined Mg-Ca alloy with 0.9wt.% calcium is named Mg-0.9Ca.

Calcium is an essential element in the human body, its salts are used to stabilize the bones and teeth and it is involved in many enzyme reactions and it takes part, together with magnesium, in the signal transmission of the neurones [37].

In You *et al.* [28] it is shown that the addition of calcium in amounts from 0.5 to 3 wt.% leads to an increasing corrosion resistance and a decrease of the oxide layer thickness compared to pure magnesium above 480 °C. Calcium also decreases the corrosion rate of magnesium [4, p. 290]. Calcium has a major influence on the sintering behaviour of magnesium as explained in section 2.4.3.

In Kammer [4, p. 158] a short overview about the advantages and disadvantages of calcium addition to magnesium is given as the follows:

Advantages:

- causes grain refinement
- increases the creep resistance
- can cause an increased tendency to sticking
- slows down the magnesium burn-off

Disadvantages:

- increased hot crack sensitivity
- aggravation of the corrosion resistance

[3] ASTM: American Society for Testing and Materials

Calcium-Magnesium Phase Diagram

Figure 2-1 shows the calculated phase diagram of magnesium and calcium. Figure 2-2 shows the area of this diagram where the maximum solubility of calcium in magnesium is apparent. The phase diagram shows a double eutectic behaviour. The maximum solubility of calcium in magnesium according to this calculation is 0.7 wt.% (0.43 at.%). This is in confirmed by Aljarrah and Medraj [38]. On the other hand, magnesium is not soluble in calcium. Magnesium has an HCP crystal structure and calcium an FCC crystal structure. The intermetallic phase Mg_2Ca divides the phase diagram at approximately 45 wt.%. Two eutectics can be found, one on the magnesium rich and also one on the calcium rich side of the diagram. The magnesium rich eutectic is at 16.33 wt.% and 516.5 °C and the calcium rich eutectic is at 80.36 wt.% and 446.3 °C. For this work, only the magnesium rich side is of importance. The heterogeneous two-phase crystal mixture α-Mg and Mg_2Ca dominate this area.

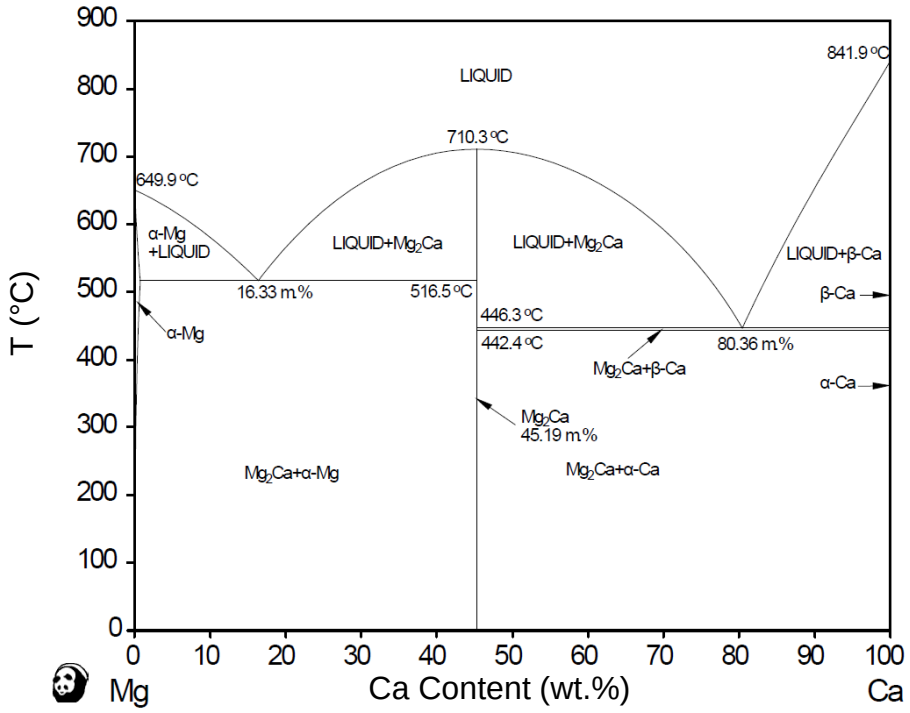

Figure 2-1 Calculated Phase diagram Mg-Ca using Pandat 8.1 with PanMagnesium 8 database [39, 40].

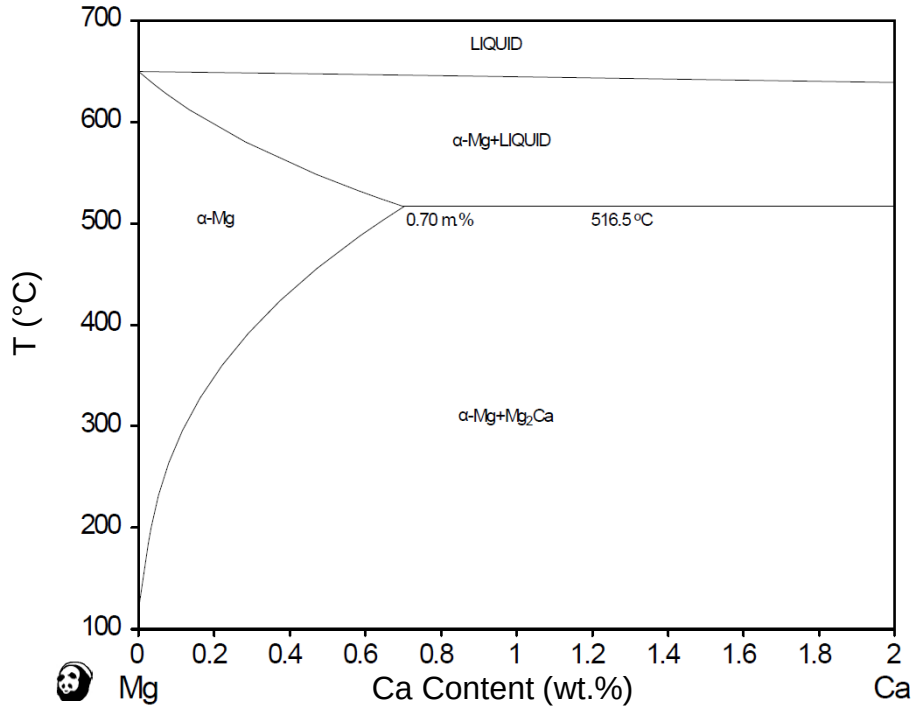

Figure 2-2 Calculated maximum solubility using Pandat 8.1 with PanMagnesium 8 database [39, 40].

2.2.5 AZ and Mg-Gd Alloys

Magnesium alloys containing aluminium and zinc (AZ alloys) are by far the most used magnesium alloys. AZ81 and AZ91 are typical cast and high pressure die casting. The mechanical strength of those alloys is high and can be modified by heat treatments. The ultimate tensile strength and yield strength very from 160-240 and 90-150 MPa, respectively and the elongation at fracture from 2% - 8% depending on the processing technique and subsequent heat treatment. The AZ alloys can be used at temperatures up to 110 °C. Typical applications are automotive, computer, phone and sports parts and cases (wearables), parts for chain saws and other tools and many more [4].

Magnesium rare earth especially Mg-Gd alloys are niche alloys that are used for special applications. Mg-Gd alloys are a suitable candidate for biomedical implant applications due to their non-toxicity, low degradation speed and comparably high strength. For Mg-2Gd, Mg-5Gd and Mg-10Gd extruded material yield strength ranging from 80 MPa to 220 MPa is reported depending on the grain size which can be controlled by the extrusion parameters [41].

2.3 Magnesium Carbon Phases and Compounds

The main element in polymeric binders is carbon. Therefore, it is quite likely that reactions between magnesium and carbon play an important role in the sintering inhibiting effect. Thus, in this chapter state-of-the-art knowledge about magnesium-carbon interactions are discussed in detail.

2.3.1 The Magnesium-Carbon Phase Diagram

From Chen and Schmid-Fetzer [42] critically reviewed older works on the Mg-C phase diagram and based on new measurements by Chen *et al* [43] a new phase diagram is calculated and discussed. In older works by Nayeb-Hashemi and Clark [44] and Hu *et al.* [45], the authors stated that magnesium carbides are present in the Mg-C phase diagram. According to Chen and Schmid-Fetzer this is based on misinterpretation of data leading to wrong calculations of the resulting phase diagram.

In their work Chen *et al* [43]. measured the solubility of carbon in liquid magnesium in a temperature range between 800 and 900 °C. They found that the solubility of carbon in liquid magnesium is in the range on tens of ppm decreasing with temperature.

Based on the coherent discussion and data measured with new methods GD-OES[4] verified by combustion analyses the calculated phase diagram of Chen and Schmid-Fetzer is used in this work.

Figure 2-3 shows the Mg-rich side of the phase diagram. It can be seen that below the solidus line at 650 °C magnesium has no solubility for carbon and that no secondary phases (carbides) are stable at these conditions. Above the solidus line, liquid magnesium and solid graphite are apparent while below the solidus line Mg + Graphite are apparent.

According to Chen and Schmid-Fetzer [42] and Chen *at al.* [43] carbon is not soluble in magnesium or able to form stable phases below the solidus line and therefore in the temperature range used in the MIM process of magnesium.

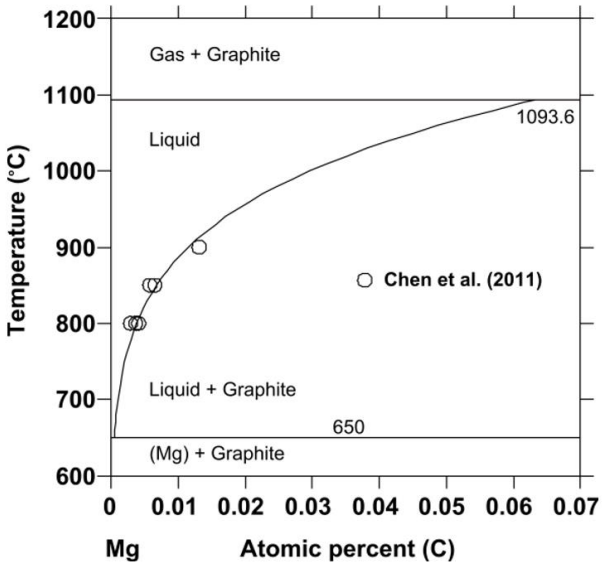

Figure 2-3 Mg rich side of the Mg-C Phase diagram at 1 bar pressure taken from [42] with experimental data points from [43]. With permission to reprint from Carl Hanser Verlag GmbH & Co. KG

[4] glow discharge optical emission spectrometry

2.3.2 Magnesium Carbides

Two kinds of magnesium carbides are reported in the literature. The magnesium acetylide (dicarbide) (MgC_2) and the magnesium allylenide (sesquicarbide) (Mg_2C_3) which is the only known alkaline-earth metal allylenide [46]. MgC_2 has a tetragonal crystal structure [47] and Mg_2C_3 an orthorhombic one [48].

Both magnesium carbides are thermally unstable and highly reactive and therefore it is impossible to form them from pure metal and carbon at low pressures [47, 48, 49, p. 920, 50]. This fits to the fact that in the Mg-C phase diagram (see 2.3.1) no carbides are present.

Most of the published works refer to the production of the magnesium carbides by passing hydrocarbons over heated magnesium [46-56]. In Schneider and Cordes [53] the synthesis from $MgCl_2$ and CaC_2 is investigated, in Reuggeberg [47] magnesium diethyl and acetylene and are investigated as starting materials. In Hick *et al.* [57] a mechanochemical route is tested and the authors report the first production of Mg_2C_3 out of the elements by high-energy ball milling. They assume that this is possible due to the locally high heat and pressure of the ball milling technique. The only relevant technique for this work is the passing of hydrocarbons over magnesium; therefore, the other techniques are not further pursued.

Novák [52, 56] was the first to investigate the formation and properties of the magnesium carbides systematically. In 1910, he already stated the composition of the two carbides to be MgC_2 and Mg_2C_3 due to the formation of acetylene and allylene under the contact of the carbides with water [56]. In this work, he used an acetylene gas flow over hot magnesium powder to produce the magnesium carbides for his investigations. With acetylene, Novák found out that the formation of MgC_2 begins at 400 °C reaching a maximum at 490 °C with higher temperatures the amount of MgC_2 decreases rapidly, above 600 °C reaction temperature only traces of MgC_2 could be found [50, 56]. The formation reaction of Mg_2C_3 starts at 460 °C and has its maximum reaction rate at 650-700 °C with higher temperature the amount decreases again rapidly and above 800 °C, no carbides are detectable [56].
Simultaneously with the formation of the carbides their decomposition takes place either according to equation (1) or directly into the elements [50].

$$2MgC_2 \rightarrow Mg_2C_3 + C \qquad \text{eq. (1)}$$

The decomposition according to equation (1) starts at 500 °C with simultaneous decomposition into the elements, above 600 °C only traces of MgC_2 are left. Under vacuum conditions the decomposition of MgC_2 into the elements happens already at 450 °C without the formation of Mg_2C_3 [50].

In his second work [56], Novák investigated the reaction of different hydrocarbons with magnesium. He determined the reaction products of the different hydrocarbons at different reaction temperatures. Besides acetylene, he investigated methane, pentane, octane, benzene, toluene and different isomers of xylene. For the alkanes he found out that the reaction starts at lower temperatures for molecules with a higher molecular weight. When comparing benzene and toluene, which has an additional methyl group, the amount of Mg_2C_3 decreases from 57% to 2%. Another additional methyl group leads to a slight increase around 7% to 11% depending on the position of the methyl groups [56].

Novak [56] as well as Irmann [50, 54] and Perret and Rietmann [58] presumed that the formation of the carbides occurs due to the reaction of the magnesium with fragments of the thermal decomposition of the hydrocarbons being radicals of the hydrocarbons.

The formation of the carbides happens typically on the surface of the magnesium, while the bulk material stays unchanged [47]. It is suggested that approximately 50 atomic layers of magnesium are involved in the carbide formation [55].

2.3.3 Further Relevant Magnesium Compounds and Reactions

Magnesium and Carbon Dioxide

Burning magnesium is known to react with carbon dioxide with the formation of magnesium oxide and carbon according to equation (2) [26]. At low temperatures carbon dioxide is adsorbed on the surface of magnesium due to chemisorption forming a carbonate and due to physisorption leading to the agglomeration of carbon dioxide on the magnesium surface [59].

$$2Mg + CO_2 \rightarrow 2MgO + C \qquad \text{eq. (2)}$$

Magnesium Oxide and Carbon / Carbon Monoxide

The formation of magnesium from magnesium oxide according to equation (3) is known as a carbothermic reaction. This reaction can take place at temperatures above 1350 °C and pressures below 100 Pa. Below 1100 °C the reverse reaction is favoured [60].

$$MgO(s) + C(s) \leftrightarrow Mg(g) + CO(g) \qquad \text{eq. (3)}$$

Magnesium Carbonate

Magnesium carbonate ($MgCO_3$) is an inorganic compound. Magnesium carbonate is a white and virtually insoluble compound in water. It decomposes at a temperature above 350 °C into magnesium oxide and carbon dioxide [61, 62].

Magnesium Stearate

Magnesium stearate ($(H_{35}C_{17}\text{-}CO\text{-}O)_2Mg$) is the magnesium salt of the stearic acid. Its melting point is approximately 140 °C [63].

During MIM, it can form on the surface of the magnesium powder due to the reaction of magnesium or the oxide layer with stearic acid, which is a typical ingredient of binders used for MIM [64, 65].
The range of its thermal decomposition goes up to 480 °C with a residual of 13% being magnesium oxide [66].

2.4 Metal Injection Moulding (MIM)

MIM combines the key benefits of plastic injection moulding with the properties of metals. These benefits are, for example, complex geometries, large quantities, short cycle times and near net shape components which results in no or minimal reworking and low costs [3, 67]. The most important property of the metals is their strength but depending on the use of the parts other properties, such as ductility, corrosion resistance, bio-compatibility [68], degradability [27], wear resistance and hardness [13] are required as well.

The term Metal Injection Moulding includes the whole process chain not only the injection moulding. According to DIN 8580 [69] it is classified as a primary shaping process. In this process the production is performed out of the shapeless state.

In the process of MIM a metal part is produced out of a powder while the shape is given by injection moulding and the metal consolidation is done by sintering [3, 13, p. 141]. Figure 2-4 shows the process chain schematically.

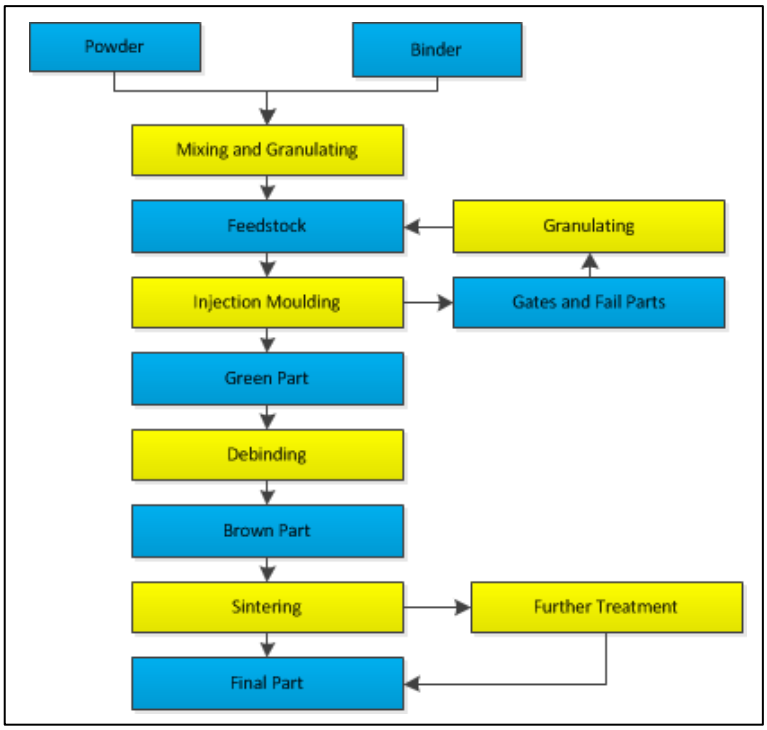

Figure 2-4 MIM processing route according to [3].

In the first step, the metal powder (base metal and alloys or pre-alloyed powder) and the binder are mixed under heat supply until a homogenous compound is reached, the so-called feedstock [3, p. 197 ff.].

The feedstock is then cooled down and granulated [3, p. 213 ff.]. This granulate can now be used in a commercial plastic injection moulding machine (with or without special adaptations in tooling) [3, p. 247 ff.]. The rheological behaviour of the feedstock needed for injection moulding is controlled by the injection temperature, binder components [3, p. 104], the size and shape of the powder particles [3, p. 61] and the powder loading in the feedstock [3, p. 128]. After injection moulding the parts are called green parts. The green part typically already consists the geometrical features of the final part with scale factors depending on the shrinkage caused by the following process steps.

The next step is the debinding where the components of the binder are removed. The debinding can be performed in one step thermally or in two steps chemically or by solvents followed by thermal debinding. The binder has to keep the powder particles together until the first sintering begins to assure the shape of the part [3, p. 281 ff.]. A debound part is called a brown part.

After the debinding step the actual sintering process takes place, in which the powder particles bond together based on diffusion mechanisms due to heat treatment, which is usually performed below the melting point of the metal (exceptions are liquid phase sintering processes). After sintering the result is a volume shrunk part with a certain rest porosity. Past sintering the parts are often completely finished otherwise further steps such as assembly, densification, heat treatment or finishing can follow [3, p. 425].

In the case of MIM of magnesium the heat treatment steps thermal debinding of the backbone polymer and the sintering are the most critical ones. Therefore, the following subchapters are mainly focussing on these process steps.

2.4.1 Thermal Debinding

Debinding is performed to remove the binder before sintering. While debinding failures can cause compact cracking and deformation due to gravity, thermal gradients or internal vapour pockets [3, p. 281].
Mostly, debinding is performed in several small steps to achieve an extraction process of the binder that is as short as possible in time and leads to no failures of the part or contamination of the powder. The binder is extracted from the pores of the compact as a liquid or vapour [3, p. 281].
To prevent deformation all debindig methods use a final thermal evaporation step prior to sintering [3, p. 322]. A common debinding process in combination with a wax and polymer based binder is to extract the waxes by solvent debinding while the polymers ensure the shape of the part. The polymers are extracted by thermal debinding prior to sintering. The polymers are cracked in shorter molecule chains and evaporate through the porous compound, which is the result of the solvent debinding step [3, p. 281 ff]. This two step process combination of solvent and thermal debinding is also used for MIM of magnesium within this work.

2.4.2 Sintering

Sintering is the final process in MIM and is responsible for densification and property development of the compact. While heated to high temperatures, the particles of the powder bind together, thereby it is important that there is a solid phase which ensures the shape retention. Sintering occurs due to material transport mechanism with the ambition to eliminate the high surface energy associated with unsintered powder. The surface energy per unit volume depends on the inverse of the particle diameter, therefore smaller particles sinter faster [3, p. 349 ff.].

The sintering process basically consists of three stages which merge without a clear differentiation. The first stage is dominated by the neck formation. The neck size ratio and shrinkage are small. The grain size is smaller than the particle size and the pores are irregularly formed and interconnected.
In the intermediate stage the most shrinkage takes place so it is characterized by large densification. The density grows to 70-92% of the theoretical value. The pore structure gets smoother, changing to a cylindrical shape, while the pores are still interconnected. At the end of this stage pore isolation and grain growth can occur.

In the final stage the interconnected pores collapse into single spherical pores. This happens at approximately 8% porosity. The shrinkage slows down and grain growth can take place. Gas trapped in the pores can limit the amount of final densification [3, p. 352 ff.].

The permanent presence of a liquid phase during the isotherm stage of sintering is typical for persistent-liquid-phase sintering. A solid phase must remain to ensure the shape stability. Therefore, the sintering temperatures for liquid phase sintering are in a temperature range between the solid and liquid phase of the phase diagram (e.g. Liquid + Mg-hcp in Figure 2-2). Due to wetting of the solid phase, capillary forces occur that lead to a faster densification and elimination of pores. Particle rearrangement is assisted by the liquid between the particle surfaces. This process is shown schematically in Figure 2-5.

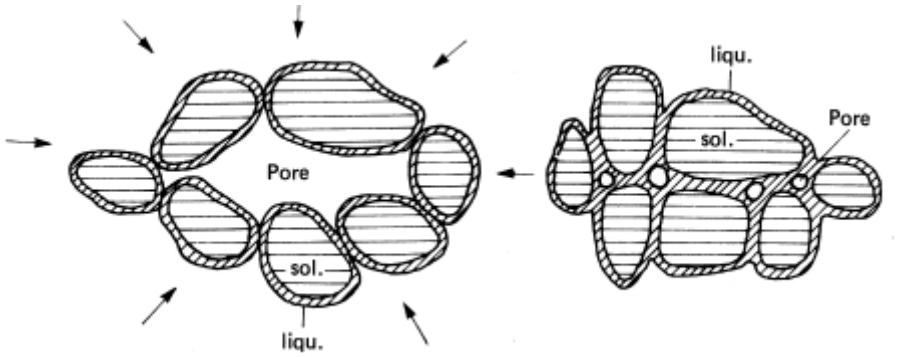

Figure 2-5 Densification due to presence of a liquid phase taken from [70, p. 187]. With permission to reprint from VDI Verlag GmbH.

When the solid phase is solvable in the liquid phase the liquid phase acts as a fast diffusion path due to dissolving and exsolution. These effects cause a much faster densification and lower rest porosity compared to solid phase sintering. [3, p. 376 ff., 70, p. 177 ff.].

Combinations of materials that have no solubility cannot be produced by melting metallurgy but by powder metallurgy. For an A-B-powder blend (A has a lower melting point) there are two possible composites: An A soaked B skeleton with connected B particles, or an A matrix with embedded B particles. For the second case, densification only occurs due to rearrangement of the A covered B particles [70, p. 178].

Within this work titanium and pure magnesium are sintered by solid stage sintering while the remaining magnesium alloys are sintered by permanent liquid phase sintering.

2.4.3 MIM of Magnesium

Sintering of Magnesium

Magnesium forms a stable oxide layer under the presence of oxygen. This oxide layer prevents the diffusion of magnesium as the diffusion rate is approximately 5.7×10^{11} times lower than in magnesium itself [71]. In some metals, e.g. titanium [72, p. 130] or iron [71, 73] the oxide layer dissolves in the metal at higher temperatures due to the changing solubility of oxygen in the solid metal or the oxide layer is removed by reducing reactions.

Hence, sintering of those metals is not inhibited by their surface oxide layer because it dissolves at sintering temperatures in a short time. This effect does not occur when heating magnesium to sintering temperatures [8, 71, 74]. Therefore, the oxide layer of the magnesium particles has to be as thin as possible or removed or reduced [74] so the sintering processes can take place.

Several experiments to reduce, remove or crack the surface layer have been undertaken by Wolff *et al.* [8, 12] and by Burke *et al.* [74, 21]. Both have investigated the sintering fundamentals of magnesium and proven the feasibility to sinter magnesium. Mechanical treatment and alloying additions were investigated Burke *et al.* [74, 21] and Wolff *et al.* [7, 75]. Mechanical treatment could not bring the desired effects but alloying with small amounts of calcium [7, 74] or lithium-hydrate [7] brings remarkable sintering results compared to pure magnesium. The addition of calcium with the master-alloy technique[5] turned out to be the most promising route with respect to the sintering results. The Ca-rich master alloy powder is added in certain amounts to pure magnesium powder to maintain the desired Mg-Ca alloy composition.

Another critical point to ensure sintering of magnesium is to protect the magnesium powder from further oxygen uptake, therefore all handling as well as the sintering process should take place under an inert gas atmosphere (e.g. argon) [7]. In Wolff *et al.* [8, 12] further investigations to protect the specimens from picking up remaining oxygen from the furnace atmosphere during sintering were made, by using magnesium getter material surrounding the crucible. It could be verified that fully surrounding the specimens by coarse magnesium powder getter material during sintering leads to improved sintering results. To protect the specimens from impurities in the atmosphere of the sintering furnace they are placed inside a labyrinth like crucible setup as shown in Figure 2-6. The magnesium getter material protects the specimens from impurities of the outer atmosphere because of its high surface area which contaminates have to pass before reaching the samples resulting in the fact that these impurities prone to react with the getter material before reaching the sintering samples. Furthermore, this protecting effect is increased by the sublimation of the magnesium getter material, caused by the high vapour pressure of magnesium (see Table 2-1), which leads to a magnesium rich atmosphere inside the crucible and the furnace [76].

[5] Master alloy technique: Addition of powders with high amount of alloying elements with pure metal powder or low alloyed powder in certain amounts resulting in the desired final alloy composition [13].

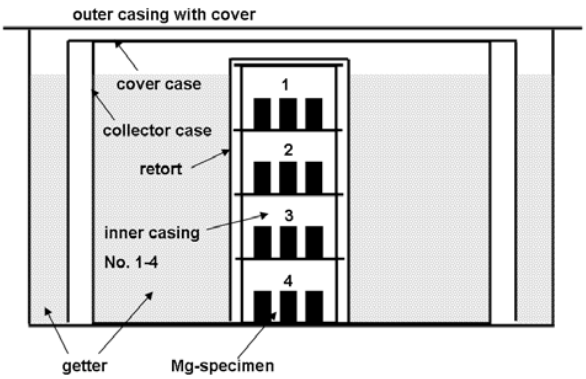

Figure 2-6 Specimen placement and sinter crucible configuration [76]. With permission to republish from Trans Tech Publications.

The vapour pressure of magnesium is so high, that it has to be considered during sintering. At the melting point of 650 °C the vapour pressure occurs at 372 Pa. This fact leads to the result that magnesium cannot be sintered for long durations under vacuum or low pressure because the magnesium would sublimate and condense on the cold parts of the furnace [4, p. 86].

Table 2-1 shows the vapour pressure of magnesium in the range of the sintering temperatures.

The intense sublimation and resublimation of magnesium material would result in loss of sample material as well as in problems of blocking of moving furnace parts (e.g. heat deflection shields during opening of the furnace after sintering).

Table 2-1 Vapour pressure of magnesium at different temperatures according to [4, p. 86].

Temperature (°C)	**Vapour pressure (Pa)**
427	0.9331
527	21.33
627	231.5
650 (solid)	372.0
650 (liquid)	358.2

It is assumed that the addition of calcium reduces the already existing oxide layer as well as protects the magnesium from additional oxygen uptake through its lower oxide formation enthalpy [8]. This also applies for the other possible contents of the surface layer that are mentioned by Burke in [74, p. 79]. The reaction equations (4) - (6) display the reactions with the magnesium compounds with calcium and their standard enthalpy of formation which are taken from the NIST Chemistry WebBook [77]. The positive resulting enthalpy means that the reactions are exothermic. This shows that calcium theoretically has the ability to reduce the magnesium surface layer.

$$MgO\left(-601\frac{\text{kJ}}{\text{mol}}\right)+Ca\left(0\frac{\text{kJ}}{\text{mol}}\right)\rightarrow Mg\left(0\frac{\text{kJ}}{\text{mol}}\right)+CaO\left(-635\frac{\text{kJ}}{\text{mol}}\right)+34\frac{\text{kJ}}{\text{mol}} \quad \text{eq. (4)}$$

$$Mg(OH)_2\left(-925\frac{\text{kJ}}{\text{mol}}\right)+Ca\left(0\frac{\text{kJ}}{\text{mol}}\right)\rightarrow Mg\left(0\frac{\text{kJ}}{\text{mol}}\right)+Ca(OH)_2\left(-986\frac{\text{kJ}}{\text{mol}}\right)+61\frac{\text{kJ}}{\text{mol}} \quad \text{eq. (5)}$$

$$MgCO_3\left(-1096\frac{\text{kJ}}{\text{mol}}\right)+Ca\left(0\frac{\text{kJ}}{\text{mol}}\right)\rightarrow Mg\left(0\frac{\text{kJ}}{\text{mol}}\right)+CaCO_3\left(-1207\frac{\text{kJ}}{\text{mol}}\right)+111\frac{\text{kJ}}{\text{mol}} \quad \text{eq. (6)}$$

The addition of different calcium amounts (0.2, 0.6 and 1 wt.%) due to master-alloyed Mg-7Ca powder were investigated by Wolff *et al.* [12]. Mg-7Ca turned out to be the best suitable master alloy concerning the sintering properties [78]. Depending on the final concentration of the alloy and the sintering temperatures either transient-liquid-phase sintering or persistent-liquid-phase sintering occurs [12, 76]. In Figure 2-2 it can be seen that the liquid phase occurs when the eutectic temperature (516 °C) is exceeded. The addition of calcium has positive effects on the sintering of magnesium. It can reduce magnesium surface oxides [79] and it assists the sintering processes due to the presence of a liquid phase [80, p. 1]. The isotherm sintering of Mg-Ca is performed under an inert argon atmosphere at a pressure of around 1000 mbar for 64 hours [8].

Numerous publications focus on the production of porous magnesium compounds by applying press and sinter techniques.

Wen *et al.* [24, 81] achieved an open porous structure with porosities ranging from 35% to 55% with a pore size varying between 70-400 µm using space holder techniques. Sintering parameters were reported to be 2 hours at 500 °C. Performing compression tests on sintered samples resulted in a peak compression strength of 17 MPa. Compression tests of unsintered samples were not reported. The results of Wolff *et al.* [8] and Schaper *et al.* [34] show that short sintering and this low temperature does not result in sufficient sintering of pure magnesium.
Čapek and Vojtěch [22, 82] also produced porous samples using space holder techniques. Sintering was performed under technical argon (purity 99.996%) as well as magnesium gettered atmosphere at 550 °C for 3, 6, 12 and 24 hours. Residual porosities were reported to be between 24% and 29%. They reported a maximum compressive strength to be 69 MPa for the samples sintered for 24 hours under gettered atmosphere. Green parts strength was reported to be 20 MPa. Comparing the results of Wen *et al.* [24, 81] and Čapek and Vojtěch [22, 82] is not possible due to the differences in compaction before sintering and different porosities and pore sizes.

MIM of Magnesium and Binder System Development for MIM of Magnesium

Due to the limited amount of peer reviewed published literature in the field of MIM of magnesium a number of references from bachelor and master theses are used within the literature review of this work.

After sintering of magnesium was proven feasible Wolff *et al.* [9] started to introduce magnesium into the MIM process. They started with a binder system designed for MIM of titanium. This binder system was a wax-based binder system with poly ethylene-vinyl acetate (PE-EVA) as the backbone polymer. Using this binder system led to bad sintering results. Using a crucible set up like that shown in Figure 2-7 with binder free and binder containing specimens they could identify the PE-EVA decomposition products as the cause for these bad sintering results as also the binder free reference sample showed bad sintering results. They assumed the oxygen of the polymer to influence the sintering performance of the magnesium but they also showed that an oxygen free polymer (polypropylene-co-1-butene (PPcoPB)) has an influence on the sintering of both binder free and binder containing specimen, respectively. However, the influence of that oxygen free polymer was considerably lower. They could also show that the usage of paraffin wax and stearic acid and their associated solvent removal in cyclohexane had no influence on the sintering results. Wolff *et al.* [10] reported the first samples successfully processed with the complete MIM process route using PPcoPB as backbone polymer in the binder system. However, problems during injection moulding still occurred.

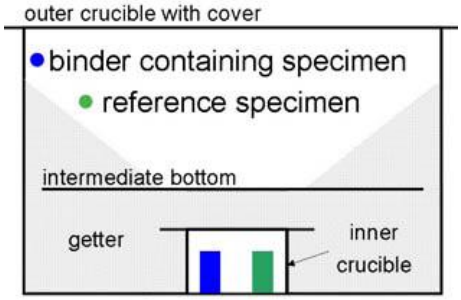

Figure 2-7 Specimen positioning for decomposition atmosphere influence [9]. With permission to republish from © European Powder Metallurgy Association (EPMA). First published in the Euro PM2011 Congress Proceedings

Wiese started his work [83] with a screening of suitable polymers by investigation of their thermal decomposition. Polyvinyl alcohols (PVA) and polyethylene glycols (PEG) were excluded because of their considerable decomposition residuals. The remaining PE-EVA, PE, PP, PPcoPB and poly-1-buten (PB) were tested on their influence on the sintering behaviour of Mg-1Ca powder. PE-EVA and PE showed a clear negative influence on the sintering, whereas PP, PPcoPB and PB showed a minor influence.

In the following work Deussing [84] investigated the influence of different polymer amounts of PP and PPcoPB on the sintering of Mg-0.9Ca. PPcoPB showed a decrease in the sintering results with increased polymer content while with PP only a minor effect of the polymer content was found. Investigations on the mouldability of PPcoPB and PP based feedstocks (feedstock with 36 vol.% binder containing 18 wt.% of polymer in the binder system) highlighted problems with the PPcoPB based feedstock causing demixing, blister formations, air entrapments, blocking of the barrel and sticking of the parts in the

mould. The PP based feedstock showed less problems, however all produced parts still showed injection moulding defects such as blisters.

Schaper followed up in [85] the work of Wiese [83] and Deussing [84]. Different Mg-0.9Ca feedstock systems based on PE-EVA, PP, PPcoPB as well as mixtures of those polymers were investigated concerning the processability and sintering results. Polymer contents of 5 wt.% and 15 wt.% were chosen for PP and PPcoPB and 5 wt.% and 35 wt.% for PE-EVA (36 vol.% binder). Two binder systems with 7.5 wt.% PP / 7.5 wt.% PPcoPB and 5 wt.% PP / 5 wt.% PPcoPB / 5 wt.% PE-EVA were evaluated. PE-EVA samples showed a strong influence of the polymer content on the sintering results. Samples with 35 wt.% PE-EVA resulted in strength of around 5 MPa after sintering where samples with only 5 wt.% PE-EVA showed strength of around 140 MPa. However, these samples could only be handled with absolute care in the brown state showing that this polymer amount is very low for production environment. The same can be concluded for the PP and PPcoPB samples with 5 wt.%. For PP and PPcoPB the influence of the polymer content was much lower as these samples showed only small differences in sintering results with increased polymer amount. However, these feedstocks showed problems during mixing and injection moulding due to the poor miscibility of the polymers with the paraffin waxes. The processability of the 5 wt.% PP / 5 wt.% PPcoPB / 5 wt.% PE-EVA feedstock was much better as PE-EVA seemed to improve the miscibility. However, the sintering results of this mixture was again lower due to the influence of the PE-EVA on the sintering of the Mg-0.9Ca.

Besides the influence of the polymer, the influence of stearic acid on the sintering was investigated. A treatment of the Mg-0.9Ca powder with stearic acid followed by removal in cyclohexane showed a positive influence of this treatment on the sintering behaviour of the powder.

Beside the work of the group of Wolff *et al.* [8-10, 75, 78, 86-88] only one other group working on the MIM processing of magnesium could be found in the literature. Harun *et al.* [89] investigated systematically the rheological behaviour of a ZK60 magnesium alloy powder (<45 µm spherical) with an LDPE and palm stearin-based binder system. They highlighted a powder loading of 64% with a binder composition of 60/40 palm stearin/LDPE as the most suitable for injection moulding. In their follow up work [90], they investigated the next step of the process route, the solvent debinding of the palm stearin leaving the LDPE and ZK60 powder for thermal debinding and sintering. No publications of thermal debinding or sintering results from this work group could be found in the literature. This together with the results of Wolff *et al.* [8- 10, 75, 78, 86-88] can lead to the conclusion that the thermal debinding of the used backbone LDPE would lead to unsatisfying sintering results.

The present work follows up on the work of Wiese [83], Deussing [84] and Schaper [85] as well as on the publications correlating to these works by Wolf *et al.* [9-11, 86-88]. The aim is to understand the principle mechanisms that cause the sintering inhibiting effects. Based on this knowledge it should be possible to find a binder system that combines good sintering results of the PP based polymers with the good injection moulding properties of binder systems that are composed with PE based polymers. The problems occurring during injection moulding and mixing of PP based binder systems are presumably caused due to insufficient miscibility of PP based polymers and the used waxes [85].

Published MIM Results Related to this Work

Within the frame of this present work which follows on the work of Schaper [85] a polypropylene-ethylene-copolymer (PPcoPE) could be identified as not being sintering inhibiting as well as being beneficial in the mixing and injection moulding step. A binder system developed within the frame of this work containing combinations of this backbone polymer, paraffin waxes and stearic acid is already used in several publications that are related to this work [34, 86-88, 91-93].

The binder system developed within this work was used to process several magnesium alloys by MIM. Table 2-2 gives an overview of the magnesium alloys that were processed with the binder system developed with correlation to this work and the mechanical properties that could be achieved.

Table 2-2 Mechanical properties of MIM processed Mg alloys related to this work.

Alloy	Yield Strength (MPa)	Ultimate Tensile Strength (MPa)	Elongation at Fracture (%)	Publication
Mg	25-40	28-80	1-5.5	[34], [91]
Mg-0.9Ca	60-68	135-142	7-8	[88], [34]
AZ81	115-120	215-255	5-7	[34], [92]
EZK400	123	164	3.4	[34], [86]
AZ91	90-105	117-140	1	[91]

2.5 Binder System Components

Polyethylene (PE)

PE belongs to the group of the polyolefins. Figure 2-8 shows the basic repeating unit of PE. The basic molecule chain of PE consists of a straight hydrocarbon chain. PE is separated in different classes depending on the crystallinity level which is linked to the amount of defects in the structure. Chains with fewer defects have a higher degree of crystallinity. The packing of crystalline regions is denser compared to non-crystalline regions resulting in higher density of PE with lower defects. Therefore, PE can be separated into different density classes with different amounts and types of defects [94, pp. 3-4].

High Density Polyethylene (HDPE) is chemically the most similar to ideal polyethylene. It contains a low amount of defects and branches leading to a high crystallinity. Typical

densities of HDPE are 0.94-0.97 g/cm³ [94, p. 2].

Low Density Polyethylene (LDPE) contains a higher amount of defects and branches which reduce the crystallinity leading to a lower density compared to HDPE. The branches are mainly ethyl and butyl groups as well as some long chain branches. Typical densities of LDPE range from 0.90-0.94 g/cm³ [94, p. 2].

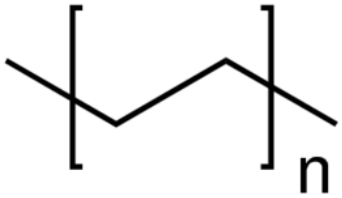

Figure 2-8 Repeating unit of PE [95]. Reproduced with permission from Merck KGaA, Darmstadt, Germany and/or its affiliates.

Polyethylene-Vinyl Acetate (PE-EVA)

Polyethylene-vinyl acetate is the most common copolymer of PE. Figure 2-9 gives the general repeating units of PE-EVA. Its general structure is comparable to the one of LDPE with additions of acetate groups. The acetate groups hinder the crystallization with increasing amount. The acetate groups interact between each other via dispersive forces forming clusters. Due to the polar groups PE-EVA has a higher chemical reactivity compared to LDPE and HDPE [94, p. 3]. PE-EVA is used as one of typical backbone polymers for MIM of titanium [9, 96].

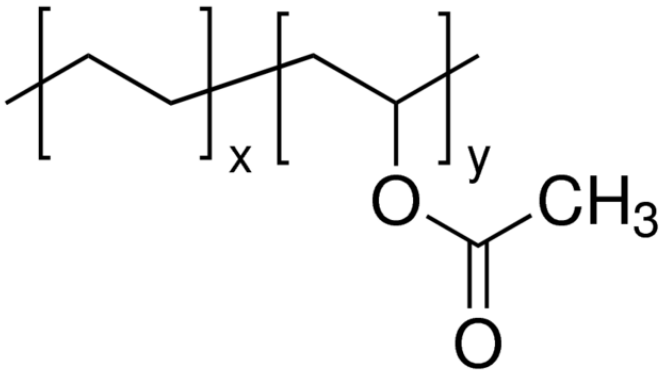

Figure 2-9 Repeating unit of PE-EVA [95]. Reproduced with permission from Merck KGaA, Darmstadt, Germany and/or its affiliates.

Polypropylene (PP)

PP belongs to the group of the polyolefins. The basic molecule chain is comparable to PE with an additional methyl group on every second carbon atom. PP can be separated into three major groups due to their differences in tacticity: isotactic, syndiotactic and atactic (amorphous). Figure 2-10 shows the repeating unit of PP. PP is produced by polymerisation of propene using Ziegler-Natta or metallocene catalysts. The typical melting point of PP is in the range of 160 °C (syndiotactic) to184 °C (isotactic). The adaption of the mole

mass can be achieved by adapting the hydrogen partial pressure during the polymerisation [97].

Beside the homopolymers which contain exclusively the repeating unit of Figure 2-10 copolymers contain additional repeating units. Depending on the distribution of these additional repeating units PP copolymers are separated into random and block copolymers. Figure 2-11 shows the structure of random and block copolymers. Random copolymers contain typically 1-7 wt.% ethylene with 75% single and 25% multiple insertions. Random copolymers have typically lower melting points compared to the homopolymers due to their lower crystallinity [98, pp. 19-21].

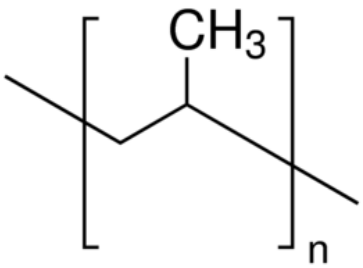

Figure 2-10 Repeating unit of PP [95]. Reproduced with permission from Merck KGaA, Darmstadt, Germany and/or its affiliates.

Repeating Units: A: Propylene B: Ethylene

Random Copolymer:

A-A-A-A-A-B-A-A-B-A-A-A-A-A-A-B-A-A-A-A-B-A-A-A-A-A

Block Copolymer:

A-A-B-B-A-A-A-A-B-B-B-A-A-A-A-A-A-A-B-B-B-B-B-B-A-A-A-A-A-A-A-A

Figure 2-11 Structure of random and block copolymers according to [98, p. 20].

Polyisobutylene (PIB)

Figure 2-12 displays the repeating unit of PIB. The basic molecule chain of PIB contains an additional methyl group when compared with PP. PIB can be separated into three product classes due to different molar weights. With molar weights of 300-3000 g/mol PIB is an oily liquid, from 50000-400000 g/mol viscous, sticky and from 1300000-4700000 g/mol elastic-rubber like bulks. PIB swells in ether, ester, oils and fats and are soluble in chlorinated hydrocarbons [99].

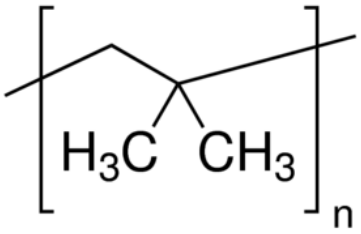

Figure 2-12 Repeating unit of polyisobutylene (PIB) [95]. Reproduced with permission from Merck KGaA, Darmstadt, Germany and/or its affiliates.

Paraffin Wax

Paraffin waxes are a mixture of saturated aliphatic hydrocarbons. The general molecular formula is C_nH_{2n+2} with a typical chain length of C_{22} - C_{40}. The melting point varies depending on the molecular weight. In the solid-state waxes are brittle while in the molten state they have a low viscosity. Paraffin waxes are soluble in several non-polar hydrocarbons e.g. hexane [100].

Stearic Acid

Stearic acid is a white solid powder with the chemical formula $C_{17}H_{35}CO_2H$. It is a saturated fatty acid. Its melting point is 69-71 °C, it is insoluble in water but soluble in e.g. lye, hot alcohol, chloroform, tetrachloromethane, non-polar hydrocarbons and carbon disulphide [101].

Stearic acid is widely used in powder injection moulding. Due to its polar end group and its long non-polar chain it acts as a surfactant improving the wettability of the powder by the binder enhancing the miscibility and the injection moulding. Moreover, it is reducing powder agglomerations and defects in the mixture of powder and polymeric components that are caused by bad adhesion between the powder and the binder [1, p. 83 ff.].

2.6 Thermal Decomposition of Polyolefins (PE and PP)

Thermal decomposition of PP occurs at slightly lower temperatures than PE. By Peterson *et al.* [102] it is shown that the thermal decomposition under nitrogen atmosphere begins at 250 °C and ends at 450 °C for PP and for PE it starts at 350 °C and ends at 490 °C, respectively. This can be explained by the differences in activation energy for the thermal decomposition of PE and PP [102]. Branching of the polymer chain influences the thermal stability. The highly branched PP is less stable than the straight chain PE [103]. PE as well as PP decomposes mainly through random chain scission, which starts at weak links of the polymer chain. For PE those weak links can be peroxides, carbonyls, chain branches, and unsaturated structures. For PP every carbon atom is a tertiary carbon atom and thus prone to attack [102, 103]. Beside the chain scission, PE begins to crosslink and branch between the polymer chains [103] this process does not occur during the decomposition of PP [102].

Random chain scission produces free radicals as shown in Figure 2-13 on the example of a straight alkane chain [103]. These free radicals tend to stabilise themselves by intramolecular hydrogen transfer (see Figure 2-13 (a)) or intermolecular hydrogen transfer (see Figure 2-13 (b)) followed by β-scission. Both, intra- and intermolecular hydrogen transfer form new radicals (propagation reaction) that can either attack other molecules or stabilise with other radicals (termination reaction) [103, 104]. Intramolecular hydrogen transfer leads to unsaturated hydrocarbons such as alkenes and intermolecular hydrogen transfer to saturated (alkanes) and unsaturated hydrocarbons [104].
In Maruta *et al.* [105], it is stated that the random chain scission of PE and PP occurs in the liquid phase leading to a decrease in molecular weight and that at the boundary between liquid and gas phase end chain scission leading to the volatile products of the thermal decomposition like shown in Figure 2-14. They could show that the pressure has a significant influence on the chain length of the decomposition products.

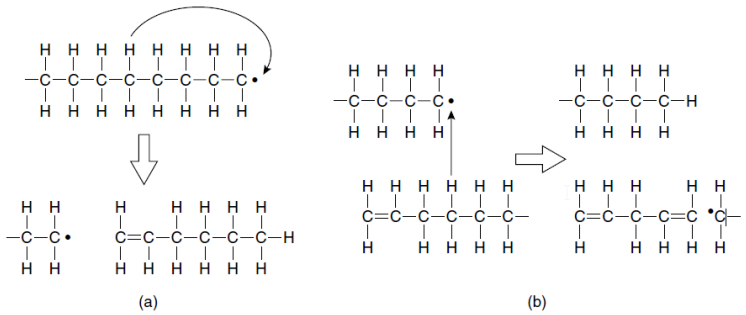

Figure 2-13 Extracted from [103] (a) intramolecular H transfer, (b) intermolecular H transfer. With permission to reprint from Springer Nature.

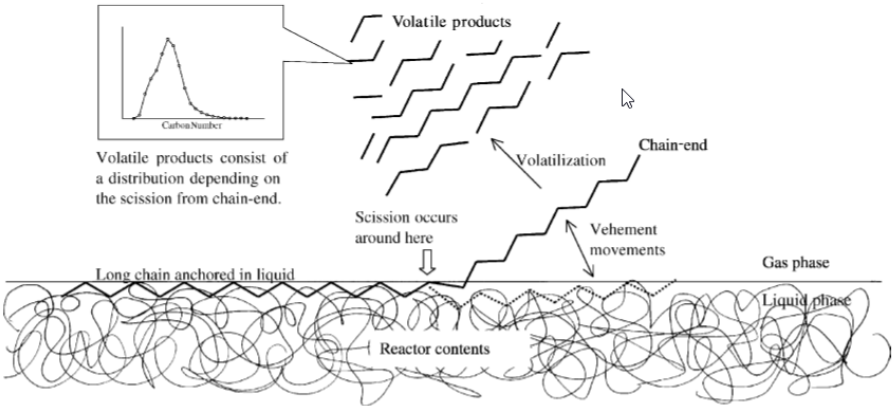

Figure 2-14 Volatile production at the gas-liquid interface extracted from [105]. With permission to reprint from Elsevier.

Depending on the detailed reaction sequences, the probability of certain reactions and the differences in the structure of PE and PP different thermal decomposition products are formed. PE mainly forms straight n-alkenes and n-alkanes and PP branched iso-alkanes and iso-alkenes [104, 106-108]. Referring to Soják *et al.* [106] the ratio in the thermal decomposition products for PE is: n-alkanes: 1-alkenes: (E)-2-alkenes: (Z)-2-alkenes: α,ω-alkadienes 1:1.2:0.07:0.05:0.08 (C_5-C_{23}) and for PP it is alkane: alkene: alkadiene

1:17:4 (C_9-C_{25}), respectively. Table 2-3 is an extract of the thermal decomposition products of PE and PP identified by Hájeková *et al.* [109]. This table highlights 2,4-dimethyl-1-heptene (structure see Figure 2-15) as the major thermal decomposition product of PP besides mainly other iso-alkenes. PE shows no outstanding thermal decomposition product but a broad distribution of 1-alkenes and n-alkanes. These results correlate with other publications about the thermal decomposition products of PE and PP [106, 110, 111, 112].

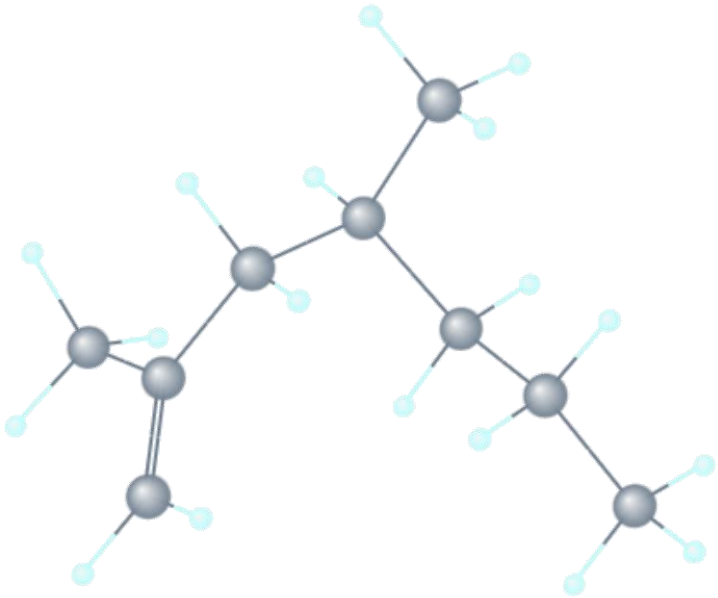

Figure 2-15 3-D-Structure of 2,4-Dimethyl-1-heptene [113]. With permission to print from NCBI.

Table 2-3 distribution of major products of PE and PP thermal decomposition extracted from [109].

Component	**LDPE (Yield/ wt.%)**	**PP (Yield/ wt.%)**
Ethane	1.3	0.9
Propane	2.2	0.5
Propene	2.1	6.1
Butane	1.9	tr.
Methylpropene	0.2	1.4
Pentane	0.9	3.6
1-Hexene, 2-Methyl-1-hexene	0.7	1.9
2,4-Dimethyl-1-heptene	-	19.0
1,3,5-Trimethylcyclohexane	-	1.2
1-Decene	1.2	0.5
Unidentified C_7—C_{10}	2.7	-
1-Undecene	1.4	-
Undecane	1.2	-
1-Dodecene	1.8	-
Dodecane	1.7	-
2,4,6-Trimethyl-1-nonene (isomers)	-	2.6
1-Tetradecene	2.6	-
Tetradecane	2.4	-
1-Pentadecene	2.5	-

Unidentified C_{11}—C_{15}	5.5	5.3
1-Hexadecene	2.2	-
Hexadecan	2.5	-
1-Heptadecene	1.7	-
Heptadecan	1.9	-
2,4,6,8,10-Pentamethyltri-1-decene (isomers)	-	2.1
1-Octadecene	1.0	-
C_{21}-Alkene	-	1.3
Unidentified C_{16}—C_{22}	1.3	5.4

2.7 Evolved Gas Analytics during Thermal Debinding of MIM and PM Compounds

Several works from the groups of Quadbeck *et al*. [114-118], Hartwig *et al*. [119] as well as of Mohsin *et al*. [120, 121] performed *in situ* evolved gas analytics mainly on copper, aluminium and steel PM and MIM components by mass spectroscopy (MS) as well as Fourier transformed infrared spectroscopy (FTIR). Those experiments aim on better understanding of the thermal debinding and sintering process to improve or to monitor the heat treatment processes.

In Quadbeck *et al.* [114] the atmosphere during thermal debinding of the production of metal hollow spheres using polystyrene (PS), polyvinyl alcohol (PVA) and tylose as organic compounds is investigated by IR absorption. The formation of CH_3OH, polymeric OH groups, CO_2, CO, alkenes, aromatic compounds, methane, water and aldehydes is qualitatively analysed under H_2 as well as Ar+5%H_2 atmospheres. The formation of CO in the used temperature range due to decarbonisation under hydrogen atmosphere as well as due to formation caused by the thermal debinding of the organic compound is investigated. Furthermore, the formation of methane due to decarbonisation of the used carbonyl iron material is discussed. It is stated that the data of this work correlates with the established mechanisms for degradation of PVA and PS. PVA decomposes into hydroxyl groups and aromatic compounds and PS degrades into styrene.

In Quadbeck *et al.* [115] the thermal debinding of ethylenbisstearamide (EBS) used in the PM processing of steel components is investigated by FTIR analysis in N_2-H_2 atmosphere. It was found that EBS in steel components decomposes mainly in CH-groups, CO, CO_2, H_2O and CH_4 with CH-groups being the dominant species. It was also found that the alloying elements can have an influence on the debinding temperature. At higher temperatures CO and H_2O have been detected correlating with oxidation reaction effects. Above 700 °C decarbonisation occurs due to methane formation. This methane formation is found to be influenced by the amount of carbon and the presence of chromium.

In Quadbeck *et al.* [116] besides the decomposition of PS and PVA as already mentioned in Quadbeck *et al.* [114] reactions of metal oxides with the used hydrogen atmosphere as

well as the decarbonisation due to reactions of carbon with the used hydrogen atmosphere and metal oxides is investigated to explain the presence of H_2O, CO, CO_2 and methane at higher temperatures.

In Quadbeck *et al.* [117] the authors show how the FTIR technique might be used to optimise or control the process parameters or to monitor the process for industrial production of PM components on the example of a continuous sintering belt furnace using aluminium components with EBS as organic pressing agent.

In Quadbeck *et al.* [118] the influence of delubrication additives on the thermal decomposition of the used lubricant for production of the FeCuC green compacts is investigated by FTIR analysis. The lubricant used in the presence of FeCuC decomposes under N_2-H_2 atmosphere with the major emission products being CO_2, CO, H_2O, NH_3, CH_4 and further CH groups. In addition, large quantities of aromatic and aliphatic compounds as well as anhydrites are identified. It is found that in the presence of the investigated delubrication additive, the formation of aromatic compounds is inhibited and around 220 °C an additive reduction step with the formation of H_2O and CO_2 is observed.

In Hartwig and Schroeder [119] mass spectrometry is used to investigate the atmosphere during thermal debinding and sintering of feedstocks consisting of a PE based binder system and two different carbonyl iron powders (non-reduced and reduced). Argon or hydrogen are used as atmospheres to investigate the influence of hydrogen on the evolving components. It is found that the reduced powder reacts intensively with the binder picking up carbon during thermal debinding which can be removed again when hydrogen is used as the atmosphere by the formation of methane. The non-reduced powder seems to be less reactive to the binder as well as to the hydrogen atmosphere. It is also found that the non-reduced powder also releases N containing compounds during the heat treatment. Furthermore, the oxide and hydroxide reduction reactions are investigated by the presence of H_2O and CO_2 in the atmosphere. The decomposition of the binder is monitored by the presence of an unknown hydrocarbon compound with the mass 27 (C_xH_y).

In Mohsin *et al.* [120] the authors investigate the thermal debinding atmosphere of MIM copper components processed with a binder containing of a mixture of PE and PP. They found that the thermal decomposition in 95%N_2+5%H_2 and Ar starts at 250 °C and ends depending on the heating rate around 450 °C. By applying FTIR and MS they found that the atmosphere during thermal debinding consists of hydrocarbons in the C1-C6 range with the majority being methane, ethylene, propylene, C4 and C5 components. Table 2-4 gives an overview of prominent IR band assignments that were observed by [120] for TGA-FTIR measurements on PE/PP mixtures in copper MIM parts. They stated that copper does not have any catalytic effect on the degradation of the polymers. Furthermore, they investigated the reduction of both copper oxides by the detection of water which is the reduction product under hydrogen containing atmospheres. In Mohsin *et al.* [121] the

same technique is used to investigate the thermal debinding of W-8%Ni-2%Cu. It is found that W has a catalytic effect on the thermal debinding of the binder used. The start of the thermal decomposition as well as the appearance of longer chain molecules in the gas phase are shifted to lower temperatures. However, the general degradation process and the degradation products do not seem to be changed by the presence of tungsten.

For magnesium no reports of evolved gas analytics during thermal debinding of PM or MIM parts could be found in the literature.

Table 2-4 Prominent IR band assignments taken from [120].

Wave Numbers	**Assignment**
888	CH_3 r, C-C s
973	CH_3 r + C-C s
997	CH_3 r
1163	C-C s +C-H w CH_3 r
1372-1381	CH_3 sb
1453-1465	CH_3 ab
1661	C=C s
2858-2972	CH_2/CH_3 as, CH/CH_2 CH_3 s
2340-2375	CO_2

ab = asymmetrical bending; as = asymmetrical stretching; r = rocking;
s = stretching; sb = symmetrical bending; w = wagging

2.8 Carbon Hydrogenation

The hydrogenation of carbon to methane equation (7) is an equilibrium reaction [122]. An equilibrium reaction is dependent on the quantity of reactants and products and the temperature and pressure [123]. In the case of equation (7) a hyperstoichiometric amount of hydrogen would shift the reaction further to the right leading to a decrease of carbon. If methane is removed from the system the amount of carbon can also be reduced.
An increase in pressure increases the yield of methane, an increase in temperature decreases the yield of methane especially at temperatures above 1000 K due to methane decomposition and formation of higher hydrocarbons like ethane and acetylene [124]. However, the yields of other hydrocarbons are by far lower compared to the methane [124, 125] and therefore not considered at this point.

$$C\ (s) + 2H_2(g) \rightleftharpoons CH_4(g) \qquad \text{eq. (7)}$$

Besides the above-mentioned influences on the equilibrium reaction the type and condition of the carbon has a great influence on the reaction kinetics [124, 126]. The reaction probability decreases with the increasing crystallinity due to the fact that carbon atoms on the edge of graphite layers are more reactive compared to atoms in the layer [126]. Therefore, amorphous carbon like active carbon, glassy carbon and pyrolytic carbon are more reactive compared to graphite [122, 124-127]. However, the source and type of the

carbon does not have an influence on the equilibrium but only on the reactivity [128]. It is assumed that hydrogen is chemisorbed on the active sites of the carbonaceous material forming a (CH_2) complex which can then react to either methane or back to hydrogen according to equation (8) [125, 126, 128, 129].

$$C + H_2 \rightleftharpoons (CH_2) + H_2 \rightleftharpoons CH_4 \qquad \text{eq. (8)}$$

In [130] it is reported that the carbon content of steel parts sintered under hydrogen is significantly lower compared to sintering under vacuum. The hydrogenation of carbon during the sintering of FeCuC components is reported by Quadbeck *et al.* [118] at approximately 600 °C.

3 Ambition of the Experiments

First of all, a polymer screening using different types of polyolefins is performed to investigate the influence of the different types of polymers on the sintering behaviour of magnesium. To investigate, if these differences are caused by differences in thermal decomposition behaviour, thermo-gravimetric measurements are performed using pure polymers as well as polymers in contact with magnesium powder under different conditions.

It is assumed that the observed sintering inhibiting effects are caused by carbon residuals, therefore different measurement setups are used to determine the influence of the used backbone polymer on the surface carbon content after thermal removal of the polymer.

To investigate the influence and potential reactions of the polyolefin thermal decomposition products with magnesium these decomposition products are analysed for pure polymers as well as in the presence of magnesium.

A literature review concerning the thermal decomposition products of PP and PE based polymers reveals that these differ by the basic molecular structure. To investigate if these basic differences can influence the sintering activity, magnesium samples are treated with assorted potential decomposition products. This is done to simulate the thermal debinding process.

Carbon and carbon compounds can be the potential residuals of the thermal decomposition of polyolefins. Therefore, the influence of pure carbon additions to pure magnesium and Mg-0.9Ca press and sinter samples and the resulting sintering activity is investigated. Also analyses of residual carbon content of samples of different experimental setups are performed.

Furthermore, sintering under hydrogen atmosphere is investigated as carbon residuals might be removed by carbon hydrogenation resulting in lower carbon contents and presumably in improved sintering activity. Using hydrogen as sintering atmosphere might result in hydride formation when alloying elements are used that prone to form hydrides. Mg-rare earth alloys are known to form hydrides [131]. To investigate the influence of hydrogen atmosphere on the sintering results of such alloys Mg-Gd is introduced in this step.

Magnesium-aluminium-zinc (AZ) alloys are widely used magnesium alloys in non-biomedical applications. Therefore, the influence of PE and PP based backbone polymers as well as the influence of hydrogen as sintering atmosphere are investigated using a commercially available AZ91 powder. This alloy was selected due to the commercial availability and the wide range of applications of the AZ alloys for magnesium parts. This makes AZ alloys attractive candidates for the production of magnesium parts using MIM techniques in the non-biomedical sector.

The differences in the sintering results of PE and PP based backbone polymers observed for MIM of magnesium might also occur when other reactive metals such as titanium are processed by MIM. Therefore, titanium is processed using PE and PP based backbone polymers and the mechanical properties as well as the residual carbon is measured. Titanium is also used as reference material in certain experimental setups to investigate if certain observations can be traced back to the presence of magnesium or in general to reactive metal powders.

4 Materials and Methods

In this chapter the materials used are listed and specified. Furthermore, the processes used for sample production as well as experimental setups are explained. Moreover, relevant measurement techniques and data evaluations are specified.

4.1 Materials

4.1.1 Powders

Table 4-1 gives an overview of the powder used for the experiments within this work.

Mg-0.9Ca was produced using the master alloy technique by mixing the pure magnesium powder and Mg-5Ca powder to achieve a calcium content of 0.9 wt.% in the resulting alloy.

Mg-5Gd was produced by mixing the pure magnesium powder and the Mg-10Gd powder to achieve a gadolinium content of 5 wt.% in the resulting alloy.

The specific surface area of the pure Mg powder used in this work is 1.6713 m²/g determined using BET methods according to ISO 9277 [132].

Table 4-1 Overview of powder used for the experiments within this work.

Powder	Composition	Particle Shape and Size	Manufacturer
Mg Grit (Getter)	Mg 98.5%	grit 0.06-0.3 mm	Merck, Germany
(pure) Mg	Mg 99.8%	spherical <45 µm	SFM SA, Switzerland
Mg-5Ca	5.3% Ca, Mg bal.	spherical <45 µm	casting: Helmholtz-Zentrum Geesthacht, Germany, atomisation: MSE Clausthal, Germany
AZ91	8.5% Al, 0.55% Zn, Mg bal.	spherical <45 µm	SFM SA, Switzerland
Mg-10Gd	9.14% Gd, Mg bal.	spherical <63 µm	casting: Helmholtz-Zentrum Geesthacht, Germany, atomisation: MSE Clausthal, Germany
Ti	99.5% Ti	spherical <45 µm	TLS, Germany
C	99.95% C	splinter 0.4-12 µm	Alfa Aesar, Germany

4.1.2 Binder Components

Table 4-2 gives an overview of the binder components used for the experiments conducted in this work.

Table 4-2 Binder components used in the frame of this work.

Component	Abbreviation	Manufacturer
Paraffin wax	PW	Merck, Germany
Stearic acid	SA	Merck, Germany
Polyethylene vinyl acetate	PE-EVA	LyondellBasell, Netherlands
Polyethylene (low density)	PE/PE-LD	LyondellBasell, Netherlands
Polyethylene (high density)	PE-HD*	LyondellBasell, Netherlands
Polypropylene (isotactic)	PP-isotak*	Sigma Aldrich, MS, USA
Polypropylene (amorphous)	PP-amorph*	Sigma Aldrich, MS, USA
Polyethylene-co-Octadiene	PPcoOc*	Borealis, Austria
Polypropylene ethylene copolymer (random)	PPcoPE (PPR7220)	Total, France
Polypropylene ethylene copolymer (random)	PPcoPE (PPR9220)*	Total, France
Polypropylene ethylene copolymer (random)	PPcoPE (QE50E)*	Ducor Petrochemicals, Netherlands
Polyisobutylene	PIB*	Sigma Aldrich, MS, USA

*only used in binder screening experiments

4.2 Sample Production

Powder Handling

All powders already had an oxide layer in the as received state from the powder production process. This passivation layer is produced on purpose due to safety reasons to prevent the powder from self-igniting. To prevent the powders used from further oxygen uptake and for safety reasons all powder handling was carried out under a protective argon atmosphere in a glove-box system (Unilab, MBraun, Germany) with oxygen levels maintained below 10 ppm and water levels below 1 ppm.

Powder Pressing

Binder free pressed samples were produced using uniaxial pressing with a pressure of 100-150 MPa (Enerpac RC55, USA). Dies with diameters of 8, 8.3 and 11 mm are used to produce cylinders. Unless otherwise stated, all samples were pressed under argon atmosphere.

4.2.1 MIM Processing

Feedstock Production

For feedstock production the magnesium powders and binder components were weighed and heated under a protective argon atmosphere in a steel cup until all binder components were molten. The cups were closed under argon atmosphere and then transferred into a planetary rotary mixer (Thinky ARE 250, Japan) and mixed for 5 min at 2000 rpm. After mixing and cooling the feedstock was granulated using a cutting mill (Wanner B08.10f, Germany). For homogenisation the feedstock was extruded through the extruder of the injection moulding machine at 160 °C. After cooling down the feedstock was again granulated. This feedstock granulate was used for the injection moulding.

Injection Moulding

Injection moulding was performed using a commercial injection moulding machine (Arburg Allrounder 320S, Germany). Dog bone tensile test specimens according to DIN EN ISO 2740 [133] were produced. Figure 4-1 shows the dimensions of the dog bone green parts after injection moulding. Figure 4-2 shows the injection moulding tool after injection and before ejecting the part from the mould.

Tool and feedstock temperatures varied depending on the binder system used. Table 4-3 shows the parameters used for the injection moulding for PP and PE based binder systems. Sprues and defect parts were granulated and reused.

Table 4-3 Injection moulding parameters for dog bone tensile test specimens for PP based binder systems.

Parameter	Value for PP based binder systems	Value for PE based binder systems
Melt temperature (°C)	80/130/135/135 (hopper to nozzle)	80/90/110/110 (hopper to nozzle)
Tool temperature (°C)	52/56 (ejector side/nozzle side)	45/45
Shot volume (cm^3)	11.5	11.5
Injection flow (cm^3/s)	3 steps 7.5/15/10	3 steps 7.5/15/10
Injection pressure (bar)	3 steps 200/800/1000	3 steps 200/800/1000
Changeover points	11 cm^3 / 1.5 cm^3 / 1.1 s	11 cm^3 / 1.5 cm^3 / 1.1 s
Holding pressure (bar)	500/200/25 each 1 s	500/200/25 each 1 s
Cooling time (s)	15	15

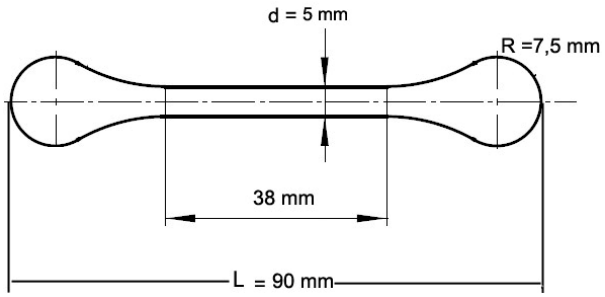

Figure 4-1 Dimension of dog bone tensile test specimens according to ISO 2740-B [133].

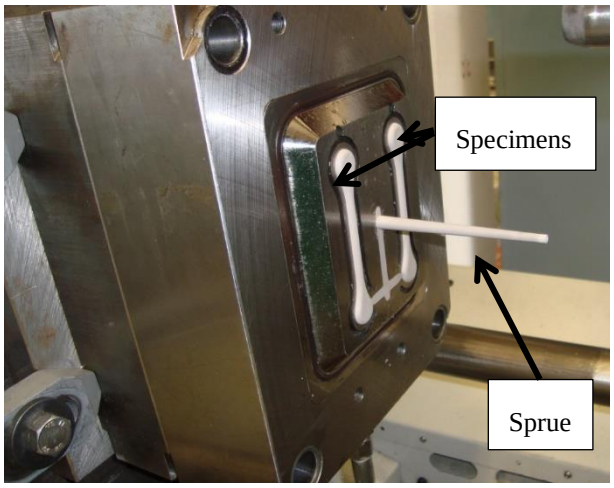

Figure 4-2 Tool of the injection moulding of dog bone tensile test specimen after injection cycle before ejecting the parts (ejector side of the mould).

Solvent Debinding

The debinding of the wax components and the stearic acid was performed by solvent debinding in hexane at 45 °C for 15 hours (Lömi EBA50/2006, Germany). After solvent debinding the specimens were transferred into a glove box system with argon atmosphere to keep the time in oxygen atmosphere as short as possible to prevent the specimens from further oxygen uptake (Unilab, MBraun, Germany).

Thermal Debinding and Sintering of MIM Samples

Figure 4-3 shows the crucible set up for the thermal debinding and sintering of the MIM samples. The samples were placed on boron nitride coated steel plates which were stacked on steel rings. This stack was surrounded by an inner crucible which was placed into an outer crucible. Inner and outer crucibles were separated by coarse magnesium powder as getter material to minimize the influence of impurities of the furnace atmosphere on the samples during the heat treatment. Thermal debinding and sintering was performed using a hot wall retort furnace (MUT RRO350-900, Germany). Figure 4-4 shows the temperature-, pressure-time course used for the thermal debinding and sintering of the MIM samples. The pressure swing during the thermal debinding, to ensure a gas exchange with the inner crucible and the furnace, was performed by opening and closing the outlet valve towards the vacuum pump. Sintering times varied for the different processed alloys. If not indicated differently sintering times and temperatures according to Table 4-4 were used.

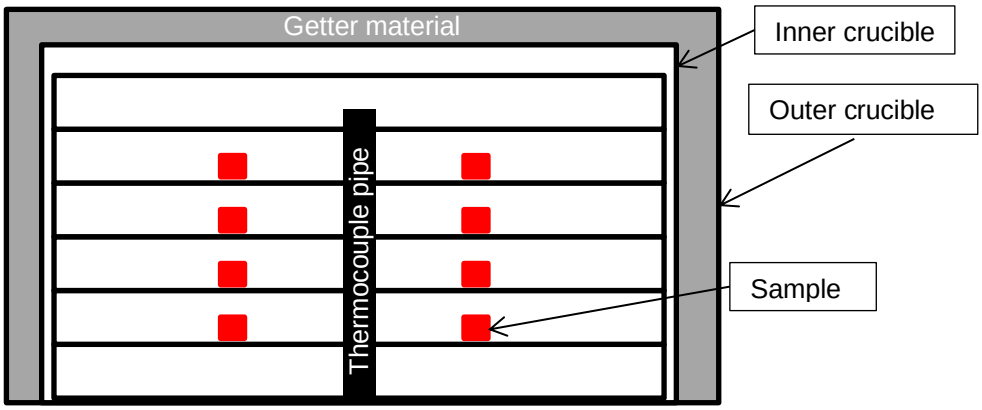

Figure 4-3 Crucible set up for thermal debinding and sintering of MIM specimens.

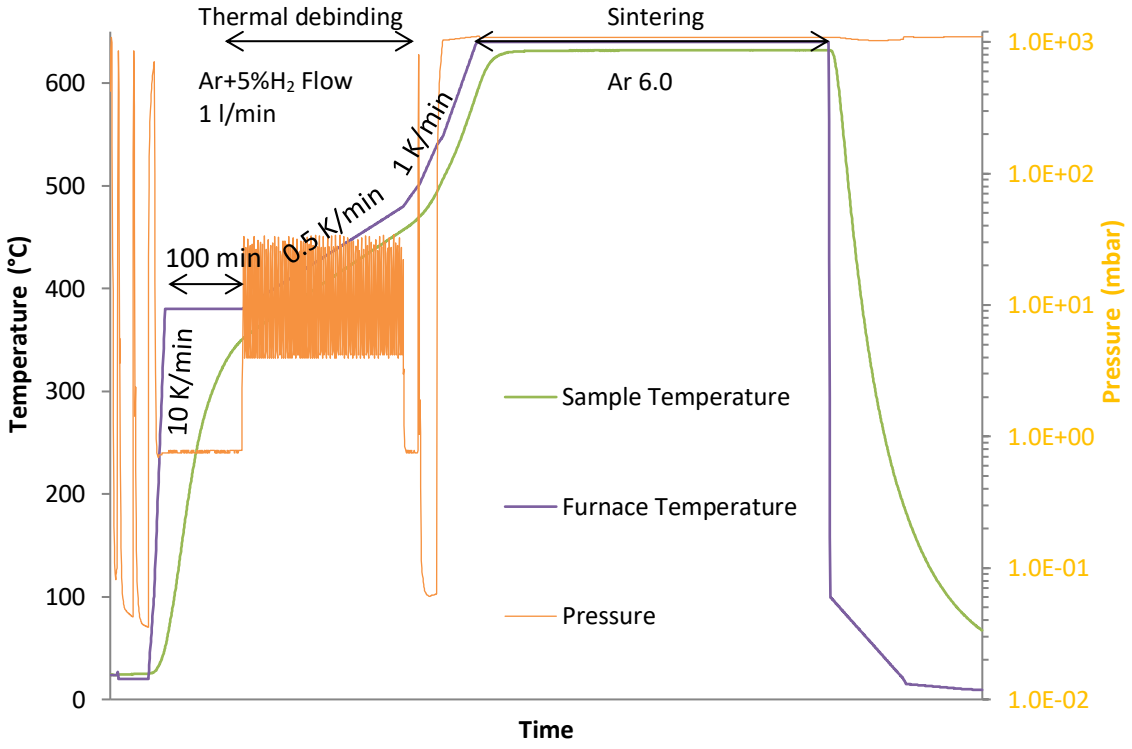

Figure 4-4 Time temperature pressure course for thermal debinding and sintering of MIM samples.

Table 4-4 Sintering temperatures (sample) and sintering times used for the different processed materials.

Material	Sintering Temperature (°C)	Sintering Time (h)
Mg	638	64
Mg-0.9Ca	638	64
AZ91	607	4
Mg-5Gd	635	4
Mg-10Gd	635	4

4.3 Experimental Setups

4.3.1 Polymer Screening

For the polymer screening Mg-0.9Ca feedstock cylinders were produced out of different polymer containing feedstocks with a powder loading of 64 vol.% with a binder system composition of 35 wt.% polymer, 60 wt.% paraffin wax and 5 wt.% stearic acid. Cylinder production was carried out by heating the cylindrical die on a heating plate with feedstock inside the die. A pressure of 5 MPa was used while the samples were cooled down inside the die. Followed by the sample production was the solvent debinding in hexane. This route was used for all but the polyisobutylene samples.

A polyisobutylene feedstock was produced using only polyisobutylene and hexane due to the solubility of polyisobutylene in hexane which prohibits a solvent debinding of this feedstock in hexane. For this feedstock the same powder loading was used with a binder system of 35 wt.% polyisobutylene and 65 m% hexane. After mixing, the hexane was removed by evaporation in vacuum. Cylinders were produced with the same technique as with the other feedstocks. For the polyisobutylene feedstock the cylinders were vacuum debound instead of solvent debinding to enable evaporation of the hexane. This set up was used due to the solubility of polyisobutylene in hexane.

Figure 4-5 shows the crucible set up used for the polymer screening. Each set of polymers was placed inside a small inner crucible with a binder free reference sample. Samples were placed on boron nitride coated steel plates. The inner crucibles were separated by getter material to minimize the influence of different sets of polymers on each other. Thermal debinding was performed between 380 °C and 550 °C with a heating rate of 0.5 K/min with an Ar+H_2 flow of 0.5 l/min at 5 mbar. Sintering was performed at 630 °C for 64 hours. Thermal debinding and sintering for the polymer screening experiments were conducted in a hot wall furnace (Xerion, XRetort, Germany).

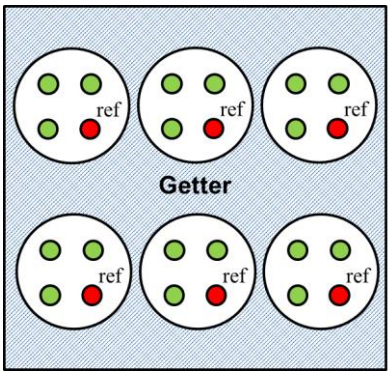

Figure 4-5 Crucible set up for polymer screening experiments with binder containing samples (green) and binder free reference samples (red).

4.3.2 Influence of Backbone Polymer on Surface Carbon Content

To investigate the carbon residuals after thermal debinding of PE and PPcoPE polymer on magnesium by XPS pure magnesium discs with a diameter of 10 mm are coated with the polymers and heat treated in the same set up as used for the polymer screening. PE and PPcoPE are used as polymers, while uncoated discs are used as reference. The discs are coated by placing them on a heating plate and melting the polymer on the magnesium discs followed by cooling of the coated discs. The time-temperature-pressure course for the thermal debinding was the same as that used for the polymer screening up to 500 °C and was then stopped. After cooling down the samples surfaces were analysed by XPS to determine the total surface carbon content. Discs instead of powder samples are used to minimize the influence of surface morphology on the measurement results.

4.3.3 Hydrocarbons as Simulated Debinding Products

To simulate the thermal debinding of PE and PP different alkanes and alkenes were chosen as potential decomposition products. Table 4-5 gives an overview of the chosen products. Short chain hydrocarbons up to C_6 are selected so that they can be used as swiping gas over the samples and due to the availability of corresponding isomers in sufficient amounts. To simulate the thermal debinding of the polymer the products were led over pure magnesium and Mg-0.9Ca cylinders with a diameter of 8 and 11 mm produced by the method described in section 4.2. For XPS measurements magnesium discs from extruded material with a diameter of 10 mm were placed inside the crucible. Discs instead of powder samples are used to minimize the influence of surface morphology on the measurement results. To ensure a homogenous contact of the samples with the test atmosphere a crucible set up as shown in Figure 4-6 was used. The products were introduced through a connector into the bottom of the crucible. The flow path was then guided through the getter into the inner crucible and then to the samples through a perforated boron nitrite coated steel plate. The products then left the crucible set up through the getter in the upper part of the crucible as indicated with the red arrows. This set up ensured a homogenous contact of the samples with the test atmosphere while the following sintering step was maintained with samples surrounded by getter material to ensure a pure sintering atmosphere.

The test atmosphere was generated by a controlled flow of the product through a flow meter connected to the inlet of the furnace to which the crucible connector is attached. The test products were led over the samples with a fluctuation in pressure between 5 and 50 mbar maintained by opening and closing the outlet valve towards the vacuum pump. The test atmosphere was introduced at a temperature between 380 and 480 °C (furnace set temperature, sample temperature ~10 K lower) with a heating rate of 1 K/min. Sintering was performed for 8 hours under 1050 mbar argon (purity 6.0) at 615 °C (sample

temperature). Treatment with the investigated hydrocarbons and sintering were conducted in a hot wall furnace (Xerion, XRetort, Germany).

Table 4-5 Overview of used products.

Name (Nomenclature)	Potential Decomposition Product of	Supplier	Purity
Ar+5%H2	Reference	Air Liquide	>99.9%
1-Butene	PE	Sigma-Aldrich	>99%
Iso-Butene (2-Methylpropene)	PP	Sigma-Aldrich	99%
1-Pentene	PE	Arcos Organics	97%
Iso-Pentene (2-Methyl-but-2-en)	PP	Arcos Organics	>99%
n-Hexane	PE	Arcos Organics	>99%
Iso-Hexane (2-Methylpentane)	PP	Arcos Organics	>99%

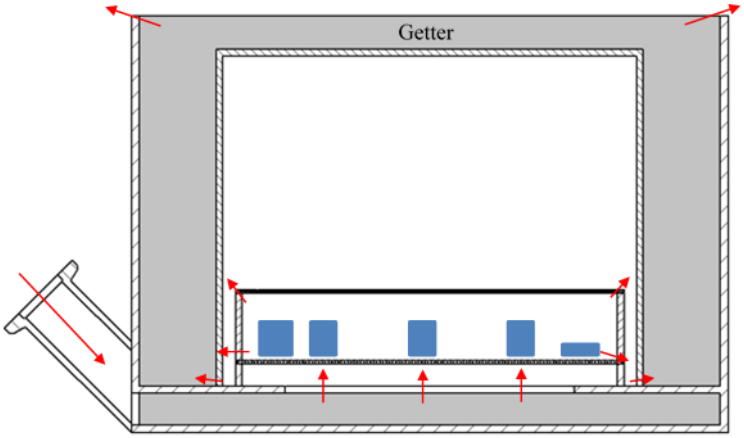

Figure 4-6 Crucible setup for experiments with hydrocarbons as simulated debinding products, gas flow path (red arrows), samples (blue).

4.3.4 Sintering Under Hydrogen Atmosphere

To investigate the influence of hydrogen as a sintering atmosphere Mg-0.9Ca as well as pure magnesium samples with PE and PP based polymers are used. All samples were produced using feedstocks with a powder loading of 64 vol.% and a binder system composition of 35 wt.% backbone polymer, 60 wt.% paraffin wax and 5 wt.% stearic acid. Samples containing PE or PE-EVA backbone polymer were placed in different levels of the same inner crucible. PPcoPE containing samples were placed in a separate crucible to prevent cross-contamination of PE based backbone decompositions onto the PPcoPE containing samples. Pure magnesium discs with a diameter of 10 mm were placed in each crucible for XPS analysis. A crucible set up as shown in Figure 4-3 is used. Thermal debinding and sintering took place in a hot wall retort furnace (MUT RRO350-900, Germany). The temperature-pressure-time curve displayed in Figure 4-4 was applied. Sintering temperatures and times as displayed in Table 4-4 were used. At 500 °C the furnace was flooded with argon (purity 5.0) and subsequently evacuated to remove remaining binder residuals from the atmosphere. At 540 °C the sintering atmosphere was introduced

up to ambient pressure. Argon (purity 5.0) was used as a reference atmosphere for comparison with the hydrogen (purity 5.0) atmosphere. To ensure a steady exchange of atmosphere a constant flow of 0.5 l/min of the sintering atmosphere was introduced resulting in a fluctuating sintering pressure between 1200 and 1250 mbar due to opening and closing of the outlet valve of the furnace.

To investigate the influence of hydrogen on the thermal debinding as well as on the sintering experiments using AZ91 samples containing PE as well as PPcoPE as backbone polymers were performed. Using argon during thermal debinding and sintering was used as reference experiment. One experiment was performed using argon during thermal debinding and hydrogen during sintering another experiment was performed using hydrogen during thermal debinding and sintering.

Mg-5Gd and Mg-10Gd samples with PPcoPE backbone polymer are processed using argon as well as hydrogen atmosphere to investigate the influence of hydrogen during sintering on magnesium alloys that contain hydride forming elements.

4.3.5 Sintering of Titanium using PPcoPE and PE-EVA Backbone Polymer

To investigate the influence of PE-EVA as well as PPcoPE backbone polymer on the sintering results as well as on the carbon content of titanium MIM samples were processed in the same way as described for the magnesium alloys. All samples were produced using feedstocks with a powder loading of 64 vol.% and a binder system composition of 35 wt.% backbone polymer, 60 wt.% paraffin wax and 5 wt.% stearic acid. Only the furnace set up varied for the sintering of the titanium MIM samples compared to the magnesium MIM process described above. Thermal debinding and sintering were performed in a high vacuum cold wall furnace with molybdenum heat deflection shields (Xerion, XVAC, Germany). Sintering time was chosen for 2 hours at 1300 °C in high vacuum ($<10^{-4}$ mbar).

4.4 Measurements and Procedures

4.4.1 Dimensions, Weight and Density

Dimension measurements were taken using callipers (Mahr 16EX, Germany). Shrinkage (S_L) is calculated according to equation (9). Weight and Archimedes density (ρ_a) were determined using a scale (Sartorius LA230S, Germany) with setup for density measurements by buoyancy method in ethanol. Geometrical density (ρ_{geo}) of cylindrical samples was calculated according to equation (12). Porosities were calculated using equations (10)-(12) with the theoretical densities (ρ_{th}) given in Table 4-6.

Table 4-6 Theoretical densities of processed alloys.

Material	Theoretical density (ρ_{th}) (g/cm³)	Reference
Mg	1.74	[4]
Mg-0.9Ca	1.73	Archimedes on bulk material
AZ91	1.81	[4]

$$S_L = \frac{l_s - l_g}{l_g} \quad \text{eq. (9)}$$

$$P_{geo} = \left(1 - \frac{\rho_{geo}}{\rho_{th}}\right) \quad \text{eq. (10)}$$

$$P_{closed} = \left(1 - \frac{\rho_a}{\rho_{th}}\right) \quad \text{eq. (11)}$$

$$\rho_{geo} = \frac{m_s}{V} \quad \text{eq. (12)}$$

4.4.2 Tensile Testing

Tensile tests were carried out on a tensile test machine (Schenck Trebel RM100 Universalprüfmaschine, Germany). The tensile tests were performed according to DIN EN ISO 6892-1:2009 B [134]. The measurements were performed on the dog bone shaped tensile test specimens in the as-sintered condition. The proportionality factor (k) was approximately 8. The traverse (v_c) speed was set constant at 0.2 mm/min. The preload was set to 1 MPa. Elongation was measured with a laser extensometer. The start length for the extensometer measurement (L_e) was approximately 30 mm. The diameter is averaged over nine measurements on the cylindrical part of the specimens.

4.4.3 Light and Electron Microscopy

Microstructural analyses were performed on samples after grinding and polishing. Microscopic images were taken using a scanning electron microscope (SEM) equipped with energy dispersive X-ray spectroscopy (EDXS) (Tescan Vega3, Czech Republic) as well as by light microscopy (Olympus PGM3, Japan).

4.4.4 TGA Measurements

For TGA measurements a Mettler Toledo SDTA 851 (Mettler Toledo, Germany) was used. Pure polymers were measured using a 70 µl aluminium oxide (Al_2O_3) crucible. Measurements with magnesium were performed using a platinum crucible to prevent reaction of the magnesium with the crucible material. Samples were weighed and placed into the TGA. Before starting a measurement, the TGA was evacuated and flooded with argon three times to ensure an oxygen free atmosphere. The samples were heated to 200 °C at a rate of 10 K/min and then heated with the desired heating rate to 550 °C.

Measurements at ambient pressure were performed using high purity argon (Ar6.0) with a flow of 50 ml/min. Measurements under vacuum were performed by connecting a vacuum pump to the outlet of the TGA. To protect the weighing cell of the TGA a small pure gas (Ar6.0) flow was used during the vacuum experiments.

4.4.5 TGA-FTIR Measurements

Figure 4-7 shows the schematic setup used for the TGA FTIR measurements. Approximately 25 mg of polymer or brown part were placed inside of a 70 µl platinum crucible located inside the TGA furnace (Mettler Toledo TGA/DSC2, Germany). Samples were heated from 30 °C to 550 °C using a heating rate of 5 K min^{-1}. The gaseous decomposition products were transported through a heated transfer line (250 °C) by an argon flow of 20 ml/min into the gas cuvette (280 °C) of the FT-IR spectrometer (Nicolet iS50, Thermo Scientific, WI, USA).

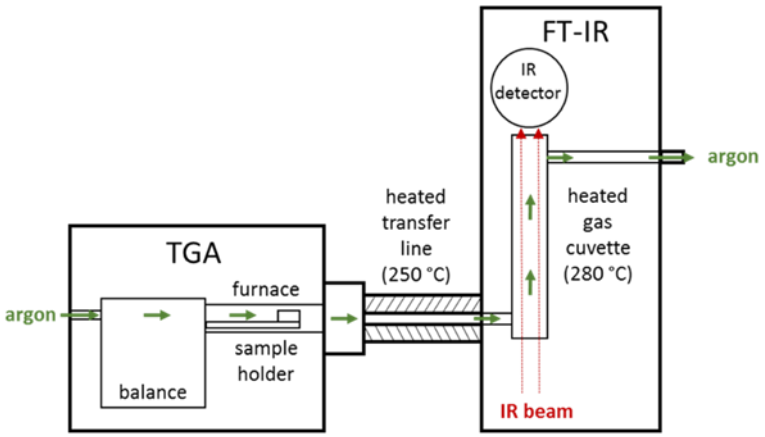

Figure 4-7 Schematic setup for TGA-FTIR measurements. With permission from Silvio Neumann.

4.4.6 XRD Measurements

XRD measurements are performed on a Bruker D8 Advance (Bruker, MA, USA) (DaVinci design) equipped with a Eulerian cradle and in Bragg-Brentano geometry using Cu kα radiation. 2θ angles have been varied stepwise between 25° and 65° with an increment of 0.01° and time of 2 s. Measurements were performed using powder mode. Data analysis was performed with the Bruker software (BrukerEVA).

4.4.7 Total Carbon Content by Combustion Analysis

The total carbon content of the magnesium and magnesium alloy samples were measured externally (HuK Umweltlabor GmbH) using a Leco CS200 (LECO Instruments GmbH, Germany). Three measurements were performed on each sample by analysing approximately 500 mg sample weight per measurement. Analyses were performed according to DIN EN ISO 15350.

Total carbon content of titanium samples was performed by analysing three times 600 mg per sample using a Leco CS444 device (LECO Instruments GmbH, Germany).

4.4.8 XPS Measurements

XPS measurements were performed using a KRATOS AXIS Ultra DLD (Kratos Analytical, United Kingdom) equipped with an Al Kα anode with monochromator working at 15 kV. For the survey spectra a pass energy of 160 was used while for the region spectra the pass energy was 20. The investigated area was 700 x 300 µm. For removal of sample contaminations from the environment, e.g. CO_2, argon etching was performed. The etching rate was 10 nm/min related to Ta_2O_5. The spectra were evaluated using the CasaXPS software. Calibration of the spectra was done by adjusting the C1s peak to 384.5 eV binding energy. After applying deconvolution of the signals, a fine calibration was done by adjusting MgO to 50.25 eV in the Mg2p signal. Table 4-7 gives an overview of the literature binding energies used for the deconvolution of the XPS region data. Magnesium carbide as well as magnesium carbonate binding energies could not be found in the literature. Therefore, literature values of silicon carbide, titanium carbide and dichromium tricarbide are used as an indication for the binding energy that could be expected for magnesium carbides in the C1s spectra. Calcium carbonate was used as a reference for the binding energy that can be expected for magnesium carbonate in the C1s spectra.

Table 4-7 Used literature binding energy values for used for XPS evaluation.

Spectra	**Formula**	**Name**	**Binding Energy (eV)**	**Literature**
C1s	C	graphite carbon	283.8	[135]
C1s	C	pyrolytic graphite	284.3	[136]
C1s	CaCO3	calcium carbonate	289.7	[137]
C1s	SiC	silicon carbide	281.45	[138]
C1s	TiC	titanium carbide	281.7	[139]
C1s	Cr2C3	dichromium tricarbide	282.8	[140]
C1s	CO/Ti	carbon monoxide/titanium	286.1	[141]
C1s	CO/Pd	carbon monoxide/palladium	286.3	[142]
C1s	CO2/Ni	carbon dioxide/nickel physisorbed	285.6	[143]
C1s	CO2/Ni	carbon dioxide/nickel chemisorbed	286.4	[143]
C1s	(-O-C(O)-C6H4-C(O)-O-CH2-CH2-)n	carboxylic acid, ester, oxygen, phenyl/benzene, polymer	288.8	[144]
C1s	CH3C(O)OH/MgO/Mg	acetic acid/magnesium oxide/magnesium carboxylic acid, organic acid, organometallic	287	[145]
C1s	HC(O)-O-CH3/MgO/Mg	methyl formate/magnesium oxide/magnesium alcohol, organometallic	287.8	[145]
Mg2p	MgO	magnesium oxide	50.25	[146]
Mg2p	Mg	magnesium	49.3	[146]

Mg2p	$Mg(OH)_2$	magnesium hydroxide	49.5	[147]
O1s	MgO	magnesium oxide	529.6	[148]
O1s	MgO	magnesium oxide	530.6	[149]
O1s	MgO	magnesium oxide	529.9	[150]
O1s	H_2O	water	533.1	[151]
O1s	CO/Cu	carbon oxide/copper	533.3	[152]
O1s	CO/Ag/Na	carbon oxide/silver/sodium	532	[153]
O1s	CO/Ag/Na	carbon oxide/silver/sodium	533.6	[153]
O1s	CO_2	carbon dioxide	532.6	[150]

4.4.9 ToF-SIMS Measurements

ToF-SIMS measurements were performed externally at the Karlsruhe Institute of Technology (KIT). The following text describes the experimental set up used for these measurements taken from the measurement report.

"ToF-SIMS was performed on a TOF.SIMS5 instrument (ION-TOF GmbH, Münster, Germany) at KIT. This spectrometer is equipped with a bismuth cluster primary ion source and a reflectron type time-of-flight analyzer. UHV base pressure was $< 3\times10^{-8}$ mbar. For high mass resolution the bismuth source was operated in "high current bunched" mode providing short Bi^+ primary ion pulses at 25 keV energy, a lateral resolution of approx. 4 µm, a target current of 1.1 pA. The short pulse length of 1.5 ns allowed for high mass resolution. The primary ion beam was rastered across a 300 × 300 μm^2 field of view on the sample, and 128×128 data points were recorded. Primary ion doses were kept below 10^{11} ions/cm^2 (static SIMS limit). Spectra were calibrated on the omnipresent C^-, C_2^-, C_3^- peaks. Based on these datasets the chemical assignments for characteristic fragments were determined.

For depth profiling a dual beam analysis was performed in fully interlaced mode. Here, the time interval of approximately 100 µs for the released secondary ions to pass the drift tube and to reach the detector is used to erode the sample with the sputter ion beam. The primary ion source was again operated in "high current bunched" mode with a scanned area of 300 × 300 μm^2 and the sputter gun (operated with cesium ions, 2 keV, scanned over a concentric field of 500 × 500 μm^2, target current 190 nA) was applied to erode the sample.

Secondary ion intensities are plotted over the sputter time, being a measure for erosion depth. It should be noted, however, that this scale is not necessarily linear, since different materials, MgO on metallic Mg, are having different erosion rates. For metals theses rates have been predicted by Yamamura, for other compounds they have to be calibrated ex-situ directly on the used material. Due to the roughness of the samples a quantification of the obtained created depths was not attempted." [154]

5 Results

5.1 Polymer Screening

The polymer screening experiments reveal that all straight chain PE based polymers have a strong sintering inhibiting effect when used as a backbone polymer. PP and PIB based polymers do not show this effect. This can be clearly seen in Figure 5-1. The first five polymers are PP based and the last four are PE based. The shrinkage of PIB cannot be compared to the other polymers because the corresponding green parts were produced differently resulting in different powder loading. However, the sintering density can be compared to the other samples. It can be clearly seen that all PP based polymers as well as the PIB show good sintering results as they have a low residual porosity of below 5%. All PE based polymers clearly show a negative influence on the sintering activity of the Mg-0.9Ca samples as they have a low shrinkage and high residual porosity of up to 30%. Compared to the other PE based polymers the PEcoOc samples show a lower residual porosity of 26% indicating that the negative influence on the sintering activity of the Mg-0.9Ca is the weakest of the PE based polymers.

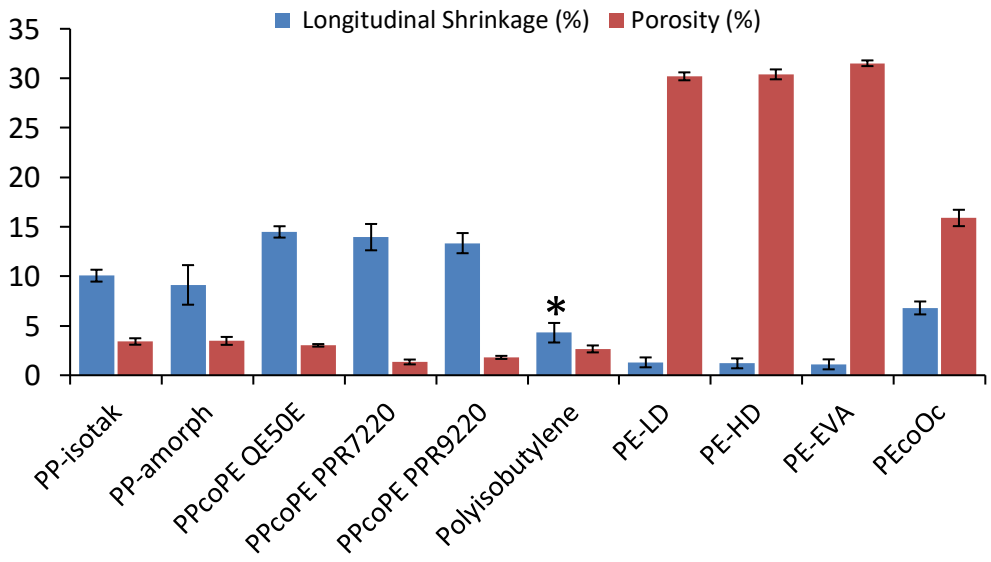

Figure 5-1 Shrinkage and density results of Mg-0.9 cylinders from polymer screening.
*Longitudinal shrinkage cannot be compared due to different production method.

The same effects can be seen on binder free reference samples placed beside the binder containing samples as shown on some selected polymers in Figure 5-2. It can be concluded that the negative influence is not only caused by the direct contact with the polymer but also through the gas phase. This gas phase contains the thermal decomposition products of the polymers.

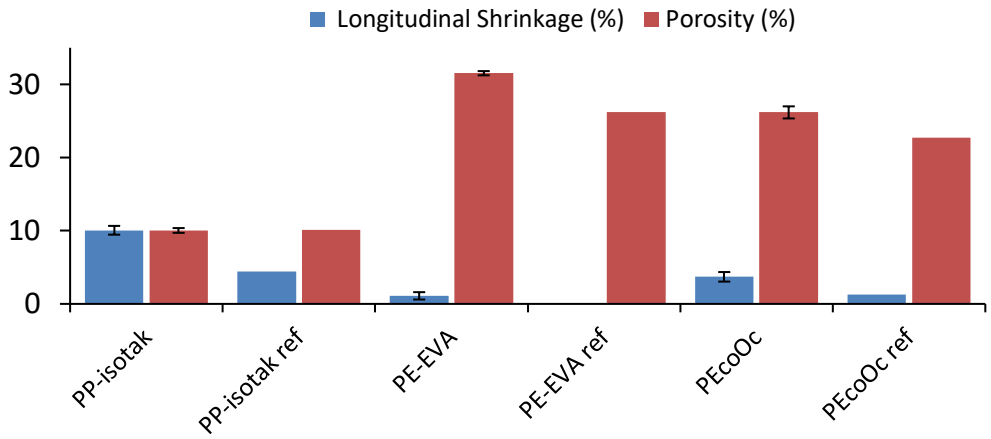

Figure 5-2 Shrinkage and residual porosity of binder containing and corresponding binder free reference (ref) samples.

The results observed for the sintering activity correlate with the investigated microstructure of the samples which can be seen in Figure 5-3 which displays the microstructures of Mg-0.9Ca samples produced using PE-EVA (a) as well as PPcoPE (b) as backbone polymer. The microstructure of the PE-EVA samples reveals high porosity and the powder shape is still visible, while for the PPcoPE microstructure the porosity is lower and the powder shape changed due to the sintering neck formation and the densification.

All PE based polymers result in a microstructure comparable to the PE-EVA microstructure, while all PP based polymers as well as the PIB result in a comparable microstructure like the one displayed for PPcoPE.

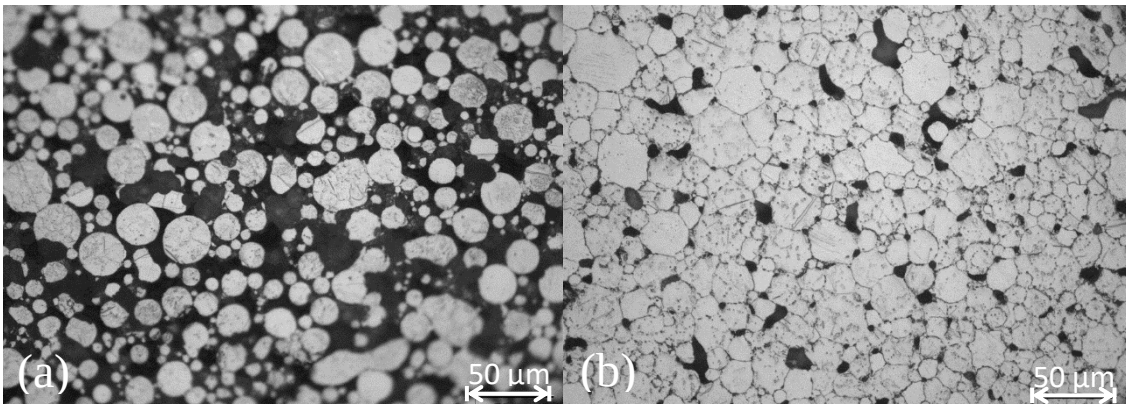

Figure 5-3 Microstructure of Mg-0.9Ca samples after sintering processed with PE-EVA (a) and PPcoPE (b).

All investigated PPcoPE polymers showed good sintering results indicated by a high densification. Furthermore, these polymers turn out to be outstanding in the mixing and injection moulding step of the MIM process compared to other PP based polymers. The isotactic as well as the amorphous PP were identified to have mixing problems during pre-mixing of the binder as displayed in Figure 5-4. It can be seen that when isotactic PP is mixed with waxes the compound is heterogeneous even after repeated mixing while PPcoPE and waxes can be homogenously mixed. These problems of isotactic PP during

feedstock production are likely caused by bad miscibility of these polymers with waxes [85, 155].

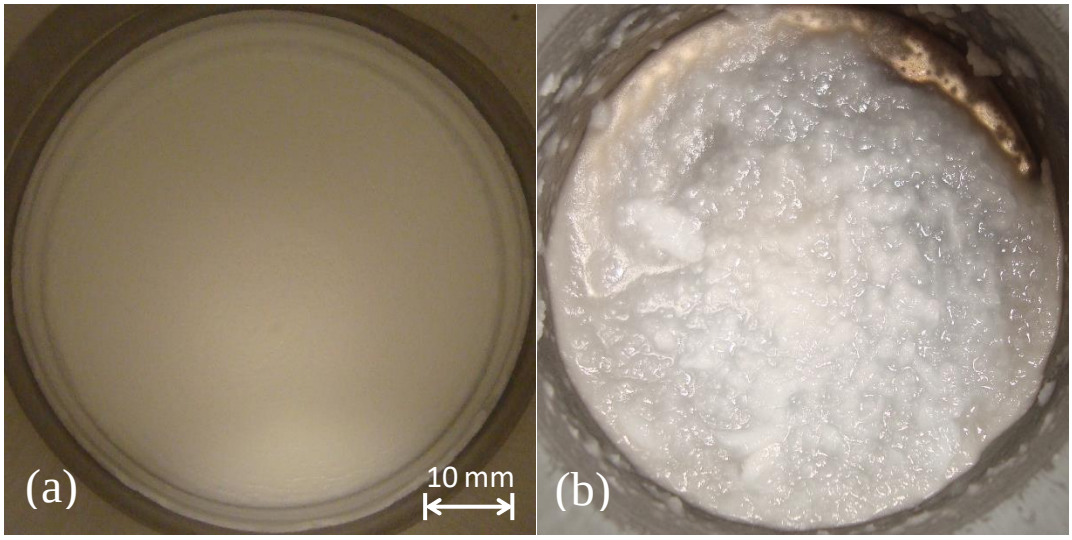

Figure 5-4 Binder system after mixing (a) homogeneous PPcoPE based binder system, (b) inhomogeneous PP isotactic based binder system.

Due to these mixing problems the resulting feedstock showed problems in the injection moulding such as demixing, air entrapments and blister formation which even increased with recycling of the feedstock as shown in Figure 5-5. PPcoPE based feedstocks did not show these problems even after recycling of the feedstock. Therefore, PPcoPE is chosen as a PP based representative backbone polymer during production of the MIM samples for the following MIM experiments and for the following investigations.

Figure 5-5 Injection moulding defects of samples with isotactic PP backbone polymer. Left top sample minor defects of non-recycled feedstock, bottom sample of recycled feedstock with demixing (different coloured areas) and improper filling (red circle). Right picture displays air entrapments inside the part.

5.2 Influence of Backbone Polymer on Surface Carbon Content

The thermal removal of the polymers as described in section 4.3.2. leads to carbon residuals on the magnesium surfaces of the samples. This can be concluded as the polymer treated samples have a higher surface carbon content compared to the reference sample as displayed in Figure 5-6. The thermal removal of PE results in higher amounts of carbon residuals compared to PPcoPE. ToF-SIMS measurements show correlating results in the depth integrated signals of the graphitisation as displayed in Figure 5-7. The PE treated sample shows the strongest intensity peak meaning that this sample has the highest

amount of graphitic residuals on its surface followed by the PPcoPE treated one. The polymer free reference sample reveals the lowest amount of graphitic residuals.

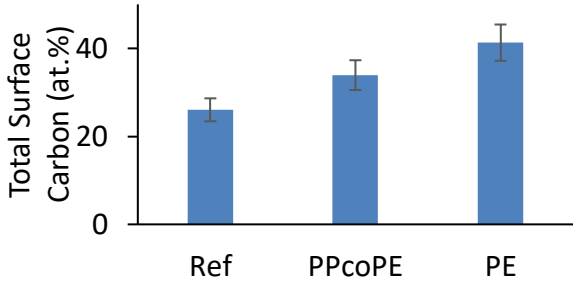

Figure 5-6 Influence of backbone polymer on the total carbon content (determined by XPS) of polymer covered Mg discs after thermal debinding.

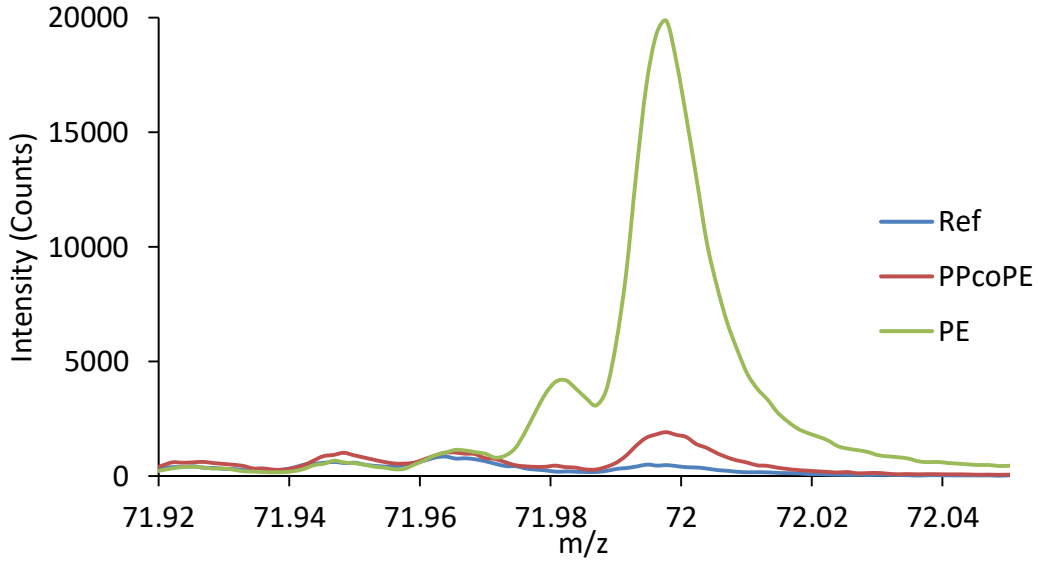

Figure 5-7 Graphitisation of Mg discs covered with different polymers after thermal debinding, depth integrated profile of ToF-SIMS measurement.

5.3 TGA Measurements

The investigated PE based polymers decompose at slightly higher temperatures compared to the investigated PP based one as it can be seen in the following graphs. Figure 5-8 shows the TGA curves of PE-EVA, HDPE, PPcoPE and isotactic PP with a heating rate of 4 K/min under vacuum. It can be seen that the decomposition of PE-EVA reveals a first small loss of weight in the range of 250-310 °C due to the decomposition of the EVA group. The main decomposition of PE-EVA is finished at around 385 °C. The end of the decomposition of HDPE is approximately 15 K lower. Both PP based polymers as well as LDPE are fully decomposed at around 360 °C.

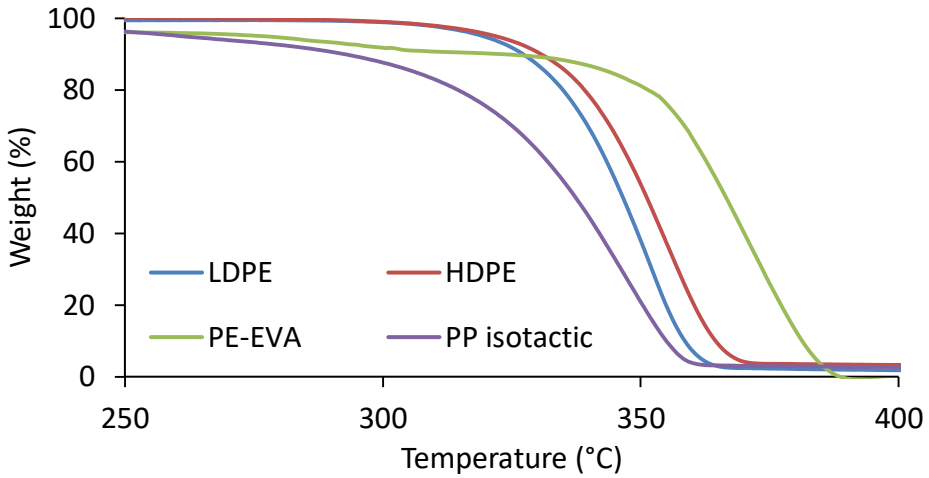

Figure 5-8 TGA curves of PPcoPE, isotactic PP, PE-EVA and HDPE under vacuum (~1 mbar + Ar flow), heating rate 4 K/min.

Applying a vacuum during the thermal treatment shifts the thermal decomposition of the polymers approximately 100 K to lower temperatures as it can be seen in Figure 5-9 on the example of PPcoPE and PE-EVA.

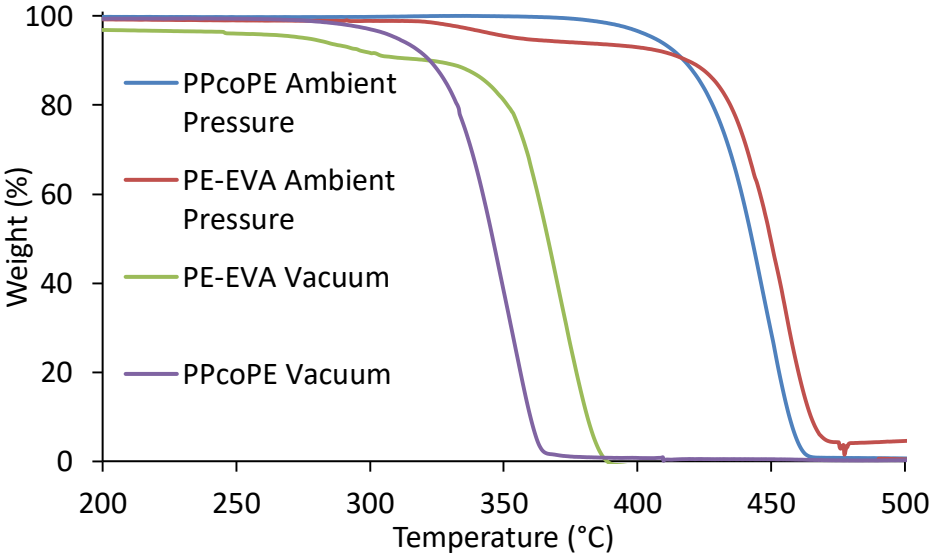

Figure 5-9 TGA curves of PE-EVA and PPcoPE under ambient pressure (Ar flow) and vacuum (~1 mbar + Ar flow), heating rate 4K/min.

Slower heating rates shift the thermal decomposition to lower temperatures as shown in Figure 5-10. The end of the thermal decomposition with a heating rate of 1 K/min compared to 4 K/min is approximately 20 K lower, while the difference from 1 K/min to 0.5 K/min is approximately 10 K. These results correlate with findings of Mohsin *et al.* [156, 120].

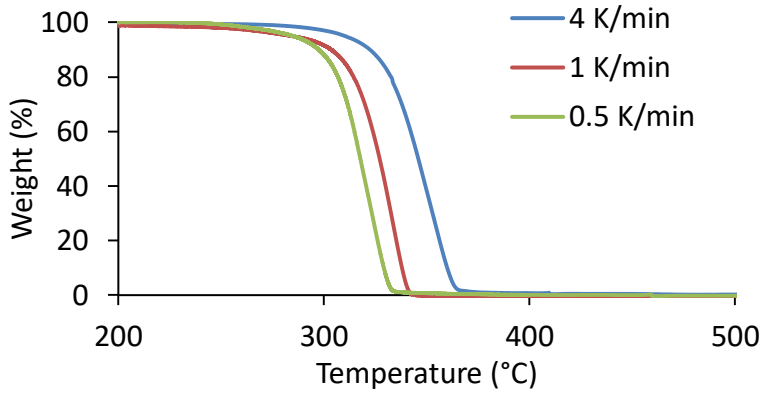

Figure 5-10 TGA curves of PPcoPE at different heating rates 4 K/min, 1 K/min and 0.5 K/min under vacuum (~1 mbar + Ar flow).

When magnesium powder is added to the polymers no significant differences in the TGA curves can be observed. Figure 5-11 shows the TGA curve of PE and PE+Mg normalized on to the polymer weight. The decomposition at the used parameters is comparable in terms of starting and end points as they start at the same temperatures. The weight loss starts at approximately 380 °C and has a maximum decrease at approximately 455 °C. The decomposition at the used parameters is finished at approximately 480 °C. The slight weight gain of the PE+Mg sample is caused by a starting oxidation of the magnesium powder due to oxygen impurities in the TGA setup which was visible due to a colour change of the sample close to the lid of the TGA crucible. This observation can also be made when pure magnesium is measured. Measurements of PPcoPE and PPcoPE+Mg show a comparable behaviour with a starting point at approximately 320 °C, a maximum decrease at approximately 450 °C and the end of decomposition at approximately 460 °C.

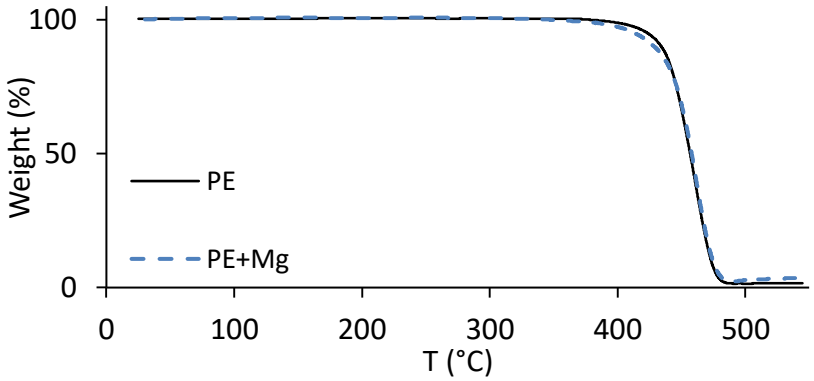

Figure 5-11 Comparison of TGA curve of PE and PE+Mg.

5.4 TGA-FTIR Measurements

The maximum decomposition rate of PE was determined at 450 °C. Figure 5-12 displays the IR spectra of the gas phase of PE, Mg+PE and Ti+PE at this temperature. No significant changes can be observed in the main peaks. However, small differences can be observed in the so-called fingerprint region (low wavenumber spectra) as displayed in Figure 5-13. PE and Ti+PE show the same bands and band positions while Mg+PE shows a

change in bands. It can be seen that in the range of 1000-900 cm^{-1} a difference in band position and band ratio is apparent. This indicates that in the presence of magnesium the thermal decomposition products in the gas phase differ from the pure polymer. The difference between the bands of PE and Mg+PE especially in the area around 965 cm^{-1} is only apparent for Mg+PE and not for Ti+PE. This shows that this difference can be traced back to the presence of magnesium as the Ti+PE and PE spectra are similar. The changes in the spectra presumably indicate a reaction of magnesium with PE or PE decomposition products or a change in the decomposition behaviour of the PE in the presence of magnesium.

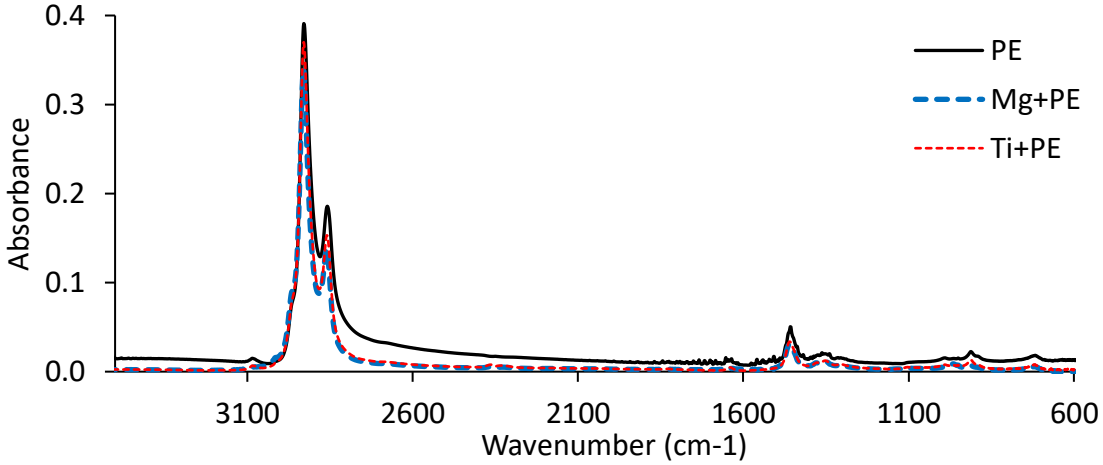

Figure 5-12 IR spectra of PE, Mg+PE and Ti+PE at 450 °C.

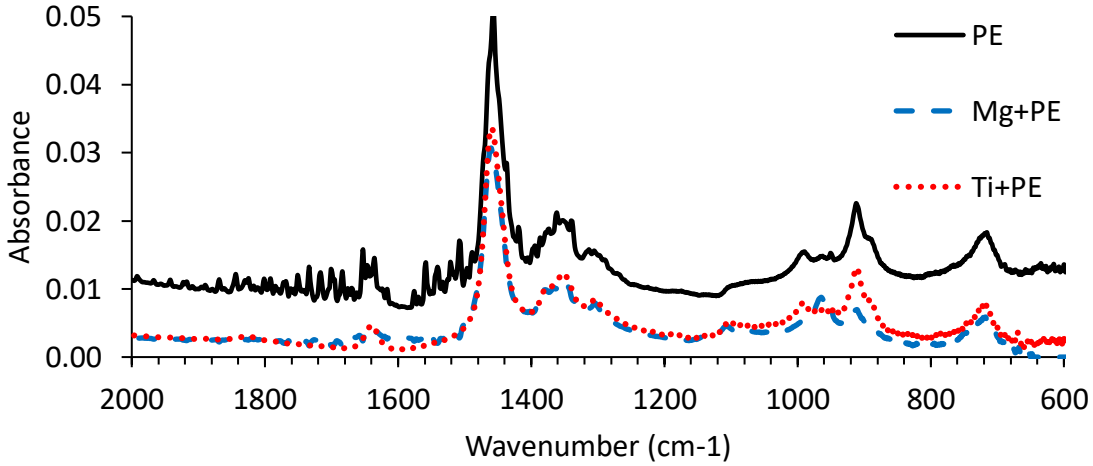

Figure 5-13 Comparison of low wavenumber spectra of the IR spectra at 450 °C of PE and PE+Mg and PE+Ti.

No changes can be observed in the low wavenumber bands of PPcoPE when magnesium is present as displayed in Figure 5-14. This means that no chemical reaction can be detected or no change in the thermal decomposition behaviour of PPcoPE can be observed in the presence of magnesium as observed for PE+Mg.

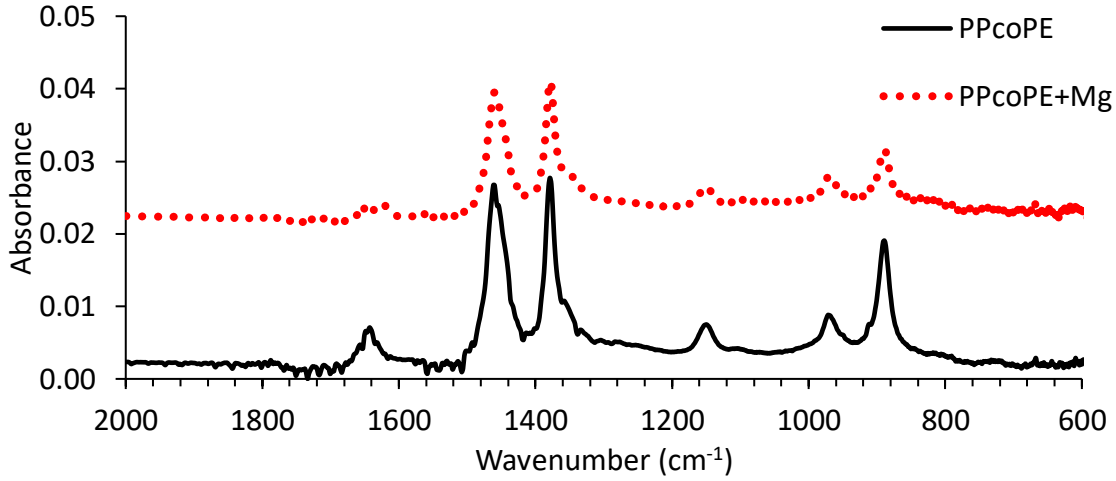

Figure 5-14 Low wavenumber IR spectra at 450 °C of PPcoPE and PPcoPE+Mg.

5.5 Hydrocarbons as Simulated Debinding Products

When pure magnesium and Mg-0.9Ca binder free pressed powder cylinders are treated with different hydrocarbon gases during a temperature profile similar to the thermal debinding in MIM significant differences in sintering activity can be observed as represented by the longitudinal shrinkage in Figure 5-15. Pure magnesium samples treated with straight hydrocarbons show a lower sintering activity (lower shrinkage) compared to samples treated with the corresponding branched isomers (higher shrinkage). For Mg-0.9Ca the same trend can be observed except for the butene isomers. It is assumed that this is caused by a reaction between iso-butene and calcium as this effect is not observed for the calcium free pure magnesium samples. Therefore, Mg-0.9Ca treated with iso-butene is excluded from further considerations.

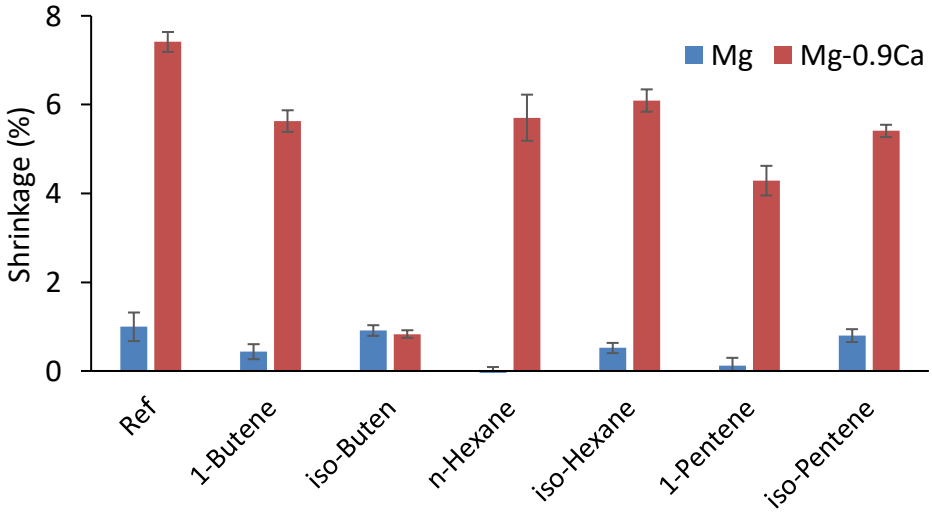

Figure 5-15 Longitudinal shrinkage of Mg and Mg-0.9Ca sintered cylinders after hydrocarbon treatment.

When the surface carbon content of pure magnesium discs placed besides the sintering samples is analysed it can be observed that the samples treated with the straight isomers have a higher carbon content compared to the samples treated with the branched ones. It

can be concluded that the treatment with the straight isomers results in higher carbon content and lower sintering activity (lower shrinkage) compared to the corresponding branched isomers. This can be seen in Figure 5-16 in which the surface carbon content of the magnesium discs as well as the longitudinal shrinkage of the corresponding pressed powder cylinders is displayed.

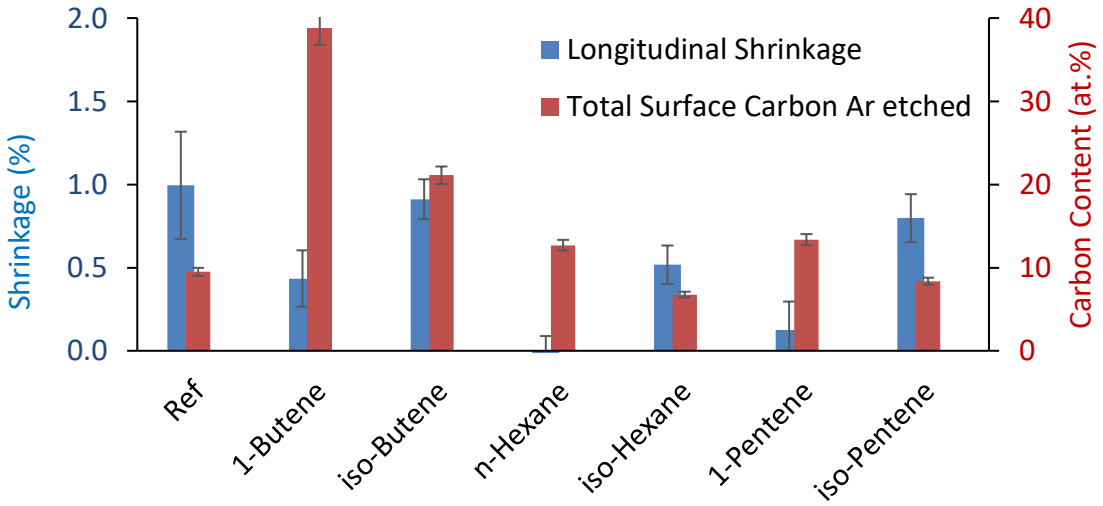

Figure 5-16 Longitudinal shrinkage of Mg sintered samples and total surface carbon of corresponding Mg discs after Ar etching after treated with different hydrocarbons.

ToF-SIMS measurements reveal congruent results in the graphitisation of the samples. This can be seen in Figure 5-17 in which the depth integrated graphitisation profiles of the magnesium discs are displayed. It can be observed that the intensity in case of straight hydrocarbons is higher compared to the corresponding branched isomer. These results underline that treatment with the straight hydrocarbons results in higher carbon residuals on the magnesium surface compared to treatment with their corresponding branched isomers.

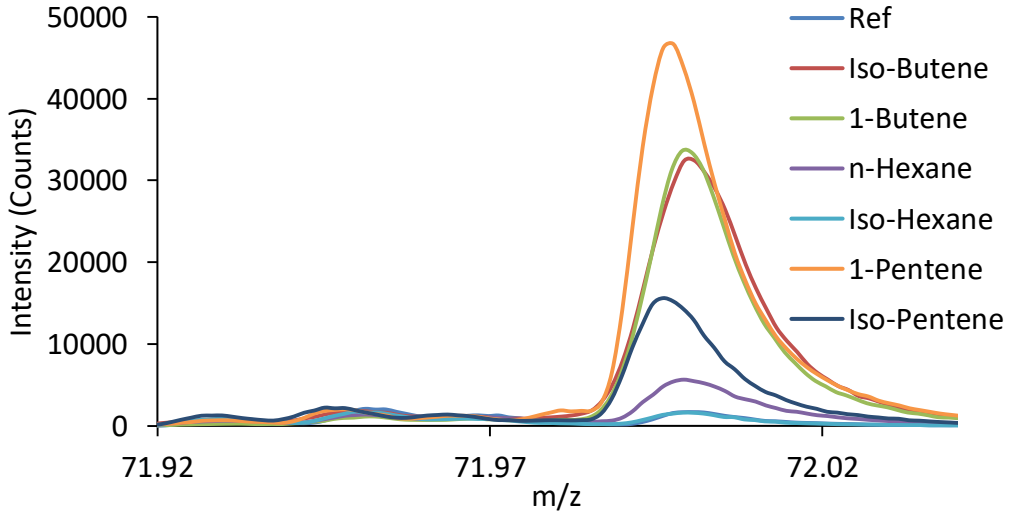

Figure 5-17 Graphitisation of Mg discs treated with different hydrocarbons, depth integrated profile of ToF-SIMS measurement.

From Figure 5-16 a correlation of sintering activity and carbon content can be presumed. Therefore, Figure 5-18 and Figure 5-19 display the longitudinal shrinkage of pure magnesium and Mg-0.9Ca sintered samples over the measured surface carbon contents determined by XPS and ToF-SIMS, respectively. A trend showing that the carbon content and sintering activity correlate can be seen. The higher the carbon content, the lower the sintering activity (shrinkage) of the samples.

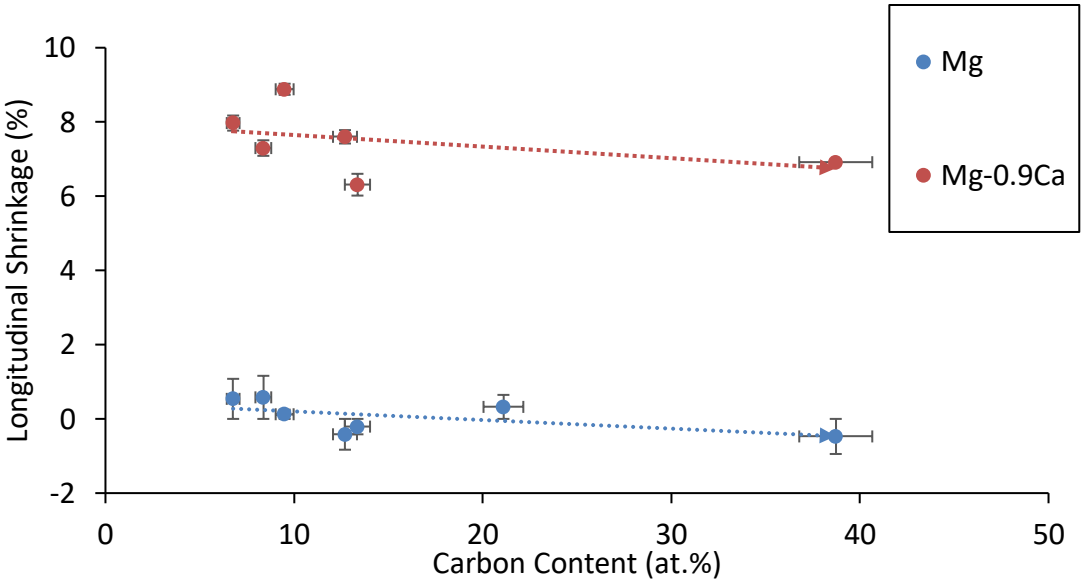

Figure 5-18 Longitudinal shrinkage of pure Mg and Mg-0.9Ca sintered samples VS total surface carbon content of corresponding Mg discs determined by XPS, samples treated with different hydrocarbons.

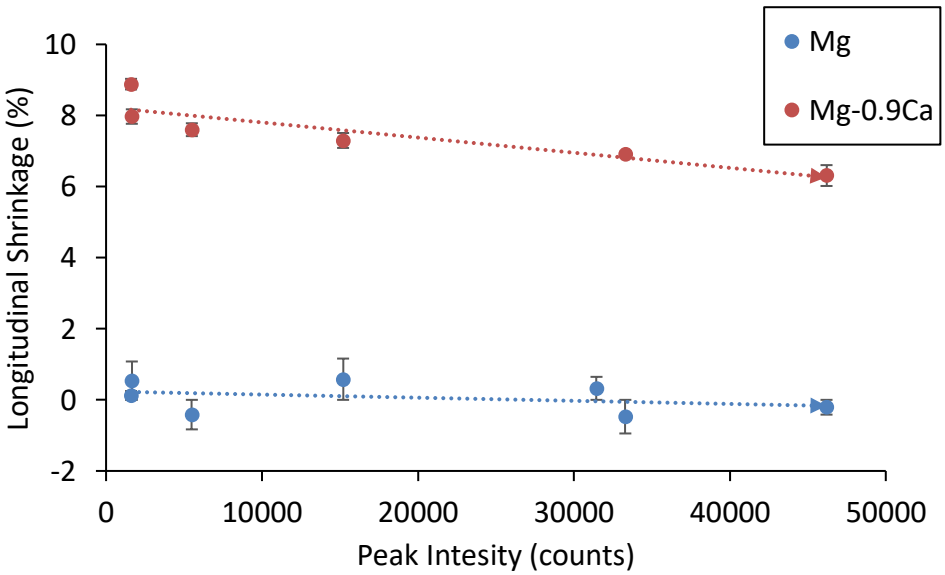

Figure 5-19 Longitudinal shrinkage of pure Mg and Mg-0.9Ca sintered samples VS max. peak height of depth integrated graphitisation of corresponding Mg discs determined by ToF-SIMS, samples treated with different hydrocarbons.

The formation of carbides is assumed therefore XRD measurements were performed on the samples. Analysing these measurements results reveal that carbides cannot be detected by this method. Only Mg and MgO can be detected as shown in Figure 5-20 on the example of a 1-butene treated magnesium sintered cylinder. It is possible that no carbides were present due to the fact that they already decomposed during the heat treatment or

the contact of the sample with air. Another explanation can be that the amount of carbides in the samples is too small to be detected by XRD measurement. Small amounts of carbides can be assumed when XPS is used as measurement method as shown in Figure 5-21 on the example of n-hexane. Even with this sensitive measurement technique the detected amount of presumed carbides is low.

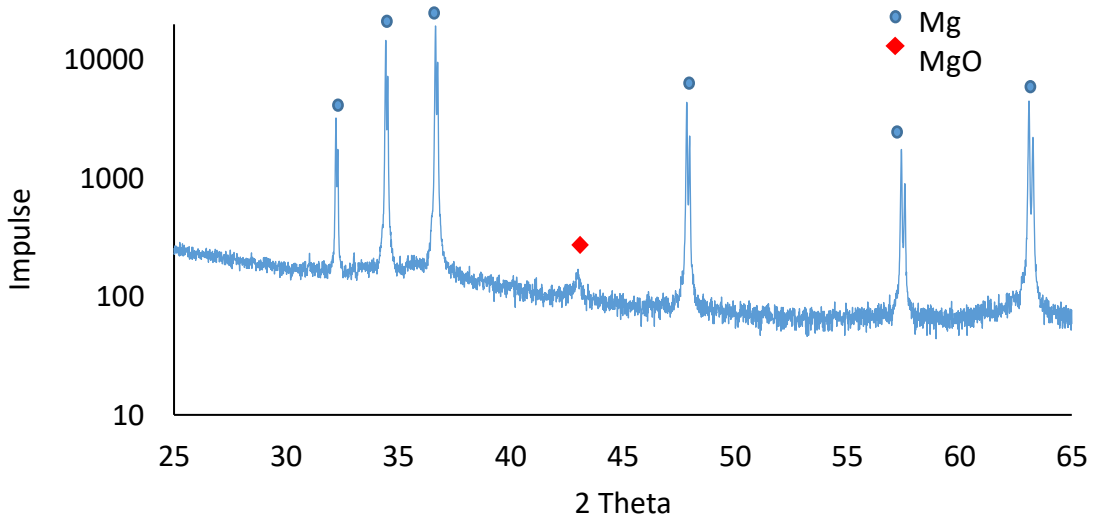

Figure 5-20 XRD measurement on Mg sintered cylinder treated with 1-butene.

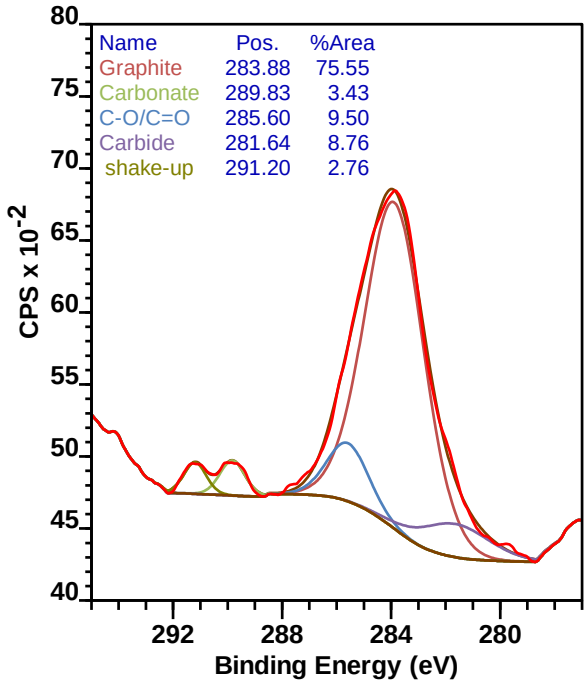

Figure 5-21 C1s signal of Mg disc treated with n-hexane. [93] With permission to reprint from John Wiley and Sons

5.6 Influence of Pure Carbon on the Sintering Behaviour of Magnesium

A correlation between carbon content and sintering activity is already shown in section 5.5. To underline this trend samples of pure magnesium and Mg0.9Ca are sintered with

and without pure carbon additions. A relatively small amount of 0.25 wt.% (equals 0.1 vol%) of graphite are added before pressing of the cylinders. After sintering the total carbon content was determined. The sintering results (longitudinal shrinkage) over the measured total carbon content is displayed in Figure 5-22. The data points with the higher total carbon content correspond to the samples with graphite addition. It can be seen that the shrinkage of the pure magnesium samples is significantly lower when small amounts of graphite are added.

Mg-0.9Ca seems to be more tolerant with respect to the graphite additions as only minor changes in the shrinkage can be observed with small graphite additions. This might be due to the higher sintering activity of Mg-0.9Ca and the presence of liquid phase.

The differences in measured total carbon content equals the amount of added graphite (0.25 wt.%). This confirms the accuracy of the measurement technique and equipment (combustion analysis) used.

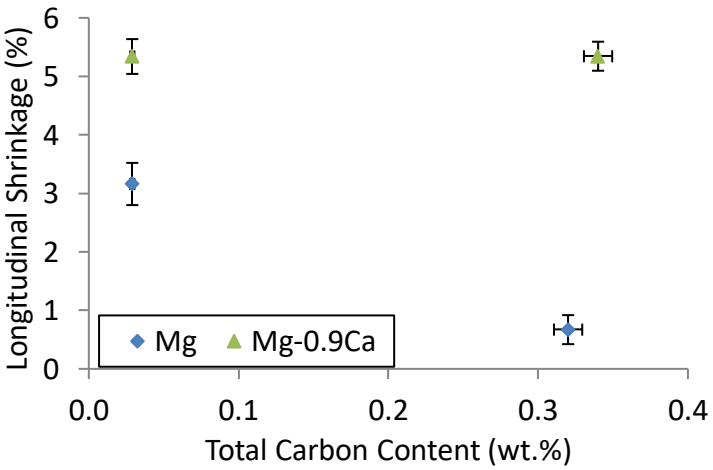

Figure 5-22 Shrinkage of pure Mg and Mg-0.9Ca press and sinter cylinders with and without graphite additions.

SEM images are taken to investigate samples before and after sintering. Figure 5-23 displays a SEM image of the sintered Mg+C sample (a) and of pure magnesium (b) after sintering. It can be seen that in the case of Mg+C no sintering neck formation can be observed, while for pure magnesium neck formation is clearly visible (see black arrows). Carbon particles are visible due to their non-spherical shape (see red arrow, confirmed by EDXS). No features such as sintering neck formation or diffusion zones in the contact points of carbon and magnesium particles can be found. When comparing to unsintered Mg+C samples as shown in Figure 5-24 it can be seen that scale like structures are visible on the powder particles of the sintered samples. As this is the case for pure magnesium as well as for Mg+C carbon can be excluded as source of these structures. It is assumed that this effect might be caused due to oxidation of the powder surfaces during the sintering process since this effect is not visible on the powder particles before sintering.

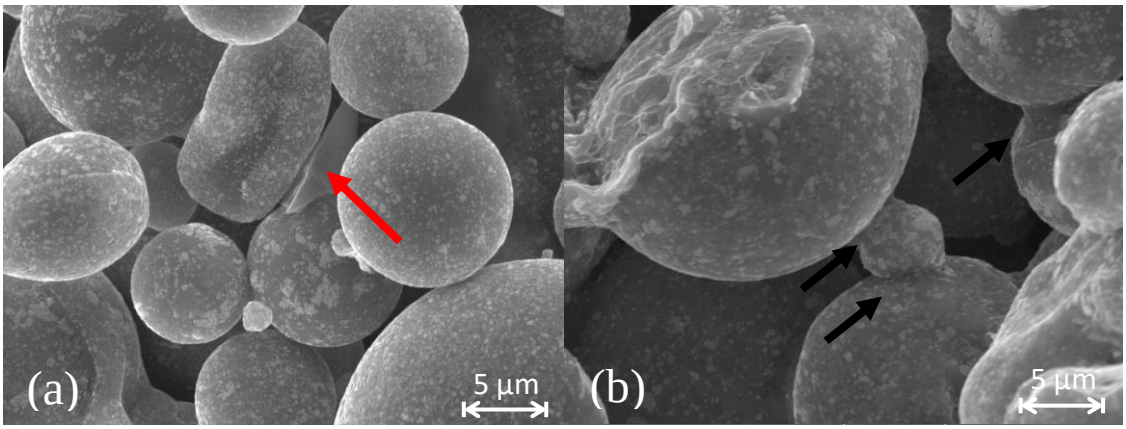

Figure 5-23 Mg+C after sintering (a) and Mg after sintering (b).

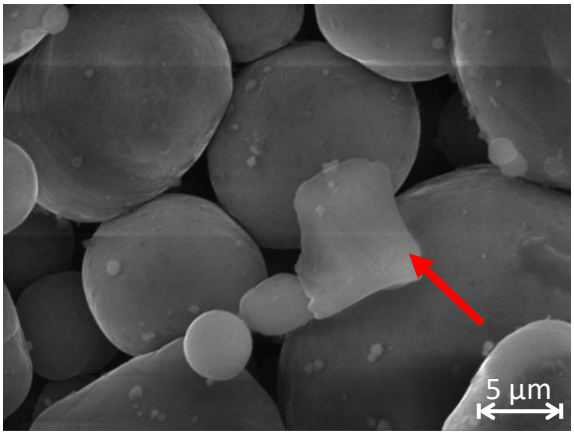

Figure 5-24 Mg+C splinter before sintering.

5.7 Sintering Under Hydrogen Atmosphere

When comparing the samples sintered under argon and hydrogen, respectively, a clear difference can be observed. Figure 5-25 displays the longitudinal shrinkage and the mechanical properties of pure magnesium MIM samples processed with different backbone polymers sintered under hydrogen and argon, respectively. It can be seen that all samples processed under argon reveal only low shrinkage.

The PPcoPE processed samples show the highest shrinkage of the samples sintered under argon. However, in general the strength of the magnesium samples sintered under argon was very low. Both sample sets processed with PE based backbone polymers had such a low strength that it was not possible to measure the samples with the used set up. For the PPcoPE processed samples ultimate tensile strength of approximately 10 MPa was still low and no elongation was measurable. However, this set of samples was at least measurable.

These results show again the strong sintering inhibiting effect of the PE based polymers compared to PP based polymers. When comparing the results of the samples sintered under hydrogen it can be noticed that the PE-EVA processed samples have the lowest shrinkage and mechanical properties. One reason can be the formation of blisters on the samples that occurred probably due to the fact that the thermal debinding process was not

optimised for the thermal decomposition of this polymer leading to the formation of blisters during the thermal debinding step as shown in Figure 5-26. This blister formation also occurred for the PE-EVA processed samples sintered under argon.

Also, the PE and PPcoPE processed samples sintered under hydrogen reveal a significant improvement in shrinkage and mechanical properties. The mechanical properties are the highest ever measured for pure magnesium MIM samples. When comparing the PPcoPE and PE processed samples sintered under hydrogen it can be observed that the mechanical properties as well as the longitudinal shrinkage are in the same range. This is in contrast to the results of these samples sintered under argon. These results show that sintering under hydrogen has a positive effect on the sintering results of pure magnesium MIM samples. Furthermore, it can be seen that the negative effect of PE on the sintering results in comparison to PPcoPE can be reversed as the results after sintering under hydrogen are comparable.

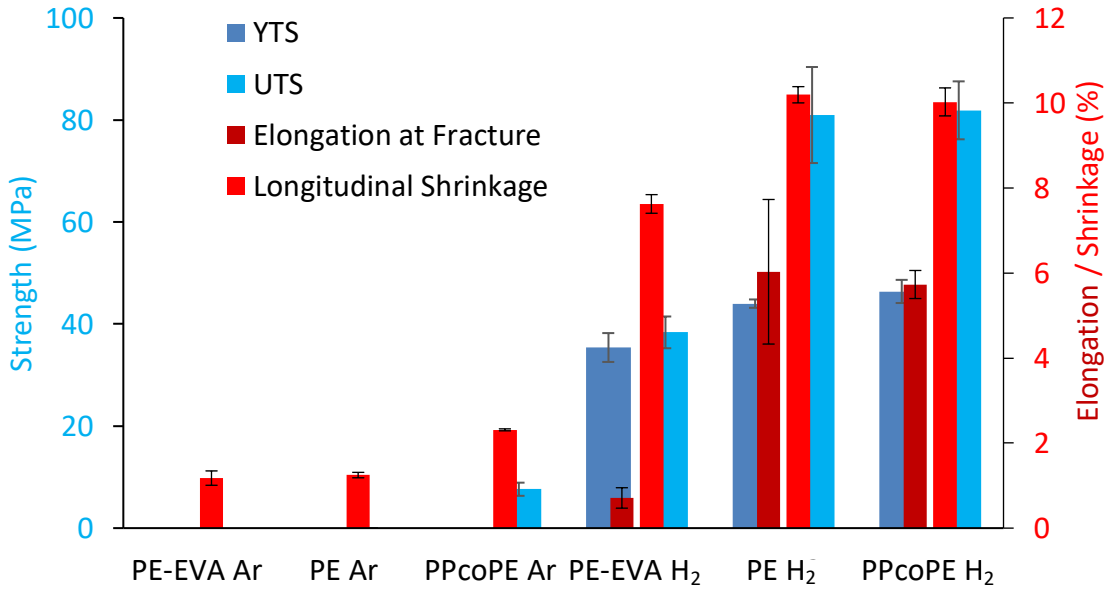

Figure 5-25 Mechanical properties and longitudinal shrinkage of pure MIM Mg samples with different backbone polymers sintered under Ar and H_2.

Figure 5-26 Blister formation on PE-EVA MIM samples after sintering.

A correlation between sintering activity and carbon residuals is assumed. Therefore, Figure 5-27 displays the longitudinal shrinkage and the total carbon content of the pure magnesium MIM of Figure 5-25. The order of the samples is changed to oppose the samples processed with same polymers but different sintering atmospheres. The total carbon content of the initial powder is displayed for comparison. It can be seen that the samples

sintered under hydrogen reveal a higher sintering activity (higher shrinkage) while their total carbon content is lower in contrast to sintering under argon. The total carbon content of the samples sintered under hydrogen is comparable to the carbon content of the initial powder. This shows that by using hydrogen as a sintering atmosphere, carbon residuals caused by the thermal decomposition of the backbone polymers can be removed from the samples.

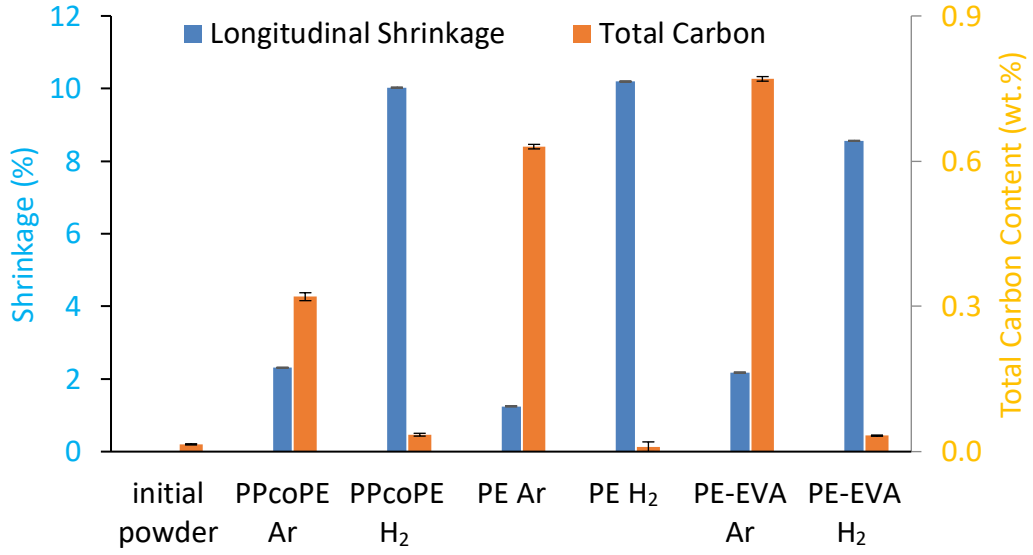

Figure 5-27 Longitudinal shrinkage and total carbon content of pure Mg MIM samples processed using different backbone polymers sintered under Ar and H_2.

To illustrate the correlation of carbon content and sintering activity Figure 5-28 displays the results of Figure 5-27 as longitudinal shrinkage VS total carbon content. Two groups can be observed, one group with high shrinkage and low carbon content and one group with low shrinkage and high carbon content. The low carbon content group implies the samples sintered under hydrogen while the other group implies the samples sintered under argon. This indicates the opposing correlation of carbon content and sintering activity. The higher the carbon content the lower the sintering activity. Furthermore, it can be concluded that by using hydrogen the carbon content can be reduced to a level comparable to the content of the initial powder.

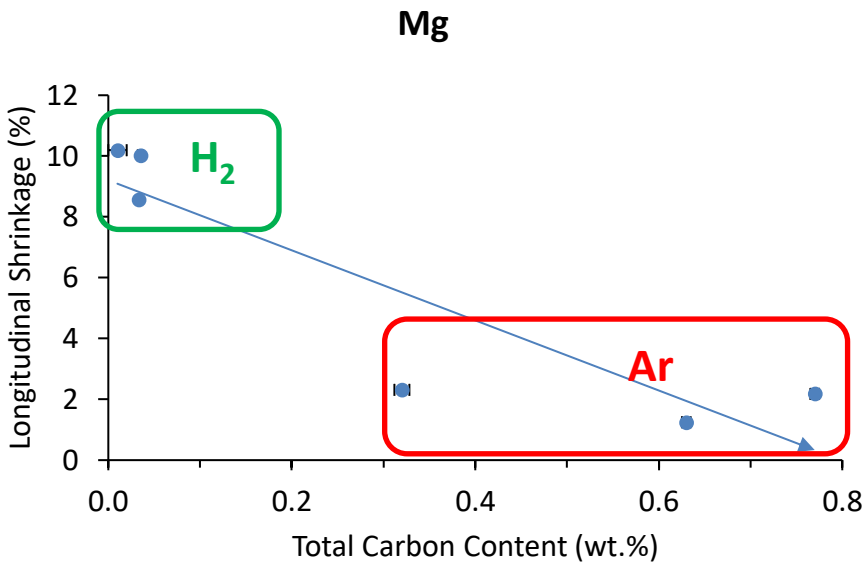

Figure 5-28 Longitudinal shrinkage vs total carbon content of pure Mg MIM samples sintered under H_2 and Ar using different backbone polymers.

Magnesium discs were placed besides MIM samples for XPS analysis. Figure 5-29 displays the results of the XPS measurements performed on these. Obviously, only the disc placed besides the PE samples sintered under argon shows a significant difference in carbon content.

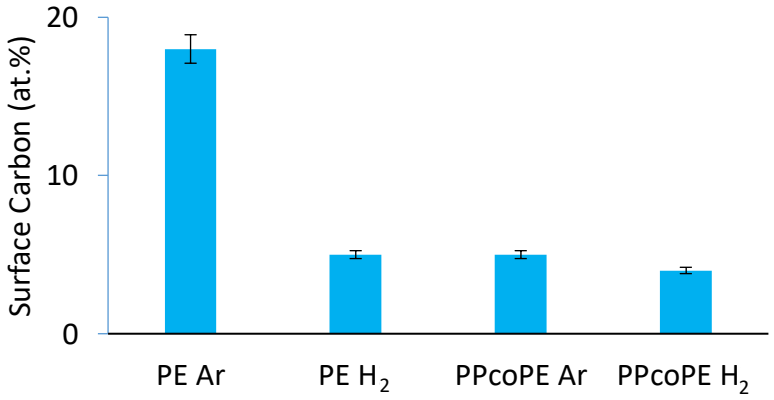

Figure 5-29 Total surface carbon by XPS after Ar etching determined of Mg discs placed besides MIM samples containing PE and PPcoPE backbone polymers sintered under Ar and H_2.

For the Mg-0.9Ca samples, Figure 5-30 displays the longitudinal shrinkage and the mechanical properties of these set of samples sintered under argon and hydrogen, respectively. When comparing the samples sintered under argon it can be observed that both PE based polymers only reveal a low sintering activity (low longitudinal shrinkage) and low mechanical properties compared to the PPcoPE samples. This again shows the strong sintering inhibiting effect of the PE based polymers compared to the PP based polymers. When comparing the samples sintered under hydrogen to the ones sintered under argon it can be seen that the shrinkage as well as the mechanical properties of the PE processed samples significantly increased. When comparing the samples sintered under hydrogen it can be seen that the mechanical results of the PE-EVA processed samples are lower. This

is presumably due to thermal debinding not being optimised for this backbone polymer resulting in blister formations as observed in Figure 5-26. These blisters caused premature failures during the tensile tests. Therefore, the results of these samples should not be considered as material but rather as individual sample properties.

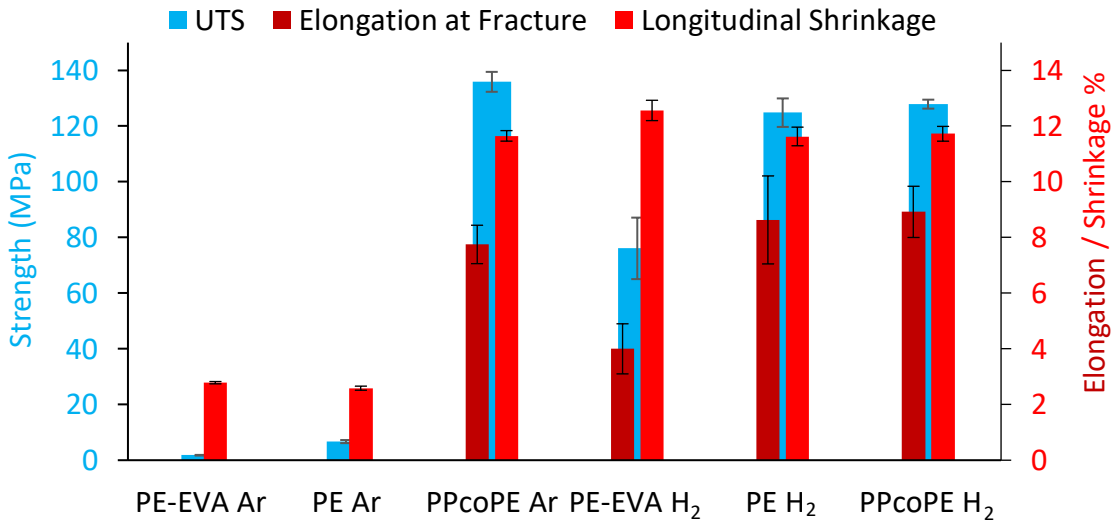

Figure 5-30 Mechanical properties and longitudinal shrinkage of Mg-0.9Ca MIM samples processed using different backbone polymers sintered under Ar and H_2.

To correlate the mechanical properties and the carbon content of samples with comparable sintering activity Figure 5-31 displays the mechanical properties in correlation with the total carbon content of the PPcoPE processed samples sintered under argon and hydrogen. It can be seen that sintering under hydrogen results in lower carbon content of the samples. When comparing the mechanical properties, it can be seen that the elongation at fracture decreases with increasing carbon content while the yield strength as well as the ultimate tensile strength increase.

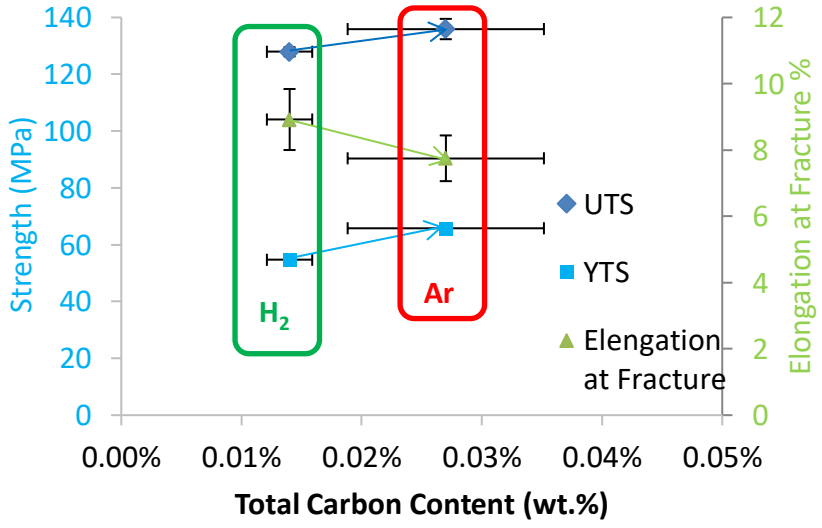

Figure 5-31 Mechanical properties of Mg-0.9Ca MIM samples processed using PPcoPE backbone polymer sintered under Ar and H_2 resulting in different carbon contents.

To investigate the influence of sintering under hydrogen to commercially used alloys, Figure 5-32 displays the total carbon content of AZ91 MIM samples processed with PE and PPcoPE backbone polymer, respectively, thermally debound and sintered under different atmospheres. Equivalent to the results shown before, both, using PPcoPE and sintering under hydrogen reduce the amount of residual carbon. Additional usage of hydrogen during thermal debinding further decreases the residual carbon content.

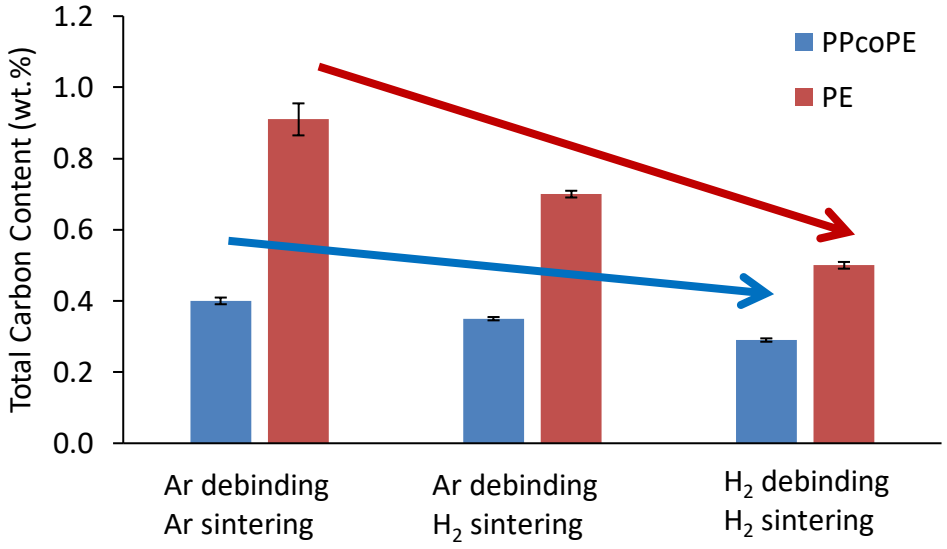

Figure 5-32 Total carbon content of AZ91 MIM samples processed with PE and PPcoPE backbone polymer, sintered under Ar, H_2 and thermal debound and sintered under Ar.

Also, for this alloy the correlation between sintering activity and carbon content can be observed as displayed in Figure 5-33. The higher the total carbon content of the samples the lower is their sintering activity (shrinkage).

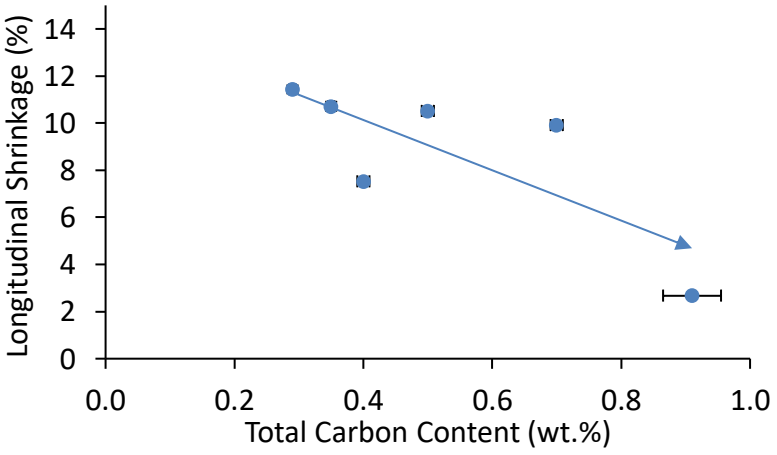

Figure 5-33 Longitudinal shrinkage VS total carbon content of AZ91 MIM samples processed with PE and PPcoPE backbone polymer sintered under Ar and H_2 atmosphere.

To investigate the influence of hydrogen sintering atmosphere on the sintering results of alloys that contain alloying elements that are known to form hydrated Mg-Gd alloys are sintered under argon and hydrogen, respectively. Figure 5-34 displays the longitudinal shrinkage of Mg-10Gd and Mg-5Gd MIM samples processed with PPcoPE backbone

polymer sintered under argon and hydrogen. It can be seen that the shrinkage of the Mg-10Gd samples is significantly lower when the samples are sintered under a hydrogen atmosphere. Mg-5Gd also shows a reduction in shrinkage when sintered under a hydrogen atmosphere but not to the same extent as Mg-10Gd. This shows that the sintering results do not improve but even decline when hydrogen is used as a sintering atmosphere instead of argon. This is in contrast to the results observed for pure magnesium, Mg-0.9Ca and AZ91 MIM samples.

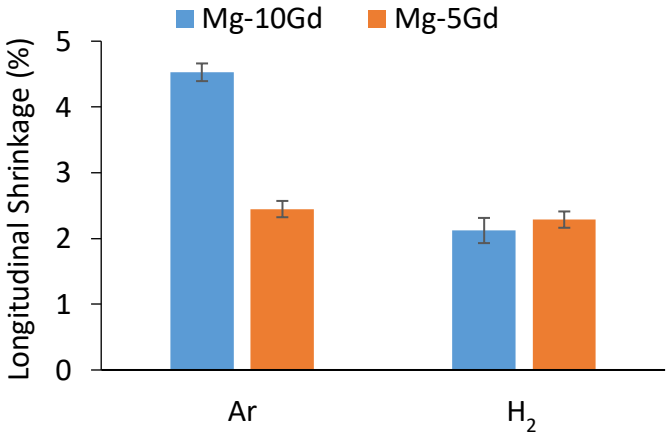

Figure 5-34 Longitudinal Shrinkage of Mg-10Gd and Mg-5Gd MIM samples sintered under Ar and H_2.

5.8 Sintering of Titanium using PPcoPE and PE-EVA Backbone Polymer

The mechanical properties of the titanium MIM samples processed using PE-EVA as well as PPcoPE as backbone polymers reveal no significant differences as shown in Figure 5-35. Figure 5-36 displays the total carbon content determined by combustion analysis. It can be seen that the carbon content does not differ significantly. This shows that the thermal decomposition of these two polymers leave the same amount of carbon residuals in the sintered titanium part. The results show that there is no significant difference between the two types of backbone polymers when used for MIM of titanium. This is in contrast to the results observed for pure magnesium, Mg-0.9Ca and AZ91 MIM samples.

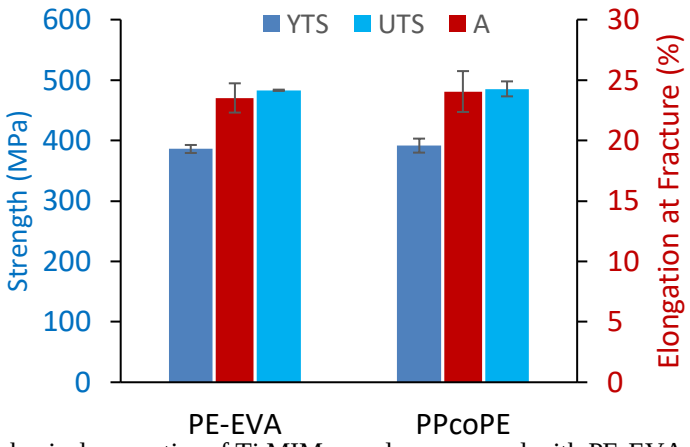

Figure 5-35 Mechanical properties of Ti MIM samples processed with PE-EVA and PPcoPE.

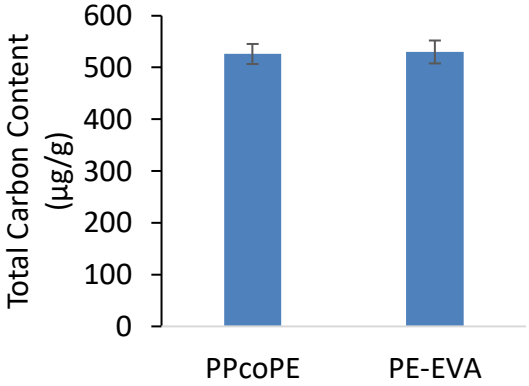

Figure 5-36 Total carbon content of Ti MIM samples processed with PPcoPE and PE-EVA backbone polymer.

6 Discussion

6.1 The Effect of Carbon on the Sintering Activity of Magnesium

The major thermal decomposition products of the investigated polyolefinic polymers are hydrocarbons [111, 112]. Therefore, it can be assumed that either a compound of carbon and magnesium or elemental carbon is causing the sintering inhibiting effect. Hence, the effect of carbon and carbon residuals on the sintering activity of magnesium is investigated and discussed in the following section.

The fact that carbon residuals have a negative influence on the sintering activity of magnesium and its alloys is proven within this work. This could be shown using different experimental setups processing pure magnesium as well as different magnesium alloys. Thereby, it is irrelevant if the carbon is added as elemental carbon (see section 5.6) or by the treatment of magnesium with hydrocarbon compounds (see sections 5.2, 5.5 and 5.7). It is found that pure magnesium is more sensitive to the carbon content compared to the tested Mg-0.9Ca and AZ81 alloy (see section 5.2, 5.5, 5.6 and 5.7). Adding small amounts of elemental carbon already results in a dramatic drop of sintering activity indicated by a decrease of shrinkage (see section 5.6). An opposing correlation between carbon content and sintering activity could be proven by producing samples of pure magnesium, Mg-0.9Ca as well as AZ81 using different backbone polymers and different sintering atmospheres (argon and hydrogen) (see sections 5.5 and 5.7). The correlation is illustrated in Figure 5-18, Figure 5-19, Figure 5-29 and Figure 5-33. The higher the carbon content of samples the lower is the sintering activity of these samples. A comparable correlation between sintering activity and carbon content was also found by Gierl *et al.* [157] for MIM of aluminium alloys.

A literature review reveals that magnesium has no measurable solubility for carbon and that there are no stable Mg-C phases according to the phase diagram [42, 43]. Therefore, it can be concluded that elemental carbon e.g. graphite on the magnesium powder particles is chemically inert. Also, magnesium oxide and carbon are chemically inert to each other at the conditions apparent during MIM [60]. This leads to the assumption that carbon is preventing inter-particle diffusion. Inter-particle diffusion is essential for the sintering process [70]. Therefore, it can be concluded, that carbon has a diffusion hindering effect comparable or even stronger like the oxide layer of magnesium powder particles [8]. SEM images of the powder surfaces do not show differences between samples with high carbon content when the carbon residuals are caused by hydrocarbon treatment. As the carbon residuals are caused by gaseous hydrocarbons such as in the case of the thermal debinding during MIM (see section 5.1) it can be supposed that the carbon residuals are homogeneously distributed over the powder surfaces. Figure 6-1 displays a model of two powder particles that are covered by the oxide layer and an additional layer of carbon

residuals. To enable sintering in this model magnesium atoms need to be able to diffuse through these layers on the powder particle surface. The position of the carbon residuals resulting from the treatment with hydrocarbons is supposed to be below the oxide layer. This is due to the fact that metastable magnesium carbides would form and decompose in the upper magnesium layers (see section 6.2). In the case of elemental carbon addition the carbon is located on top of the oxide layer.

In the following section a theoretical estimation is made to calculate the amount of carbon needed to fully cover the surface of the pure magnesium powder used for the experiments. To estimate the carbon amount needed for a single layer on the magnesium powder the following input is used: the BET surface area of the used magnesium powder is 1.6713 m²/g. The appearance of the carbon residuals is unknown but a graphene structure is used for simplification. The theoretical specific surface area of graphene is 2630 m²/g according to Bonaccorso *et al.* [158]. When a single layer graphene crystal is considered to cover the magnesium powder surfaces only half of the surface of graphene is in contact to the magnesium. When the BET surface area of magnesium ($A_{BET,Mg}$) and half of the theoretical surface area of graphene ($A_{th,C}$) are set in relation according to equations (13)-(15) only 0.13 wt.% of carbon is needed to cover the magnesium powder with a single layer of graphene. This value is in the range of the carbon contents that were found to have a negative influence e.g. in Figure 5-28 it can be seen that a carbon amount of below 0.1 wt.% does not have a negative influence while a carbon content above 0.3 wt.% shows a significant sintering inhibiting effect.

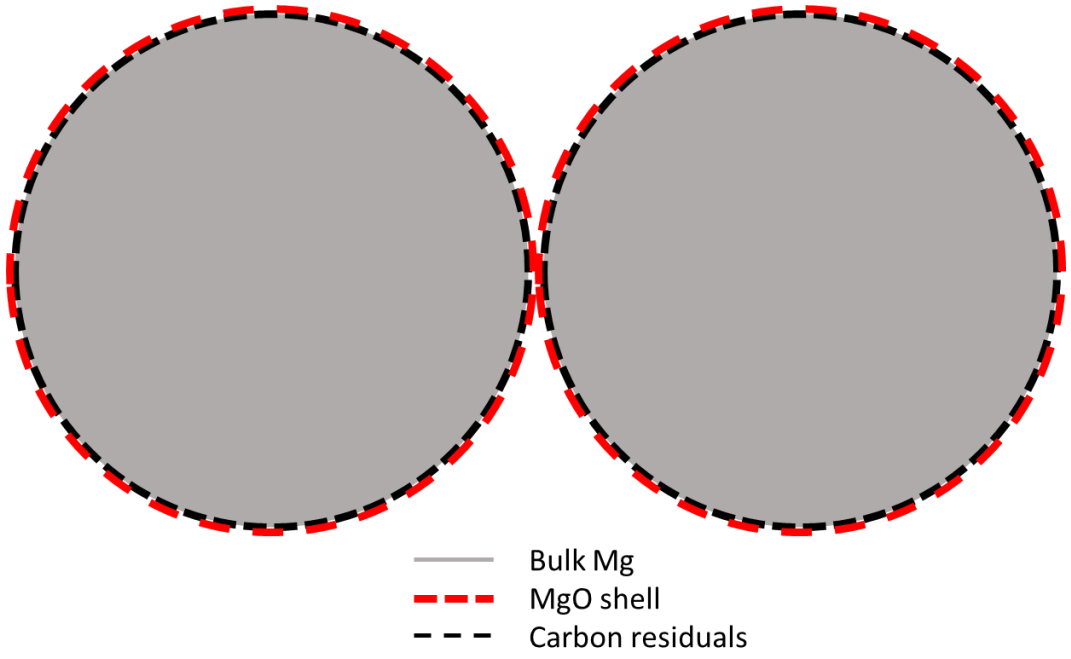

Figure 6-1 Model of Mg powder particles surrounded by magnesium oxide and carbon residuals.

$$A_{Mg} = \frac{A_C}{2} \qquad \text{eq. (13)}$$

$$A_{BET,Mg} = \frac{A_{Mg}}{m_{Mg}} \; ; \; A_{th,C} = \frac{A_C}{m_C} \qquad \text{eq. (14)}$$

$$\frac{m_C}{m_{Mg}} = \frac{2 * A_{BET,Mg}}{A_{th,C}} \qquad \text{eq. (15)}$$

Alloys that form a liquid phase during sintering like the tested Mg-0.9Ca and AZ91 are less sensitive to carbon. This is presumably due to a barrier bridging effect of the liquid phase. The liquid phase might be enabling inter-particle diffusion paths between neighbouring powder particles due to wetting of the surface areas that are not totally covered by carbon. This effect could be similar to the wetting of the oxide layer described by Wolff *et al*. [8]. Also, a breaking of the layer or displacement due to the liquid phase could be possible.

6.2 Carbon Residuals in Dependence of Polyolefins, Hydrocarbons and Atmosphere

As discussed and proven in section 6.1, carbon has a strong sintering inhibiting effect when it is apparent on the magnesium powder surface. Now it will be shown that based on this effect the different sintering behaviour of PE and PP based samples during MIM processing of magnesium can be explained. Therefore, *i.a.* the thermal decomposition products of the polyolefins are simulated using different isomers of short chain hydrocarbons. In addition, it is shown that removing carbon residuals by hydrogenation leads to improved sintering activity.

6.2.1 Carbon Residuals in Dependence of Polyolefins

In section 5.2 it can be seen that the thermal removal of PE and PPcoPE ends up in different surface carbon content of the flat surface of magnesium discs. Therefore, a correlation can be made between the differing thermal decomposition of these polymers with the different amounts of carbon on the surface of magnesium powder samples. Due to the high surface area of the magnesium powder an even more dramatic effect can be expected when powder is used instead of a flat magnesium surface leading to significant differences in carbon content of samples that are processed with PE or PPcoPE, respectively.

The results of the polymer screening (section 5.1) reveal that PE based polymers have a strong sintering inhibiting effect compared to PP based polymers and higher branched polymers like PIB. This leads to the assumption that the basic polymer chain of the backbone polymer used has a major influence on the sintering results. PE is based on a straight hydrocarbon chain. The structure of PP is similar, the only difference is an additional methyl group on every second carbon atom. This gives PP a branched structure. Adding an additional methyl group to the basic structure of PP results in the polymer PIB. If the

branched structure has an influence using PIB as a backbone polymer this should result in comparable sintering results to PP, which is shown in section 5.1. This confirms the assumption that the basic structure of the backbone polymer used has a major influence on the sintering results of magnesium. Wolff *et al.* [9] assumed that the negative influence of the PE-EVA polymer used in comparison to the poly(1-butene) as well as the poly(propylene-co-1-butene) is caused by the oxygen of the EVA group. In section 5.1 it could be shown that other PE based polymers that do not contain any oxygen in their molecular chain show comparable sintering inhibiting results compared to the PE-EVA polymer. This disproves the assumption of Wolff *et al*. [9]. In fact, it seems that the inhibiting effect is linked to the straight basic chain of the PE polymers. This link will be explained below.

From the sintering results of binder free reference samples placed besides binder containing samples (see section 5.1) it can be concluded that the sintering inhibiting effect is caused by the gaseous thermal decomposition products of the backbone polymer used. The results of the binder free samples placed beside binder containing ones correlate with the sintering results of the corresponding binder containing samples. This proves that not only the direct contact of the PE based polymer and the magnesium powder results in a sintering inhibiting effect but also the contact of the magnesium powder with the gaseous polymer decomposition products is causing this effect. This effect was also described by Wolff *et al.* [9]. This leads to the conclusion that specific decomposition products of the different polyolefins can cause significantly higher carbon residuals causing differences in sintering activity.

A literature review concerning the thermal decomposition of PE and PP based polymer chains is given in section 2.6. PE based polymers decompose at slightly higher temperatures compared to PP based ones [102]. In Figure 5-8 the TGA results show that under vacuum conditions the differences in the thermal decomposition temperature of the tested polyolefins is only around 30 K. It is unlikely that the differences in the sintering results are caused by this slight difference in the thermal decomposition temperature. Vacuum as well as low heating rates shift the thermal decomposition to lower temperatures as it is shown in section 5.3.

PP and PE based polymers are thermally decomposed by a random chain scission process [102, 103]. Moreover, it was found that the major difference in the thermal decomposition of PE and PP is that PE decomposes mainly into straight n-alkanes and 1-alkenes while PP decomposes mainly into branched iso-alkanes and iso-alkenes [104, 106-108].

TGA-FTIR measurements performed on pure polymers and polymers in contact with magnesium powder highlighted that when comparing the spectra of PE and PE+Mg an additional band occurs at around 965 cm^{-1} when magnesium is present during the thermal decomposition of PE (see Figure 5-13). This indicates a change in the gas phase of the thermal decomposition products of PE. Bands around 965 cm^{-1} are typical for double

bonds of hydrocarbons [159]. This additional band indicates a chemical reaction taking place between the thermal decomposition products of PE and the magnesium powder. The reaction cannot only be traced back to the presence of any metal powder as the same polymer together with titanium powder does not reveal an additional band. When comparing PPcoPE and PPcoPE+Mg no additional bands are present (see Figure 5-14). This proves that the reaction assumed for PE+Mg is not occurring for the combination of PPcoPE and magnesium. As PPcoPE only contains a few randomly distributed PE monomers and PPcoPE and PP polymers show comparable results in the binder screening experiments (see section 5.1) it can be assumed that the reaction found for the combination of PE and magnesium is not taking place for PP and PIB based polymers.

Experiments using PE-EVA and PPcoPE for the production of titanium MIM samples reveal that samples processed with either backbone polymers have comparable carbon contents (see section 5.8). This is in contrast to the results with PP and PE polymers in combination with magnesium. Therefore, it can be concluded that the differences in carbon content of magnesium samples in combination with PE and PP based polymers is a result of a chemical reaction linked to the presence of magnesium. This reaction is not taking place if titanium is used instead of magnesium. However, it must be considered that due to the higher sintering temperature of titanium and the solubility of titanium for carbon [160] the conditions are not comparable. Still the IR measurements show no hints for a reaction between the polymers and titanium as observed for magnesium (see section 5.4).

6.2.2 Carbon Residuals in Dependence of Different Hydrocarbons, Carbide Formation and Decomposition

In section 5.5 results of the experiments conducted using different straight and branched alkanes and alkenes to treat pure magnesium and Mg-0.9Ca samples at temperatures typically used for the thermal debinding in the MIM process are shown. Straight hydrocarbons were chosen to simulate the thermal debinding products of PE while the corresponding branched ones are used to simulate the thermal debinding products of PP. By correlating the results of PE and PP produced samples it is expected that samples treated with the straight alkanes or alkenes show less sintering activity and higher carbon content compared to the ones treated with the corresponding branched isomers. The experiments confirm these predicted sintering results. The only exception was found for the combination of Mg-0.9Ca treated with iso-butene. It is assumed that a reaction between calcium and the iso-butene is taking place as the results of 1-butene and iso-butene with pure magnesium are as expected. No literature for a reaction between iso-butene and calcium could be fund so it was not possible to prove or disprove this assumption within this work. Based on these facts the results of this combination are not further pursued. XPS and ToF-SIMS measurements on magnesium discs placed besides the sintering samples show

that the straight hydrocarbons leave higher amounts of carbon in the surfaces compared to the corresponding branched isomers. From these experiments in combination with the literature about typical thermal decomposition products of PE and PP it can be concluded that the different sintering results of PE and PP are based on the reaction of the magnesium with the thermal decomposition products of these polymers. The different carbon contents caused by different thermal decomposition products of PE and PP are therefore the reason for the different influence on the sintering activity of the magnesium powder. Furthermore, the differences in the thermal decomposition temperatures of PE and PP can be excluded as reason for the different sintering inhibiting effect as the treatment of the hydrocarbons were performed using the same temperature profile.

Following now is the discussion how certain hydrocarbons react with the magnesium resulting in higher carbon content of the samples leading to lower sintering activity. Potential reaction products of the reaction between straight hydrocarbons and magnesium could be carbides. Even if they are not thermodynamically stable two types of magnesium carbides (Mg_2C_3, MgC_2) are known to exist [54]. However, they cannot be formed from the metal and elemental carbon under the temperature and pressure conditions given in the MIM process [47, 48, 49, p. 920, 50]. On the other hand, Irmann, Novák as well as many other authors used hydrocarbons over heated magnesium to produce magnesium carbides [46-54, 56]. Novák [52, 56] investigated the formation as well as the decomposition of the carbides systematically. Using acetylene, he found that the formation of Mg_2C starts at 400 °C and has a maximum at 490 °C. The formation of Mg_2C_3 begins at 460 °C and has its maximum at 650-700 °C [56]. These temperature ranges match the thermal debinding and sintering temperatures used in the MIM process for magnesium (see section 4.2.1). Especially the formation temperatures of Mg_2C fit to the thermal debinding temperatures used during MIM processing of magnesium. Therefore, the formation of carbides out of the thermal debinding products of PE and magnesium is possible. These carbides would form on the surface of the powder particles as it is reported by Reuggeberg [47] and Gault [55].

It was suggested by different authors that the carbides form due to the reaction of magnesium with fragments of the thermal decomposition of the hydrocarbons being radicals of the hydrocarbons [54, 50, 56, 58]. During the thermal decomposition of PE as well as PP radicals form due to a random chain scission process [102, 103]. Therefore, it is likely that the carbides can form from these radicals and the magnesium powder. However, it seems that the decomposition products of PE (straight hydrocarbons) are more likely to form carbides compared to the ones of PP (branched hydrocarbons). Novák found that the number and positions of methyl groups can have an influence on the carbide yield on the example of benzene, toluene and different isomers of xylene [56]. This underlines that the differences in the decomposition products of PE and PP can be a reason for different amounts of carbide formation as these decomposition products also differ by the presence

and position of methyl groups. The different amount of carbide formation would explain the different total carbon content measured for samples processed with PE and PP based polymers. Magnesium carbides are reported to form on the surface of the magnesium while the bulk material stays unchanged [47]. It is suggested that approximately 50 magnesium layers are involved in the carbide formation [55]. This means that if carbides do form during MIM they would form on the outer layers of the powder particles.

Simultaneously with the formation of the carbides their decomposition takes place either according to equation (1) or directly into the elements [50]. The decomposition according to equation (1) starts at 500 °C with simultaneous decomposition into the elements, above 600 °C only traces of MgC_2 are left. Under vacuum conditions the decomposition of MgC_2 into the elements happens already at 450 °C without the formation of Mg_2C_3 [50]. As vacuum is applied during the thermal debinding of the MIM magnesium samples it can be concluded that if the carbides form during the process they directly decompose into carbon. The direct decomposition of the carbides would explain why carbides could not been detected by XRD measurements. The formation of MgC_2 and the direct decomposition into magnesium and carbon is more likely to happen due to the typical temperature during the thermal debinding process which is completed below 460 °C. The resulting carbon distributed at the powder particle surfaces can act as barrier between powder particles preventing the sintering process as discussed in section 6.1. The reactions and mechanisms leading to carbon residuals on the magnesium powder surfaces causing the sintering inhibiting effect when PE is used as a backbone polymer are represented in the chemical equations (16)-(18). Equation (16) describes the decomposition of the PE polymer chain under heat and vacuum into straight n-alkanes and 1-alkenes. Equation (17) describes the formation of magnesium carbide from the straight hydrocarbons and magnesium under heat. The resulting unknown hydrocarbon rest "z" is presumably causing the changes detected in the IR-bands observed during TGA-FTIR (see section 5.4). The formation of the metastable carbides is followed by their decomposition into the elements (equation (18)) which is promoted by heat and vacuum conditions. Equation (17) and (18) also apply for the straight hydrocarbon isomers of the simulated debinding products in section 5.5.

$$PE \xrightarrow[vacuum]{heat} CH_3 - [CH_2]_x - CH = CH_2 \;/\; CH_3 - [CH_2]_y - CH_3 \qquad \text{eq. (16)}$$

$$CH_3 - [CH_2]_x - CH = CH_2 \;/\; CH_3 - [CH_2]_y - CH_3 + Mg \xrightarrow{heat} MgC_2 + z \qquad \text{eq. (17)}$$

$$MgC_2 \xrightarrow[vcuum]{heat} Mg + C \qquad \text{eq. (18)}$$

Other magnesium carbon compounds besides carbides are unlikely to cause the sintering inhibiting effect. Magnesium carbonate would decompose during the thermal debinding step leaving magnesium oxide in the compound [61, 62]. As carbon could be correlated

with the sintering inhibiting effect magnesium carbonate can be excluded. Magnesium stearate which can form out of the used stearic acid and the magnesium can be excluded to be the reason for the sintering inhibiting effect because it would decompose during the thermal debinding leaving MgO. Furthermore, stearic acid can be excluded as a cause for the sintering inhibiting effect because it is used in combination with both PP and PE backbone polymers. Moreover, in [85] a positive effect of a stearic acid treatment on the sintering results could be shown.

6.2.3 Influence of Hydrogen Atmosphere on Carbon Content

If carbon residuals from the thermal decomposition of the backbone polymer cause a sintering inhibiting effect, removal of the carbon should lead to increased sintering activity. This could be proven in section 5.7 and has been published in [91, 93] by using hydrogen during thermal debinding and sintering. Carbon control by using hydrogen containing atmospheres is a common technique in powder metallurgy e.g. for iron-based materials [118, 130].

The total carbon content of magnesium samples sintered under hydrogen atmosphere is comparable to the carbon content of the initial powder while samples sintered under argon possess a significantly higher carbon content (see section 5.7). This highlights that the carbon residuals caused by the thermal decomposition of the backbone polymers can be removed when hydrogen is used as a sintering atmosphere. Carbon can be removed by hydrogen due to the hydrogenation reaction forming methane as described in more detailed in section (2.8). R. de Oro Calderon *et al.* [161] found, that methane formation in PM steels is strongly enhanced by oxygen sensitive alloying elements. Therefore, it is possible that the hydrogenation of the carbon on the powder surface is enhanced due to the contact with the magnesium which is also an oxygen sensitive material [4].

When, instead of argon, hydrogen is used during thermal debinding the carbon content can be further decreased (see section 5.7 and [91]). This is presumably due to the extended treatment time with hydrogen allowing more carbon residuals to react with the hydrogen. In addition, it is possible that hydrogen reacts with hydrocarbon radicals that form during the thermal debinding of the polyolefins [103, 162]. The resulting saturated hydrocarbons are presumably less reactive when in contact with the magnesium powder. This can be concluded from different publications [50, 54, 56, 58] in which it is suggested that radicals of the hydrocarbons are reacting with the magnesium to form magnesium carbides. However, the possibility to use hydrogen can be limited by alloying elements as discussed in section 6.3.

6.3 Effects of Carbon on Mechanical Properties and Processing Limitations with a Hydrogen Sintering Atmosphere

The following findings have stemmed from the main topic of this thesis and are therefore discussed in their own dedicated section. On the one hand it is discussed that carbon residuals in low amounts can have a strengthening effect and on the other hand possible processing limitations of the thermal treatment with hydrogen containing atmosphere are discussed.

Evaluating the mechanical results of the Mg-0.9Ca samples with different amounts of residual carbon in the range where the sintering activity is not negatively influenced it can be found that samples with lower carbon amount have a higher elongation at fracture with lower strength compared to samples with slightly higher carbon content (see Figure 5-31). This leads to the conclusions that carbon residuals in low amounts can have a strengthening effect. An explanation for this effect could be that the insoluble carbon residuals at the grain boundaries hinder the dislocation movement resulting in a strengthening effect resulting in higher strength and lower elasticity [163, p. 13 ff.].

In section 6.2 a positive effect of sintering under hydrogen was proven. However, the use of hydrogen as sintering atmosphere might be limited to alloys that do not contain elements that tend to form hydrides such as gadolinium [131, 91]. In section 5.7 and in [91] it is shown that using hydrogen atmosphere for the sintering of Mg-Gd samples has a negative influence on the sintering results compared to argon sintering atmosphere. This effect is presumably caused by the reaction of the hydrogen with the gadolinium resulting in the formation of hydrides. The formation of hydrides in combination of magnesium and gadolinium has been reported in by Huang *et al.* [131]. Alloying elements that have been hydrated cannot alloy with the magnesium which results in *i.a.* in differing amounts of the liquid phase during sintering. The amount of liquid phase can have a strong effect on the sintering results. Typically, a higher amount of liquid phase will increase the sintering activity [80]. Using the Mg-Gd alloy (see section 5.7 in particular Figure 5-34) as an example, the hydration of the Gd would result in a reduced amount of liquid phase which explains the reduced sintering activity (reduced shrinkage) of samples treated with hydrogen. Therefore, it can be concluded that the alloying elements and sintering atmospheres have to be considered when choosing a magnesium alloy for the MIM process.

6.4 Ideal Backbone Polymer and Processing Conditions

Based on the analysis of the results of this work the following recommendations for choosing backbone polymers and processing conditions for MIM of magnesium and its alloys can be made.

Branched polyolefins like PP or PIB based polymers should preferably be used while straight unbranched hydrocarbon-based polymers like PE based ones should be avoided. PPcoPE polymers show beneficial mixing with wax compared to isotactic PP resulting in improved mixing and injection moulding properties of the resulting feedstock. Even though this polymer contains PE monomers no negative effect on the sintering activity could be found (see section 5.1). This is presumably due to the fact that this polymer type only consists of low PE monomers (typically 1-7 wt.%) that are randomly distributed in the polymer chain. Typically, 75% of the monomers are single and 25% multiple insertions in the polymer chain [97, pp. 19-21]. If this polymer decomposes the resulting fragments will still have a branched structure which was proven to have no negative effect (see section 6.2).

To lower the reaction possibility between the magnesium powder and the thermal decomposition products slow heating rates and low pressures should be used during thermal debinding. These conditions will shift the thermal decomposition to lower temperatures (see section 5.3). Sweep gas can help to remove decomposition products away from the samples. Hydrogen can be beneficial during this step as hydrogen can saturate hydrocarbon radicals resulting in lower reactivity [123]. On the other hand, hydrogen can be used to remove carbon residuals by hydrogenation resulting in improved sintering activity (see section 4.3.4). However, the use of hydrogen can be limited due to reactions with alloying elements resulting in negative effects on the sintering results (see section 4.3.4). If hydrogen cannot be used high purity argon can be used. The furnace should provide a low leakage rate to prevent further oxidation of the magnesium MIM parts during thermal treatment.

Similar recommendations can be made for the sintering atmosphere. If possible due to alloy composition hydrogen should be preferred as sintering atmosphere, if not high purity argon can be used. Loose magnesium powder as described by Wolff *et al.* [8] should be used to surround the samples as getter material. The pressure during sintering should be chosen high enough to prevent extensive evaporation of the magnesium which would result in material loss of the samples.

7 Conclusions

Within this work the basic mechanism causing the different sintering results of PE and PP backbone polymers when used for MIM of magnesium could be identified and understood. With the fundamental understanding of the different reactivity between the thermal decomposition products of different polyolefins with magnesium a suitable binder system for MIM of magnesium and its alloys based on a PP based backbone polymer could be developed. The results and main findings of this work can be concluded as the following:

Using PE based polymers as a backbone polymer for MIM of magnesium and its alloys results in a strong sintering inhibiting effect while the use of PP based polymers does not result in such an effect. This effect is caused by a reaction taking place between the thermal decomposition products of PE, being mainly straight n alkanes and 1 alkenes, and the magnesium powder. The thermal decomposition products of PP, being mainly branched iso alkanes and iso alkenes, do not show this reaction with magnesium. The reaction products are metastable magnesium carbides that decompose in the conditions apparent during thermal debinding of the MIM processing (temperature and vacuum) leaving carbon residuals on the magnesium powder surfaces. Carbon is not soluble in magnesium and no compounds of magnesium and carbon are stable at the conditions that are apparent during MIM processing. Therefore, carbon residuals that form on the magnesium powder surface are able to form a layer that can prevent interparticle diffusion of neighbouring powder particles. A correlation between carbon content and sintering activity could be found. With increasing carbon content, the sintering activity decreases due to a barrier effect of the carbon residuals on the powder surfaces.

When using PE as a backbone polymer, the amount of carbon on the powder surfaces after thermal debinding is high enough to hinder interparticle diffusion between the magnesium powder particles which act as a barrier preventing sintering. When using PP based polymers the amount of carbon on the powder surfaces is significantly lower and thus sintering can still take place.

It was also found that hydrogen as a sintering atmosphere can significantly reduce the residual carbon content resulting in improved sintering even in combination with PE based polymers. This effect is caused due to hydrogenation of carbon residuals. However, the use of hydrogen can be limited by alloying elements that tend to form hydrides.

Based on this understanding of the decomposition of the polyolefins and the reactions of their decomposition products a suitable binder system for MIM of magnesium can be formulated. The binder system should be based on a branched polyolefin like PP or PIB. Within the frame of this work, PPcoPE as backbone polymer shows a good combination of low influence on sintering and good miscibility in combination with the remaining binder components such as waxes and stearic acid which ensures good mouldability.

The amount of carbon residuals should be kept as low as possible during the heat treatment steps. Thermal debinding and sintering should be performed preferably in combination with hydrogen containing atmospheres. However, this can be limited by the reactivity of alloying elements with the hydrogen. When hydrogen cannot be used vacuum and protective gases such as argon should be used. However, the use of low pressures is also limited to lower temperatures and short times due to the high vapour pressure of magnesium leading to evaporation of magnesium.

If MIM of magnesium is performed using a binder system based on the results of this work and within the determined limits, a commercial application of this process can be attractive not only in the biomedical sector to produce small complex shaped parts in high quantities with unique microstructure and properties. In fact, a small series of parts (components for “wearables”) have already been produced using the binder system developed within the frame of this work.

8 References

[1] R. M. German, Injection Molding of Metals and Ceramics, Princeton, New Jersey: Metal Powder Industries Federation, 1997.

[2] R. M. German, “Progress in Titanium Metal Powder Injection Molding,” *Materials,* vol. 6, pp. 3641-3662, 2013.

[3] R. M. German, Powder Injection Molding, Princeton, New Jersey: Metal Powder Industries Federation, 1990.

[4] C. Kammer, Magnesium Taschenbuch, Düsseldorf: Aluminium Verlag, 2000.

[5] K. U. Kainer, Magnesium Alloys and theri Applications, Weinheim: Wiley-VCH Verlag GmbH, 2006.

[6] K.-U. Kainer, T. Ebel, O. Ferri, W. Limberg, F. Pyczak, F.-P. Schimansky and M. Wolff, “From titanium to magnesium: processing by advenced metal injection moulding,” *Powder Metallurgy,* vol. 55, no. 4, pp. 315-312, 2010.

[7] M. Wolff, W. Limberg, T. Ebel and R. Bormann, “Towards Producing Magnesium Parts by Powder Metal Injection Moulding (MIM),” *Euro PM2008 Proceedings,* vol. 2, pp. 221-226, 2008.

[8] M. Wolff, T. Ebel and M. Dahms, “Sintering of Magnesium,” *Advanced Engineering Materials,* vol. 12, no. 9, pp. 829-836, September 2010.

[9] M. Wolff, B. Wiese, M. Dahms and T. Ebel, “Binder development for Magnesium Powder Injection Moulding,” in *Euro PM2011 Congress Proceedings*, vol. 2, Barcelona, Spain, European Powder Metallurgy Association (EPMA), 2011, p. 271.

[10] M. Wolff, J. Deussing, M. Dahms, T. Ebel, K. U. Kainer and T. Klassen, “Advances in the Metal Injection Moulding of Mg-Ca alloys for biomedical applications,” *Powder Injection Moulding International,* pp. 57-61, December 2012.

[11] M. Wolff, M. R. Suckert, J. G. Schaper, M. Dahms, T. Ebel, K. U. Kainer and T. Klassen, “Metal Injection Molding (MIM) of Magnesium Alloys for Orthopedic Implant Applications,” in *Proceedings of the FiMPART 2015*, Hyderabad, India, 2015.

[12] M. Wolff, T. Gülck and T. Ebel, “Sintering of Mg and MgCa Alloys for Biomedical Applications,” in *Euro PM2009 Proceedings*, vol. 1, 2009, p. 417.

[13] W. Schatt, K.-P. Wieters and B. Kieback, Pulvermetallurgie Technologien und Werkstoffe, 2. ed., Berlin-Heidelberg: Springer Verlag, 2007.

[14] W. Schatt and K.-P. Wieters, Powder Metallurgy Processing and Materials, Shrewsbury, UK: EPMA, 1997.

[15] S. Kajala, J. Ryhänen, A. Danilov and J. Tuukkanen, "Effect of porosity on the osteointegration and bone ingrowth of a weight-bearing nickel-titanium bone graft substitute," *Biomaterials,* vol. 24, no. 25, pp. 4691-4697, November 2003.

[16] P. A. Clark, E. K. Moioli, D. R. Sumner and J. J. Mao, "Porous implants as drug delivery vehicles to augment host tissue integration," *The FASEB Journal,* vol. 22, no. 6, January 2008.

[17] W. E. Frazier, "Metal Additive Manufacturing: A Review," *Journal of Materials Engineering and Performance,* vol. 23, no. 6, pp. 1917-1928, June 2014.

[18] C. Kukla, J. Gonzalez, C. Burkhardt, O. Weber and C. Holzer, "The Production of Magnets by FFF-Fused Filament Fabrication," in *EuroPM2017,* Milano, Italy, 2017.

[19] C. Berger, J. Abel, J. Pötschke and T. Moritz, "Properties Of Additive Manufactured Hardmetal Components Produced By Fused Filament Fabrication (FFF)," in *EuroPM2018,* Bilbao, Spain, 2018.

[20] I. Agote, N. Azumendi, C. Guraya, M. Lagos and A. Lores, "Binder Jetting of High Dimensional Stability Alloy For Space Applications," in *EuroPM2018,* Bilbao, Spain, 2018.

[21] P. Burke, G. Kipouros, D. Fancelli and V. Laverdiere, "Sintering Fundamentals of Magnesium Powders," *Canadien Metallurgical Quarterly,* vol. 48, no. 2, pp. 123-132, 2009.

[22] J. Čapek and D. Vojtěch, "Effect of sintering conditions on the microstructural and mechanical characteristics of porous magnesium materials prepared by powder metallurgy," *Materials Science and Engeneering C,* vol. 35, pp. 21-28, 2014.

[23] M. A. J. Teleghani, PHD Thesis: Processing and properties of high performance 7075 Al and AZ91 Mg powder metallurgy alloys, Universidad Carlos III de Madrid, 2014.

[24] C. E. Wen, M. Mabuchi, Y. Yamada, K. Shimojima, Y. Chino and T. Asahina, "Processing of biocompatible porous Ti and Mg," *Scripta Materialia,* vol. 45, pp. 1147-1153, 2001.

[25] M. Gupta and N. M. L. Sharon, Magnesium, Magnesium Alloys, and Magnesium Composites, John Wiley & Sons, Inc.,, 2010.

[26] Thieme Verlagsgruppe, "Thieme Römpp, Keyword: Magnesium," Georg Thieme Verlag KG, [Online]. Available: https://roempp.thieme.de/roempp4.0/do/data/RD-13-00108. [Accessed 8 August 2017].

[27] G.Song and S. Song, "MAGNASIUM AS A POSSIBLE DEGRADABLE BIO-COMPATABLE MATERIAL," in *Magnesium Technology in the Global Age,* Montreal, Quebec, Canada, Canadian Institute of Mining, Metallurgy and Petrolium, 2006, pp. 345-358.

[28] B.-S. You, W.-W. Park and I.-S. Chung, "THE EFFECT OF CALCIUM ADDITIONS ON THE OXIDATION BEHAVIOR IN MAGNESIUM ALLOYS," *Scripta Materialia,* no. 42, pp. 1089-1094, 31 May 2000.

[29] International Magnesium Association, "IMA Awards of Excellence Winners," *Mg Showcase,* vol. 18, 2012.

[30] R. Willumeit, J. Fischer, F. Feyerabend, N. Hort, U. Bismayer, S. Heidrich and B. Mihailova, "Chemical surface alteration of biodegradable magnesium exposed to corrosion media," *Acta Biomaterialia,* vol. 6, no. 7, pp. 2704-2715, 2011.

[31] E. C. Huse, "A New Ligature," *CHICAGO MEDICAL JOURNAL AND EXAMINER,* vol. 37, no. 2, pp. 171-172, 1878.

[32] C. Plaass, C. v. Falck, S. Ettinger, L. Sonnow, F. Calderone, A. Weizbauer, J. Reifenrath, L. Claassen, H. Waizy, K. Daniilidis, C. Stukenborg-Colsman and H. Windhagen, "Bioabsorbable magnesium versus standard titanium compression screws for fixation of distal metatarsal osteotomies – 3 year results of a randomized clinical trial," *Journal of Orthopeadic Science,* vol. 23, no. 2, pp. 321-327, 2018.

[33] M. Ezechieli, M. Ettinger, C. König, A. Weizenbauer, P. Helmecke, R. Schavan and A. Lucas, "Biomechanical characteristics of bioabsorbable magnesium-based (MgYREZr-alloy) interference screws with different threads," *Knee Surgery, Sports Traumatology, Arthroscopy*, vol. 24, no. 12, pp. 3976-3981, 2016.

[34] J. G. Schaper, M. Wolff, T. Ebel, M. Dahms and R. Willumeit-Römer, “MIM-Processing of Complex Mg-Alloys,” in *Proceedings of the EuroPM2017*, Milano, Italy, 2017.

[35] *ASTM B275-05.*

[36] M. Peters and C. Leyens, Titan und Titanlegierungen, Weinheim: WILEY-VCH Verlag, 2002.

[37] Thieme Verlagsgruppe, "Thieme RÖMPP, Keyword: Calcium," Georg Thieme Verlag KG, [Online]. Available: https://roempp.thieme.de/roempp4.0/do/data/RD-03-00107. [Accessed 20 May 2014].

[38] M. Aljarrah and M. Medraj, “Thermodynamic modelling of the Mg–Ca, Mg–Sr, Ca–Sr and Mg–Ca–Systems using the modified quasichemical model,” *Calphad,* pp. 240-251, June 2008.

[39] CompuTherm, L.L.C., *Pandat 8.1 with PanMagnesium 8 database,* 2012.

[40] B. Wiese, Projektarbeit: Thermodynamische Berechnung des Mg-Ca-Phasendiagramms, Flensburg/Geesthacht: FH Flensburg, 2012.

[41] J. Harmuth, B. Wiese, J. Bohlen and R. Willumeit-Römer, “Tailoring of Material Properties of Mg-Gd Alloys for Biomedical Applications,” in *Proceedings of the 11th International Conference on Magnesium Alloys and their Applications*, Brunel University London, UK, 2018.

[42] H.-L. Chen and R. Schmid-Fetzer, “The Mg–C phase equilibria and their thermodynamic basis,” *International Journal of Materials Research,* vol. 103, no. 11, pp. 1294-1301, 2012.

[43] H.-L. Chen, N. Li, A. Klostermeier and R. Schmid-Fetzer, “Measurement of carbon solubility in magnesium alloys using GD-OES,” *Journal of Analytical Atomic Spectrometry,* vol. 26, pp. 2189-2196, 23 August 2011.

[44] A. Nayeb-Hashemi and J. B. Clark, “Phase diagrams of binary magnesium alloys,” *ASM International,* 1988.

[45] B. Hu, Y. Du, H. Xu, W. Sun, W. Zhang and D. Zhao, “THERMODYNAMIC DESCRIPTION OF THE C-GeAND C-Mg SYSTEMS,” *Journal of Mining and Metallurgy,* pp. 97-103, 2010.

[46] U. Ruschewitz, “Binary and ternary carbides of alkali and alkaline-earth metals,” *Coordination Chemistry Reviews,* vol. 244, pp. 115-136, 2003.

[47] W. H. C. Reuggeberg, “The Carbides of Magnesium,” *Journal of the American Chemical Society,* vol. 65, 1943.

[48] H. Fjellvåg and P. Karen, “Crystal Structure of Magnesium Sesquicarbide,” *Inorganic Chemistry,* vol. 31, pp. 3260-3263, 1992.

[49] G. Brauer, Handbook of Preperative Inorganic Chemistry, New York, London: Academic Press, 1963.

[50] F. Irmann, Promotionsarbeit: Zur Kenntnis der Magnesiumcarbide, Zürich: Grütli-Buchdruckerei, 1949.

[51] P. Karen, A. Kjekshus, Q. Huang and V. L. Karen, “The crystal structure of magnesium dicarbide,” *Journal of Alloys and Compounds,* vol. 282, pp. 72-75, 1999.

[52] J. Novák, “Über die Einwirkung von metallischem Magnesium auf Acetylen,” *Berichte der deutschen chemischen Gesellschaft,* vol. 42, pp. 4209-4213, 1910.

[53] A. Schneider and J. F. Cordes, “Zur Darstellung und thermischen Stabilität der Magnesiumcarbide MgC2 und Mg2C3,” *Zeitschrift für anorganische und allgemeine Chemie,* vol. 279, pp. 94-103, 1955.

[54] F. Irmann, “Zur Kenntnis der Magnesiumcarbide,” *Helvetica Chimica Acta,* vol. 31, no. 6, pp. 1584-1602, 1948.

[55] Y. Gault, “Reactions of Propyne and Propadiene on Magnesium Films,” *Journal of the Chemical Society, Faraday Transactions 1: Physical Chemistry in Condensed Phases,* vol. 74, pp. 2678-2688, 1978.

[56] J. Novák, “Zur Kenntnis der Magnesiumcarbide,” *Zeitschrift für Physikalische Chemie,* pp. 513-546, 1910.

[57] S. M. Hick, C. Griebel and R. G. Blair, “Mechanochemical Synthesis of Alkaline Earth Carbides and Intercalation Compounds,” *Inorganic Chemistry,* vol. 48, pp. 2333-2338, 2009.

[58] A. Perret and J. Rietmann, “Sur l'affinité du magnésium pour le carbone,” *Helvetica Chimica Acta,* vol. 30, pp. 218-224, 1947.

[59] H. J. Freund and M. W. Roberts, “Surface chemistry of carbon dioxide,” *Surface Science Reports,* vol. 25, pp. 225-273, 1996.

[60] Y. Tian, T. Qu, B. Yang, H.-x. Liu, C.-b. Yang and Y.-n. Dai, “Mechanism of Carbothermic Reduction of Magnesia and Reverse Reaction,” in *Magnesium Technology 2012*, Springer , 2016, pp. 511-516.

[61] W. Bandi and G. Krapf, “The Effect of CO2 Pressure and Alkali Salt on the Mechanism of Decomposition of Dolomite,” *Thermochimica Acta,* vol. 14, pp. 221-243, 1976.

[62] Institut für Arbeitsschutz der Deutschen Gesetzlichen Unfallversicherung (IFA), “GESTIS-Stoffdatenbank Suchbegriff Magnesiumcarbonat,” [Online]. Available: http://gestis.itrust.de/nxt/gateway.dll/gestis_de/021530.xml?f=templates$fn=default.htm$3.0. [Accessed 8 August 2017].

[63] Institut für Arbeitsschutz der Deutschen Gesetzlichen Unfallversicherung (IFA), “GESTIS-Stoffdatenbank Suchbegriff Magnesiumstearat,” [Online]. Available: http://gestis.itrust.de/nxt/gateway.dll/gestis_de/021530.xml?f=templates$fn=default.htm$3.0. [Accessed 8 August 2017].

[64] J.-l. FAN, Y. HAN, T. LIU, H.-c. CHENG and J.-m. T. Yang GAO, “Influence of surfactant addition on rheoliogical behaiviors of injection-moded ultrafine 98W-1Ni-1Fe suspension,” *Transactions of Nonferrous Metals Society of China,* vol. 23, pp. 1709-1717, 2013.

[65] Y.-m. LI, X.-q. LIU, f.-h. LUO and J.-l. YUE, “Effects of surfactant on properties of MIM feedstock,” *Transactions of Nonferrous Metals Society of China,* vol. 17, pp. 1-8, 2007.

[66] M. Wesolowski, “The influence of Various Tablet Components on Thermal Decomposition of Some Pharmaceuticals,” *Mikrochimica Acta,* pp. 199-213, 1980.

[67] D. F. Heaney, Handbook of metal injection molding, Cambridge: Woodhead Publishing Limited, 2012.

[68] T. Ebel, “Titanium and titanium alloys for medical applications: opportunities and challenges,” *Powder Injection Moulding International,* vol. 2, pp. 21-30, June 2008.

[69] *DIN 8580:2003-09.*

[70] W. Schatt, Sintervorgänge Grundlagen, Düsseldorf: VDI Verlag, 1992.

[71] Z. Munir, “Analytical treatment of the role of surface oxide layers in the sintering of metals,” *Journal of Materials Science,* vol. 14, pp. 2733-2740, 1979.

[72] G. Welsch, R. Boyer and E. W. Collins, Materials Properties Handbook: Titanium Alloys, Ohio: ASM International, 1994.

[73] Z. A. Munir, “Surface Oxides and Sintering of Metals,” *Powder Metallurgy,* vol. 4, pp. 177-180, 1981.

[74] P. Burke, “Investigation of the Sintering Fundamentals of Magnesium Powders,” Dalhousie University, Halifax, Nova Scotia, 2011.

[75] M. Wolff, “Looking to the future: Magnesium powder injection moulding,” *Powder Injection Moulding International,* vol. 2, pp. 63-65, 2008.

[76] M. Wolff, C. Blawert, M. Dahms and T. Ebel, “Properties of Sintered Mg Alloys for Biomedical Applications,” in *Proceedings of the Fifth International Light Metals Technology Conference 2011,* Durnten-Zurich, Switzerland, Trans Tech Publications, 2011, pp. 491-494.

[77] “NIST Chemistry WebBook,” U.S. Department of Commerce, [Online]. Available: http://webbook.nist.gov/chemistry/. [Accessed 23 May 2014].

[78] M. Woff, M. Dahms, T. Ebel and T. Klassen, “Production of biodegradable Mg-0.9Ca implants by Powder Injection Moulding (PIM),” in *9th International Conference on Magnesium Alloys and their Applications*, Vancouver, 2012.

[79] M. Wolff, *Diploma thesis: Experimentelle Untersuchungen zur Verarbeitung von Magnesium nach dem Metallpulverspritzgießverfahren (MIM-Technik),* Flensburg: Fachhochschule Flensburg, 2006.

[80] R. M. German, Liquid Phase Sintering, New York: Plenum Press, 1985.

[81] C. E. Wen, Y. Yamada, K. Shimojima, Y. Chino, H. Hosokawa and M. Mabuchi, “Compressibility of porous magnesium foam: dependency on porosity and pore size,” *Materials Letters,* vol. 58, pp. 357-360, 2004.

[82] J. Čapek and D. Vojtěch, “Properties of porous magnesium prepared by powder,” *Materials Science and Engineering C,* vol. 33, pp. 564-569, 2013.

[83] B. Wiese, *Bachelor-Thesis: Binder für die MIM-Verarbeitung von Magnesium,* Flensburg: Fachhochschule Flensburg, 2010.

[84] J. Deussing, *Bachelor-Thesis: Entwicklung eines Bindersystems für den Metallpulverspritzguss von Magnesium,* Flensburg: Fachhochschule Flensburg, 2012.

[85] J. G. Schaper, *Master-Thesis: Metal Injection Moulding Processing of Mg-0.9Ca for Biomedical Applications,* Flensburg: Flensburg Univerity of Applied Sciences, 2014.

[86] M. Wolff, J. G. Schaper, M. Dahms, T. Ebel, R. Willumeit-Römer and T. Klassen, "Metal Injection Molding (MIM) of Mg-Alloys," in *TMS 2018 147th Annual Meeting & Exibition Supplemental Proceedings,* Phoenix, AZ, USA, 2018.

[87] M. Wolff, J. G. Schaper, M. R. Suckert, M. Dahms, T. Ebel, R. Willumeit-Römer and T. Klassen, "Enhancement of Thermal Debinding and Sintering of Biodegradable MIM-Magnesium Parts for Biomedical Applications," in *Proceedings of the WorldPM2016,* Hamburg, Germany, 2016.

[88] M. Wolff, J. G. Schaper, M. R. Suckert, M. Dahms, F. Feyerabend, T. Ebel, R. Willumeit-Römer and T. Klassen, "Metal Injection Moulding (MIM) of Magnesium and Its Alloys," *Metals,* vol. 6, May 2016.

[89] M. Harun, N. Muhamad, A. Sulong, N. M. Nor and M. Ibrahim, "Rheological Investigation of ZK60 Magnesium Alloy Feedstock for Metal Injection Moulding using Palm Stearin Based Binder System," *Applied Mechanics and Materials,* Vols. 44-47, pp. 4126-4130, 2010.

[90] M. R. Harun, N. Muhamad, A. B. Sulong, N. H. M. Nor, K. R. Jamaludin and M. H. Ibrahim, "Solvent Debinding Process for ZK60 Magnesium Alloy Mim Compact," *Jurnal Teknologi,* vol. 59, pp. 159-168, 2012.

[91] J. G. Schaper, M. Wolff, T. Ebel and R. Willumeit-Römer, "Sintering of Mg and its Alloys under Hydrogen Atmospheres," in *Euro PM2018,* Bilbao, Spain, 2018.

[92] J. G. Schaper, M. Wolff, B. Wiese, T. Ebel and R. Willumeit-Römer, "Powder Metal Injection Moulding and Heat Treatment of AZ81 Mg Alloy," *Journal of Materials Processing Technology,* vol. 267, pp. 241-246, May 2019.

[93] J. G. Schaper, N. Scharnagl, M. Wolff, T. Ebel, S. Neumann and R. Willumeit-Römer, "Polyolefin-Magnesium Interactions Performing Powder Injection Molding Process," *Advanced Engineering Materials,* 06 August 2018.

[94] A. Peacock, Handbook of Polyethylene: Structures, Properties, and Applications, New York, Basel: Marcel Dekker, INc, 2000.

[95] Sigma-Aldrich, “Sigma-Aldrich,” [Online]. Available: http://www.sigmaaldrich.com. [Accessed 05 09 2017].

[96] G. Wen, P. Cao, B. Gabbitas, D. Zhang and N. Edmonds, “Development and Design of Binder Systems for Titanium Metal Injection Molding: An Overview,” *METALLURGICAL AND MATERIALS TRANSACTIONS A,* vol. 44A, pp. 1530-1547, March 2013.

[97] Thieme Verlagsgruppe, “Thieme RÖMPP, Keyword: Polypropylene,” Georg Thieme Verlag KG, [Online]. Available: https://roempp.thieme.de/roempp4.0/do/data/RD-16-03538. [Accessed 30 November 2017].

[98] C. Maier and T. Calafut, Polypropylene: The Definitive User's Guide and Databook, Plastics Desing Library, 1998.

[99] Thieme Verlagsgruppe, “Thieme Römpp, Keyword: Polyisobutene,” Georg Thieme Verlag KG, [Online]. Available: https://roempp.thieme.de/roempp4.0/do/data/RD-16-03335. [Accessed 30 November 2017].

[100] Christen and Vögtle, Grundlagen der organischen Chemie, Frankfurt a.M.: Otto Salle Verlag, 1989.

[101] Thieme Verlagsgruppe, “Thieme Römpp, Keyword: Stearinsäure,” Georg Thieme Verlag KG, [Online]. Available: https://roempp.thieme.de/roempp4.0/do/data/RD-19-03880. [Accessed 5 September 2017].

[102] J. D. Peterson, S. Vyazovkin and C. A. Wight, “Kinetics of the Thermal and Thermo-Oxidative Degradation of Polystyrene, Polyethylene and Poly(propylene),” *Macromolecular Chemitry and Physics,* vol. 202, pp. 775-784, 2001.

[103] C. L. Beyler and M. M. Hirschler, “Thermal Decomposition of Polymers,” in *SFPE Handbook of Fire Protection Engineering*, Quincy, Massachusetts: NFPA, 2002, pp. 110-131.

[104] H. Bockhorn, A. Hornung, U. Hornung and D. Schawaller, “Kinetic study on the thermal degradation of polypropylene and polyethylene,” *Journal of Analytical and Applied Pyrolysis,* vol. 48, pp. 93-109, 1999.

[105] K. Murata, K. Sato and Y. Sakata, “Effect of pressure on thermal degradation of polyethylene,” *Journal of Analytical and Applied Pyrolysis,* vol. 71, pp. 569-589, 2004.

[106] L. Soják, H. J. R. Kubinec and M. B. E. Hájeková, “High resolution gas chromatographic-mass spectrometric analysis of polyethylene and polypropylene thermal cracking products,” *Journal of Analytical and Applied Pyrolysis,* vol. 78, pp. 387-399, 2007.

[107] T. M. Kruse, H.-W. Wong and L. J. Broadbelt, “Mechanistic Modeling of Polymer Pyrolysis: Polypropylene,” *Macromolecules,* vol. 36, pp. 9594-9607, 2003.

[108] S. E. Levine and L. J. Broadbelt, “Detailed mechanistic modeling of high-density polyethylene pyrolysis: Low molecular weight product evolution,” *Polymer Degradation and Stability,* vol. 94, pp. 810-822, 2009.

[109] E. Hájeková, L. Špodová, M. Bajus and B. Mlynková, “Separation and Characterization of Products from Thermal Cracking of Individual and Mixed Polyalkenes,” *Chemical Papers,* vol. 61, no. 4, pp. 262-270, 2007.

[110] L. Ballice, M. Yüksel and M. Saglam, “Classification of Volatile Products from the Temperature-Programmed Pyrolysis of Low- and High-Density Polyethylene,” *Energy and Fuels,* vol. 12, pp. 925-928, 1998.

[111] Y. Tsuchiya and K. Sumi, “Thermal Decomposition Products of Polypropylene,” *Journal of Polymer Science Part A: Polymer Chemistry*, vol. 7, pp. 1599-1607, 1969.

[112] Y. Tsuchiya and K. Sumi, “Thermal Decomposition Products of Polyethylene,” *Journal of Polymer Science Part A: Polymer Chemistry*, vol. 6, pp. 415-425, 1968.

[113] U.S. National Library of Medicine, “Pubchem,” [Online]. Available: https://pubchem.ncbi.nlm.nih.gov/compound/2_4-Dimethyl-1-heptene#section=Top. [Accessed 21 August 2017].

[114] P. Quadbeck, S. Pohl, H.-D. Böhm, F. Hempel and J. Röpcke, “Debinding Control of Metal Hollow spheres by IR-Absorbtion Analysis,” in *MetFoam: Porous Metals and Metallic Foams: Proceedings of the Fifth International Conference on Porous Metals and Metallic Foams* , Montreals, Canada, 2007.

[115] P. Quadbeck, B. Schreyer, A. Strauß, T. Weißgräber and B. Kieback, “In-Situ Monitoring of Gas Atmospheres During Debinding and Sintering of PM Steel Components,” in *Prceddings of the WorldPM2010,* Florence, Italy, 2010.

[116] P. Quadbeck, A. Strauß and B. Kieback, “In-situ atmosphere monitoring of the debindering of PM steel components with large organic additive volume fractions,” in *Proceedings of the WorldPM2016*, Hamburg, Germany, 2016.

[117] P. Quadbeck, A. Strauß, S. Müller and B. Kieback, “Atmosphere monitoring in a continuous sintering belt furnace,” *Journal of Materials Processing Technology,* vol. 231, pp. 406-411, 2016.

[118] P. Quadbeck, A. Strauß, L. Wimbert, R. Lindenau and B. Kieback, “Atmosphere Study on the Thermal Decomposition Behavior of Delubrication Aiding Additives,” *Proceedings of the Euro PM2017*, 2017.

[119] T. Hartwig and R. M. Schroeder, “Analysing Debinding and Sintering of Iron Feedstocks by Mass Spectrometry,” in *Proceedings of the WorldPM2012*, Yokohama, Japan, 2012.

[120] I. Mohsin, D. Lager, C. Gierl, W. Hohenauer and H. Danninger, “Thermo-kinetics study of MIM thermal de-binding using TGA coupled with FTIR and mass spectrometry,” *Thermochimica Acta,* Vols. 503-504, pp. 40-45, 2010.

[121] I. U. Mohsin, C. Gierl, H. Danninger and M. Momeni, “Thermal de-binding kinetics of injection molded W-8%Ni-2%Cu,” *Int. Journal of Refractory Metals and Hard Materials,* vol. 29, pp. 729-732, 2011.

[122] C. Wen and J. Huebler, “Kinetic Study of Coal Char Hydrogasification,” *Industrial & Engineering Chemistry Process Design and Development,* vol. 4, no. 2, pp. 142-147, April 1965.

[123] G. Wedler, Lehrbuch der Physikalischen Chemie, Weinheim: VCH, 1985.

[124] R. A. Krakowski and D. R. Olander, “Survey of the Literature on the Carbon-Hydrogen System,” Lawrence Radiation Laboratory University of California, Berkeley, 1970.

[125] J. F. Espinal, F. Mondragón and T. N. Truong, “Mechanisms for methane and ethane formation in the reaction of hydrogen with carbonaceous materials,” *Carbon*, no. 43, pp. 1820-1827, 2005.

[126] R. R. RYE, “Reaction of Thermal Atomic Hydrogen with Carbon,” *Surface Science,* vol. 49, pp. 653-667, 1977.

[127] E. Berl and R. Bemmann, “Über die Einwirkung von Wasserstoff auf Holzkohle und aktive Kohle und über die Methansynthese,” *Zeitschrift für physikalische Chemie,* vol. 162, pp. 71-93, 1932.

[128] J. D. Blackwood, B. D. Cullis and D. J. McCarthy, “Reactivity in the System Carbon-Hydrogen-Methane,” *Australian journal of chemistry,* vol. 20, pp. 1561-1570, 1967.

[129] E. Vietzke, K. Flaskamp and V. Philipps, “Hydrocarbon Formation in the Reaction of Atomic Hydrogen with Pyrolytic Graphite and the Synergyistic Effect of Argon Ion Bombardment,” *Journal of Nuclear Materials,* Vols. 111, 112, pp. 763-768, 1982.

[130] H. Zhang, “Carbon Control in PIM Steel,” *Materials and Manufacturing Process,* vol. 12, no. 4, pp. 673-679, 1997.

[131] Y. Huang, L. Yang, S. You, W. Gan, K. U. Kainer and N. Hort, “Unexpected formation of hydrides in heavy rare earth containing magnesium alloys,” *Journal of Magnesium and Alloys,* vol. 4, pp. 173-180, 2016.

[132] *ISO 9277: Determination of the specific surface area of solids by gas adsorption using the BET method.*

[133] *DIN EN ISO 2740:2009: Sintermetalle, ausgenommen Hartmetalle - Zugprobestäbe.*

[134] *DIN EN ISO 6892-1:2009: Metallische Werkstoffe - Zugversuch - Teil 1: Prüfverfahren bei Raumtemperatur.*

[135] W. M. Lau, L. J. Huang, I. Bello and Y. M. Yiu, “Modification of surface band bending of diamond by low energy argon and carbon ion bombardment,” *Journal of Applied Physics,* vol. 75, p. 3385, 1994.

[136] R. P. Vasquez, “Highly Oriented Pyrolytic Graphite by XPS,” *Surface Science Spectra,* vol. 1, no. 2, p. 238, June 1992.

[137] E. Kurmaev, V. Fedorenko, V. Galakhov, S. Bartkowski, S. Uhlenbrock, M. Neumann, R. S. P., C. Greaves and Y. Miyazaki, “Analysis of oxyanion (BO33−, CO32−, SO42−, PO43−, SeO44-) substitution in Y123 compounds studied by X-ray photoelectron spectroscopy,” *Journal of Superconductivity,* vol. 9, no. 1, pp. 97-100, February 1996.

[138] J. R. Waldrop and R. W. Grant, “Formation and Schottky barrier height of metal contacts to β-SiC,” *Applied Physics Letters,* vol. 56, p. 557, 1990.

[139] A. A. Galuska, J. C. Uht and N. Marquez, “Reactive and nonreactive ion mixing of Ti films on carbon substrates,” *Journal of Vacuum Science & Technology A: Vacuum, Surfaces, and Films,* vol. 6, p. 110, 1988.

[140] L. Ramqvist, K. Hamrin, G. Johansson, A. Fahlman and C. Nordling, “Charge transfer in transition metal carbides and related compounds studied by ESCA,” *Journal of Physics and Chemistry of Solids,* vol. 30, no. 7, pp. 1835-1847, July 1969.

[141] M. K. Rajumon, M. S. Hegde and C. N. R. Rao, “Adsorption of carbon monoxide on Ni/Ti and Ni/TiO2 surfaces preparedin situ in the electron spectrometer: A combined UPS-XPS study,” *Catalysis Letters,* vol. 1, no. 11, pp. 351-359, November 1988.

[142] L. Pedocchi, M. R. Ji, S. Lizzit, G. Comelli and G. Rovida, “CO adsorption on Pd: An XPS and density functional approach,” *Journal of Electron Spectroscopy and Related Phenomena,* vol. 76, no. 29, pp. 383-387, December 1995.

[143] G. Illing, D.Heskett, E. W. Plummer, H.-J. Freund, J. Somers, T. Lindner, A. M. Bradshaw, U. Buskotte, M. Neumann, U. Starke, K. Heinz, P. L. D. Andres, D.Saldin and J. B. Pendry, “Adsorption and reaction of CO2 on Ni{110}: X-ray photoemission, near-edge X-ray absorption fine-structure and diffuse leed studies,” *Surface Science,* vol. 206, no. 1-2, pp. 1-19, November 1988.

[144] L. J. Gerenser, “Photoemission investigation of silver/poly(ethylene terephthalate) interfacial chemistry: The effect of oxygen-plasma treatment,” *Journal of Vacuum Science & Technology A: Vacuum, Surfaces, and Films,* vol. 8, p. 3682, September 1190.

[145] X. D. Peng and M. A. Barteau, “Spectroscopic characterization of surface species derived from HCOOH, CH3COOH, CH3OH, C2H5OH, HCOOCH3, and C2H2 on MgO thin film surfaces,” *Surface Science,* vol. 224, no. 1-3, pp. 327-347, December 1989.

[146] R. Jerome, P. Teyssie, J. J. Pireaux and J. J. Verbist, “Surface analysis of polymers end-capped with metal carboxylates using x-ray photoelectron spectroscopy,” *Applied Surface Science,* vol. 27, no. 1, pp. 93-105, October 1986.

[147] D. E. Haycock, C. J. Nicholls, D. S. Urch, M. J. Webber and G. Wiech, “The electronic structure of magnesium dialuminium tetraoxide (spinel) using X-ray emission and X-ray photoelectron spectroscopies,” *Journal of the Chemical Society, Dalton Transactions,* vol. 12, pp. 1785-1790, 1978.

[148] R. P. Vasquez, “MgO(100) by XPS,” *Surface Science Spectra,* vol. 2, p. 13, 1993.

[149] J. He, J. S. Corneille, C. A. Estrada, M. Wu and D. W. Goodman, “CO interaction with ultrathin MgO films on a Mo(100) surface studied by infrared reflection–absorption spectroscopy, temperature programmed desorption, and x-ray photoelectron spectroscopy,” *Journal of Vacuum Science & Technology A: Vacuum, Surfaces, and Films,* vol. 10, p. 2248, 1992.

[150] H. Onishi, C. Egawa, T. Aruga and Y. Iwasawa, “Adsorption of Na Atoms and Oxygen Containing Molecules os MgO(I00) and (111) Surfaces,” *Surface Science,* vol. 191, pp. 479-491, 1987.

[151] C. D. Wagner, D. A. Zatko and R. H. Raymond, “Use of the oxygen KLL Auger lines in identification of surface chemical states by electron spectroscopy for chemical analysis,” *Analytical Chemistry,* vol. 52, no. 9, pp. 1445-1451, 1980.

[152] W. Wurth, C. Schneider, R. Treichler, E. Umbach and D. Menzel, “Evolution of adsorbate core-hole states after bound and continuum primary excitation: Relaxation versus decay,” *Physical Review B,* vol. 35, p. 7741, 1987.

[153] M. C. Wu, S. Z. Dong and A. R. Zhu, “Studies of CO dissociation promoted by Na on Ag(110),” *Surface Science,* vol. 216, no. 3, pp. 420-428, 1989.

[154] D. A. Welle, “Measurment report: "aw1245t",” Karlsruher Institut für Technologie, 2018.

[155] I. Krupta and A. Luyt, “Thermal properties of polypropylene/wax blends,” *Thermochemica Acta,* no. 372, pp. 137-141, 2001.

[156] I. U. Mohsin, D. Lager, W. Hohenauer, S. Ata, C. Gierl and H. Danninger, “Finite element investigation of backbone binder removal from MIM copper compact,” *Powder Metallurgy,* vol. 55, pp. 333-339, 2012.

[157] C. Gierl, H. Danninger, A. Avakemian, J. Synek, J. Sattler, B. B. Zlatkov, J. t. Maat, A. Arzl and H. Neubing, “Carbon removal as a crucial parameter in the Powder Injection Moulding of aluminium alloys,” *Powder Injection Moulding International,* vol. 6, no. 4, pp. 65-71, December 2012.

[158] F. Bonaccorso, L. Colombo, G. Yu, M. Stoller, V. Tozzini, A. C. Ferrari, R. S. Ruoff and V. Pellegrini, “Graphene, related two-dimensional crystals, and hybrid systems for energy conversion and storage,” *Science,* vol. 347, no. 6217, 02 January 2015.

[159] M. Hesse, H. Meier and B. Zeeh, Spektroskopische Methoden in der organischen Chemie, Stuttgart: Georg Thieme Verlag, 1984.

[160] T. Ebel, T. Beißig, S. Ebner, X. Luo, A. B. Nagaram and D. Zhao, "Reduction of the embrittlment effect of binder contamination in MIM processing of Ti alloys," *Powder Metallurgy,* pp. 1743-2901, 2017.

[161] R. d. O. Calderon, M. Jaliliziyaeian, C. Gierl-Mayer and H. Danninger, "Effects of H2 Atmospheres on Sintering of Low Alloy Steels Containing Oxygen-Sensitive Masteralloys," *Journal of Metals,* vol. 69, no. 4, pp. 635-644, April 2017.

[162] J. A. Miller and S. J. Klippstein, "Solution of Some One- and Two-Dimensional Master Equation Models for Thermal Dissociation: The Dissociation of Methane in the Low-Pressure Limit," *The Journal of Physical Chemistry A,* vol. 106, pp. 4904-4913, 202.

[163] H.-J. Bargel and G. Schulze, Werkstoffkunde, Springer-Verlag Berlin Heidelberg GmbH, 2004.

[164] D. C. Wirtz and F. Niethard, "Etiology, diagnosis and therapy of aseptic hip prosthesis loosening - a status assessment," *Zeitschrift für Orthopädie und ihre Grenzgebiete,* vol. 4, no. 135, pp. 270-280.

[165] T. Albrektsson and C. Johansson, "Osteoinduction, osteoconduction and osseointegration," *European Spine Journal,* vol. 2, pp. 96-101, October 2001.

Eigenanteil des Doktoranden an Veröffentlichungen

1. Johannes G. Schaper, Martin Wolff, Thomas Ebel, Michael Dahms, Regine Willumeit-Römer, *MIM Processing of Complex Mg-Alloys,* Conference oral presentation and Proceedings, EuroPM2017, Milan, Italy, 2017.

Die Experimente in dieser Veröffentlichung wurden unter Absprache der zuständigen Betreuer vom Doktoranden konzipiert, durchgeführt und ausgewertet. Ideen und Herangehensweisen wurden vom Doktoranden eigenständig entwickelt. Die Erstellung der Diskussion entstand durch eigene Gedankengänge des Doktoranden. Die Veröffentlichung wurde vom Doktoranden eigenständig vorbereitet und erstellt und nach einer Prüfung der Betreuer und Co-Autoren eingereicht.

2. Johannes G. Schaper, Nico Scharnagl, Martin Wolff, Thomas Ebel, Silvio Neumann and Regine Willumeit-Römer, *Polyolefin-Magnesium Interactions Performing Powder Injection Molding Process*, Advanced Engineering Materials, 2018.

Die Experimente dieses Papers wurden unter Absprache der zuständigen Betreuer und genannten Co-Autoren vom Doktoranden durchgeführt und ausgewertet. Ideen und Herangehensweisen wurden vom Doktoranden selbständig erarbeitet. TGA-FTIR Messungen wurden mit Hilfe von Silvio Neumann und XPS Messungen mit Hilfe von Nico Scharnagl durchgeführt und ausgewertet. Die Erstellung der Diskussion entstand durch eigene Gedankengänge des Doktoranden und wurde anschließend mit Hilfe der Co-Autoren überarbeitet und finalisiert. Das Manuskript wurde vom Doktoranden eigenständig erstellt und wurde nach Rücksprache mit den Co-Autoren zur Veröffentlichung eingereicht. Wesentliche Teile dieser Veröffentlichung sind in der Dissertation enthalten.

3. Johannes G. Schaper, Martin Wolff, Thomas Ebel, Regine Willumeit-Römer, *Sintering of Mg and its alloys under Hydrogen Atmospheres*, Conference oral presentation and Proceedings, EuroPM2018, Bilbao, Spain, 2018.

Die Experimente in dieser Veröffentlichung wurden unter Absprache der zuständigen Betreuer vom Doktoranden konzipiert, durchgeführt und ausgewertet. Ideen und Herangehensweisen wurden vom Doktoranden eigenständig entwickelt. Die Erstellung der Diskussion entstand durch eigene Gedankengänge des Doktoranden. Die Veröffentlichung wurde vom Doktoranden eigenständig vorbereitet und erstellt und nach einer Prüfung der Betreuer und Co-Autoren eingereicht. Teile dieser Veröffentlichung sind in den Kapiteln 5.7. und 6.2.3. der Dissertation enthalten.

4. Johannes G. Schaper, Martin Wolff, Björn Wiese, Thomas Ebel, Regine Willumeit-Römer, *Powder metal injection moulding and heat treatment of AZ81 Mg alloy*, Journal of Materials Processing Technology, 2019, 267, 241-246.

Die Experimente in dieser Veröffentlichung wurden unter Absprache der zuständigen Betreuer vom Doktoranden konzipiert, durchgeführt und ausgewertet. Ideen und Herangehensweisen wurden vom Doktoranden eigenständig entwickelt. Die Erstellung der Diskussion entstand durch eigene Gedankengänge des Doktoranden. Die Veröffentlichung wurde vom Doktoranden eigenständig vorbereitet und erstellt und nach einer Prüfung der Betreuer und Co-Autoren eingereicht.

Geesthacht,
20. Mai 2019

Ort, Datum, Unterschrift Betreuer

Prof. R. Willumeit-Römer

Kiel, 20.05.19, J. Schaper

Ort, Datum, Unterschrift Doktorand

Helmholtz-Zentrum
Geesthacht
Zentrum für Material- und Küstenforschung
Institut für Werkstofforschung
Metallische Biomaterialien
Max-Planck-Straße 1 · 21502 Geesthacht
Deutschland